SKB

# TECHNICAL REPORT 91-42

## Sensitivity analysis of the groundwater flow at the Finnsjön study site

Yung-Bing Bao, Roger Thunvik

Dept. Land and Water Resources,
Royal Institute of Technology, Stockholm
Sweden

September 1991

**SVENSK KÄRNBRÄNSLEHANTERING AB**
*SWEDISH NUCLEAR FUEL AND WASTE MANAGEMENT CO*
BOX 5864 S-102 48 STOCKHOLM
TEL 08-665 28 00 TELEX 13108 SKB S
TELEFAX 08-661 57 19

# SENSITIVITY ANALYSIS OF THE GROUNDWATER FLOW AT THE FINNSJÖN STUDY SITE

Yung-Bing Bao, Roger Thunvik

Dept. Land and Water Resources,
Royal Institute of Technology, Stockholm, Sweden

September 1991

# SENSITIVITY ANALYSIS OF THE GROUNDWATER FLOW AT THE FINNSJÖN STUDY SITE

**Yung-Bing Bao** **Roger Thunvik**

**September, 1991**

**Dept. Land and Water Resources**
**Royal Institute of Technology**
**Stockholm, Sweden**

## ABSTRACT

The objective of the present investigation was to study, by means of sensitivity analysis, the impact on the solutions to flow calculations of some major fractures zones and the boundary conditions applied in the previous numerical modelling of the groundwater flow conditions at the Finnsjön site. Sensitivity analysis is a useful complementary tool in groundwater flow modelling by making it possible to analyze qualitative as well as quantitative effects of various flow modelling concepts or model strategies on the flow solutions and to gain a general insight into the geohydraulic behaviour of the flow system studied. The sensitivity of the piezometric head and the sensitivity of the flux across an imaginary region of a hypothetical radioactive waste repository due to perturbations of the permeability in two major fracture zones were analyzed. The influence of uncertainties in the prescribed piezometric head boundary conditions, applied in the previous groundwater flow modelling of the Finnsjön study site, was studied. The uncertainties were due to a procedure used for transferring the boundary conditions from a "regional model" to a "local model" area. The study was performed by means of sensitivity analysis using an adjoint technique. The sensitivity of the piezometric head as well as the Darcy flux, both point-wise and integrated over the imaginary repository region, was calculated. Similarly, the sensitivity at a discharge area of interest was calculated. The groundwater flow calculations are part of the SKB 91 performance assessment study of a generic high-level waste repository at the Finnsjön site. Two different sensitivity methods, one called the direct method and the other the variational or the adjoint sensitivity method were applied. The numerical method for solving the flow equation or the so-called "primary problem" as well as the sensitivity equation were based on the Galerkin finite element method.

## CONTENTS

## FIGURE CAPTIONS



## FIGURE CAPTIONS (APPENDIX A)

### Graphical display of the primary solutions

Figure A5. Contour lines showing the distribution of the piezometric head (m) in a horizontal section (z = -500 m) through the flow domain in case 3DLSB.

Figure A6. Contour lines showing the distribution of the piezometric head (m) in a horizontal section (z = -200 m) through the flow domain in case 3DLSB.

Figure A7. Contour lines showing the distribution of the piezometric head (m) in a vertical section through the north-eastern corner of flow domain in case 3DLSR.

Figure A8. Contour lines showing the distribution of the piezometric head (m) in a vertical section through the north-eastern corner of flow domain in case 3DLSB.

Figure A9. Contour lines showing the distribution of the Darcy flux (ml/$m^2$.year) in a vertical section through the flow domain in case 3DLSB.

Figure A10. Contour lines showing the distribution of the Darcy flux (ml/$m^2$.year) in a horizontal section (z = -500 m) through the flow domain in case 3DLSB.

Figure A11. Contour lines showing the distribution of the Darcy flux (ml/$m^2$.year) in a vertical section through the north-eastern corner of in case 3DLSB.

Figure A12. Contour lines showing the distribution of the Darcy flux (ml/$m^2$.year) in a vertical section through the flow domain in case 3DLSR.

## FIGURE CAPTIONS (APPENDIX B)

### Graphical display of the sensitivity to perturbation of permeability

Figure B1. Contour lines in a vertical section through the flow domain in case 3DLSR, showing distribution of the piezometric head sensitivity to perturbation of the hydraulic conductivity in zone H1.

Figure B2. Vertical profiles of the piezometric head sensitivity to perturbation of the hydraulic conductivity in zone H1 in the case 3DLSR. (The profiles were defined as: X = 15682 m, Y = 96362 m, -1500 < Z < 0 m and X = 15500 m, Y = 95725 m, -1500 < Z < 0 m, respectively).

Figure B3 Contour lines in a horizontal cross-section (z = -500 m) through the flow domain in case 3DLSR, showing the distribution of the piezometric head sensitivity to perturbation of the hydraulic conductivity in zone H1.

Figure B4 Contour lines in a horizontal cross-section (z = -200 m) through the flow domain in case 3DLSR, showing the distribution of the piezometric head sensitivity to perturbation of the hydraulic conductivity in zone H1.

Figure B5. Contour lines in a vertical cross-section through the flow domain in case 3DLSB, showing distribution of the piezometric head sensitivity to perturbation of the hydraulic conductivity in zone H1.

## FIGURE CAPTIONS (APPENDIX C)

### Graphical display of the sensitivity to perturbation of prescribed pressure boundary

## LIST OF TABLES

## NOMENCLATURE

| | |
|---|---|
| $c^f$ | compressibility of the fluid |
| $c^r$ | compressibility of the rock |
| $g$ | acceleration of gravity |
| $h$ | piezometric head ($h = \frac{p}{\rho g} + (x_3 - x_3^{ref})$ $(x_3^{ref} = \text{reference datum})$ |
| $k$ | permeability |
| $n$ | normal inward vector |
| $N$ | basis function |
| $p$ | pressure |
| $\hat{p}$ | prescribed pressure |
| $P$ | performance function |
| $q_i$ | Darcy flux |
| $\hat{q}_i$ | prescribed Darcy flux along an exterior boundary |
| $Q(x_i, t)$ | source-sink term (known) |
| $S$ | water saturation |
| $t$ | time |
| $T$ | fluid temperature |
| $x_i$ | space coordinates |
| $x_i^c$ | point at the centroid of an element |
| $x_i^l$ | coordinates of a selected point for performance function |
| $w$ | dimensionless weights in the performance function |
| $\alpha$ | perturbation parameter |
| $\beta$ | thermal volume expansion of the fluid |
| $\rho$ | density of water |
| $\mu$ | dynamic viscosity |
| $\phi$ | porosity |
| $\Omega$ | flow region |
| $\Gamma_1, \Gamma_2$ | boundaries of the flow domain |
| $\tau$ | final time of an interval |
| $\psi$ | state sensitivity |
| $\psi^*$ | adjoint state sensitivity |

# 1 INTRODUCTION

Sensitivity analysis is a useful complementary tool in the modelling of a groundwater flow problem by making it possible to check both the qualitative as well as the quantitative effects of various flow modelling concepts. The possibility of studying the influence of various input parameters, whose geometrical or physical properties are uncertain in some sense, on various output parameters or certain user-defined performance measures according to the problem of interest, allows the technique presented here, although it is purely deterministic in its current form, to be regarded as a "tentative" uncertainty analysis.

In recent years the groundwater flow conditions at the Finnsjön site have been extensively modelled. However, some issues requiring further investigation, such as uncertainties concerning the influence, the characteristics, or even the existence of some major fracture zones, as well as uncertainties in the specification of the boundary conditions, have arisen in the Lindbom study (Lindbom et al. [1991]). The present study is aimed at analyzing some of the problems encountered in the previous flow modelling by means of sensitivity analysis techniques. Subsequently, all physical properties as well as the element grids used in the present study were those from the Lindbom study.

Essentially, the object of the present sensitivity analysis is to analyze, qualitatively as well as quantitatively, the impact on the flow solutions due to perturbations, or say uncertainties, of (i) the permeability of some major fracture zones of importance and (ii) the specification of the boundary conditions at some critical regions of the conceptual flow model of the Finnsjön site. The performance measures considered are the piezometric head and flux, both integrated and point-wise.

In the Lindbom flow modelling, the regional topography defined the top boundary conditions for the regional model. Accordingly, the local topography was applied on the top of the local mesh at the local scale model. Representation of the topography in the semi-regional and local scale are shown in Figures 1 and 2, respectively. It is apparent that the two contour maps differ with respect to their representation of the topography, in particular along fracture zone 4 and at the north-eastern corner.

The lateral boundary conditions for the local model were in the previous studies obtained from the regional scale model. In certain cases, especially where vertical fracture zones are located close to the boundary, such an approach may lead to inconsistencies between the upper and lateral boundary conditions of the local model, thus creating artificial gradients between nodal points on top and downwards along the lateral boundaries. Therefore, it is of interest to study how the ambiguities, associated with the transition procedure used in the previous calculations for setting the boundary conditions, will affect the flow solutions.

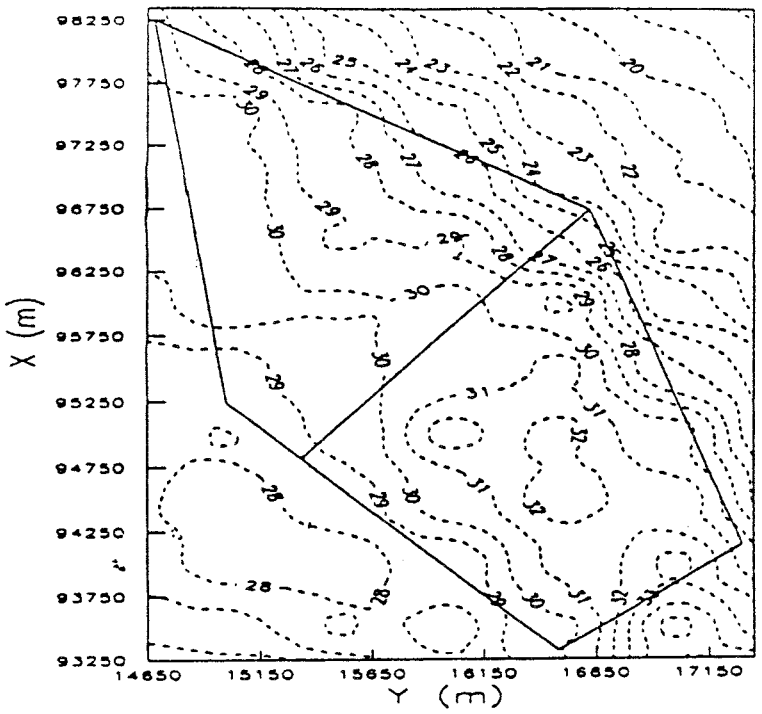


Figure 1. Topography of the local area as represented on the semi-regional scale. Note that the aspect ratio is not 1 to 1.

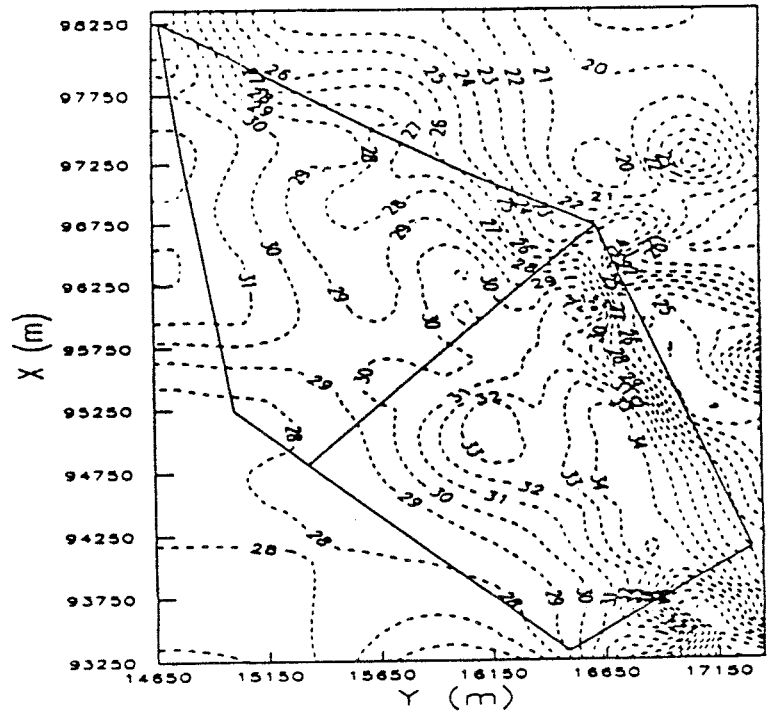


Figure 2. Topography of the local area as represented on the local scale. Note that the aspect ratio is not 1 to 1.

Sensitivity analysis may be characterized as a mathematical means for determining the relationships between the input and output variables of a mathematical model. The sensitivity of one variable to another in the mathematical model is described by the partial derivative of an output variable of interest versus an input variable. The present work is based on a previously developed computer model (Thunvik and Bao, [1989]) for determining the so-called state sensitivity coefficients and for the determination of the sensitivity of a selected performance measure to the permeability for a steady state groundwater flow problem. The theoretical foundation for the computer model used for the sensitivity analysis is thoroughly described by Bao [1990] and therefore only briefly stated in the present study. Two different sensitivity methods are considered in the present study, one which is called the direct method and the other the variational method.

In the direct method the partial derivatives of the model output variables versus the model input variables are obtained by direct differentiation of the algebraic equations resulting from the finite element integration of the flow equations. The variational method is based on adjoint sensitivity theory and is suitable for calculation of the sensitivity of various performance functions, selected according to the phenomena of interest, such as a specified piezometric head responses, point or integrated flux responses at regions of interest in the flow domain. As an example of the latter performance function the total flux across an interior or exterior boundary of the flow domain could be mentioned.

## 2 DESCRIPTION OF THE FLOW PROBLEM

According to the previous modelling of the groundwater flow conditions at the Finnsjön study site (Lindbom et al. [1991]), the extent of the local model of the site is shown in Figure 3, corresponding to an area of 6.6 km.

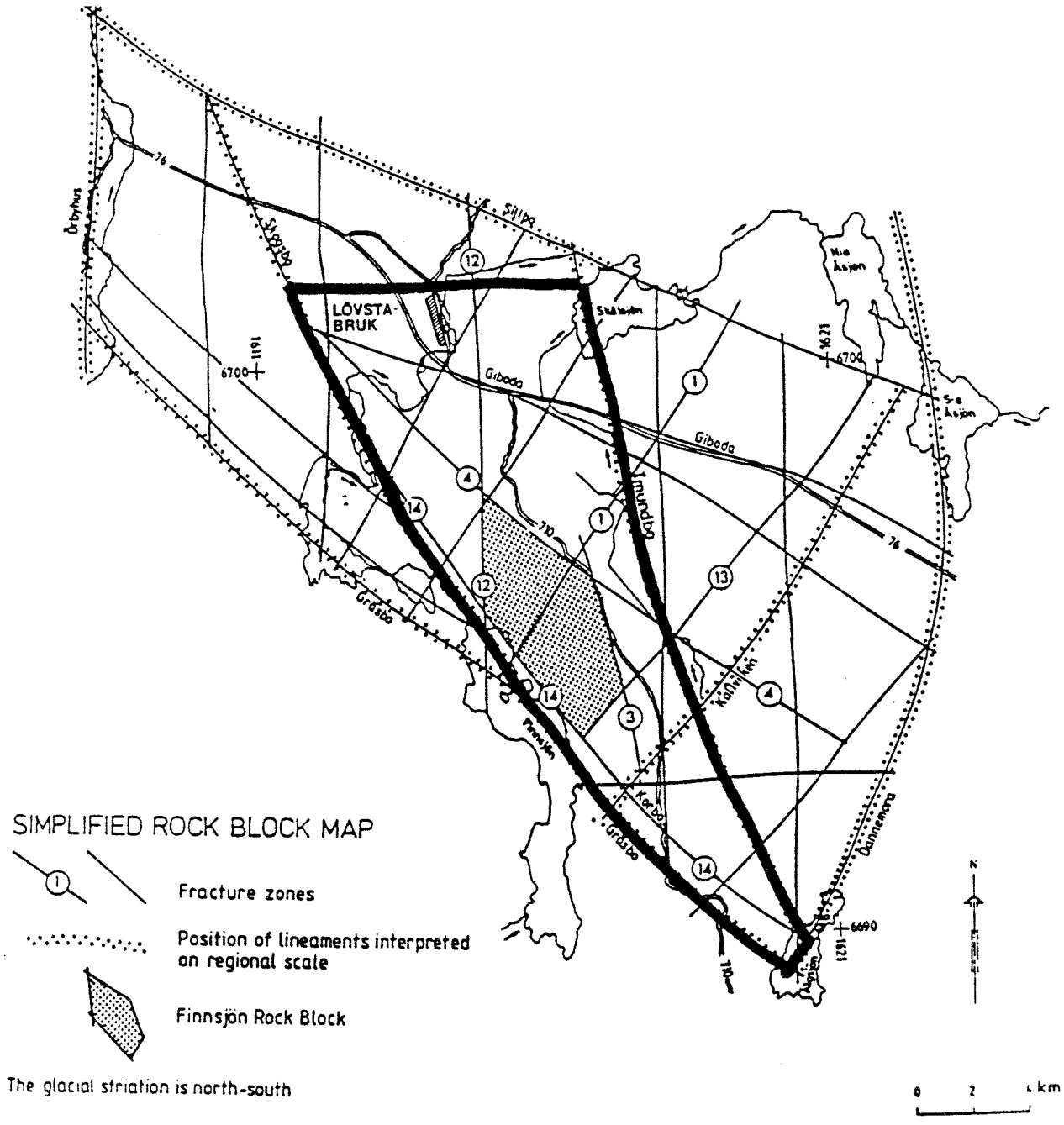


Figure 3. The extent of the local area (shaded) of the Finnsjön study site (from Lindbom et al. [1991]).

In the previous modelling (Lindbom et al. [1991]), the local flow domain was modelled to a depth of 1500 m assuming a no-flow bottom boundary. The fracture zones are comprised both of major regional lineaments and smaller "local scale" zones. The fracture zones on the local scale domain are illustrated in Figure 4. Fracture zones 3, 4, 12, 13 and 14 in the flow domain were coinciding with lateral boundaries. Fracture zone 1 is sloping downwards from the top.

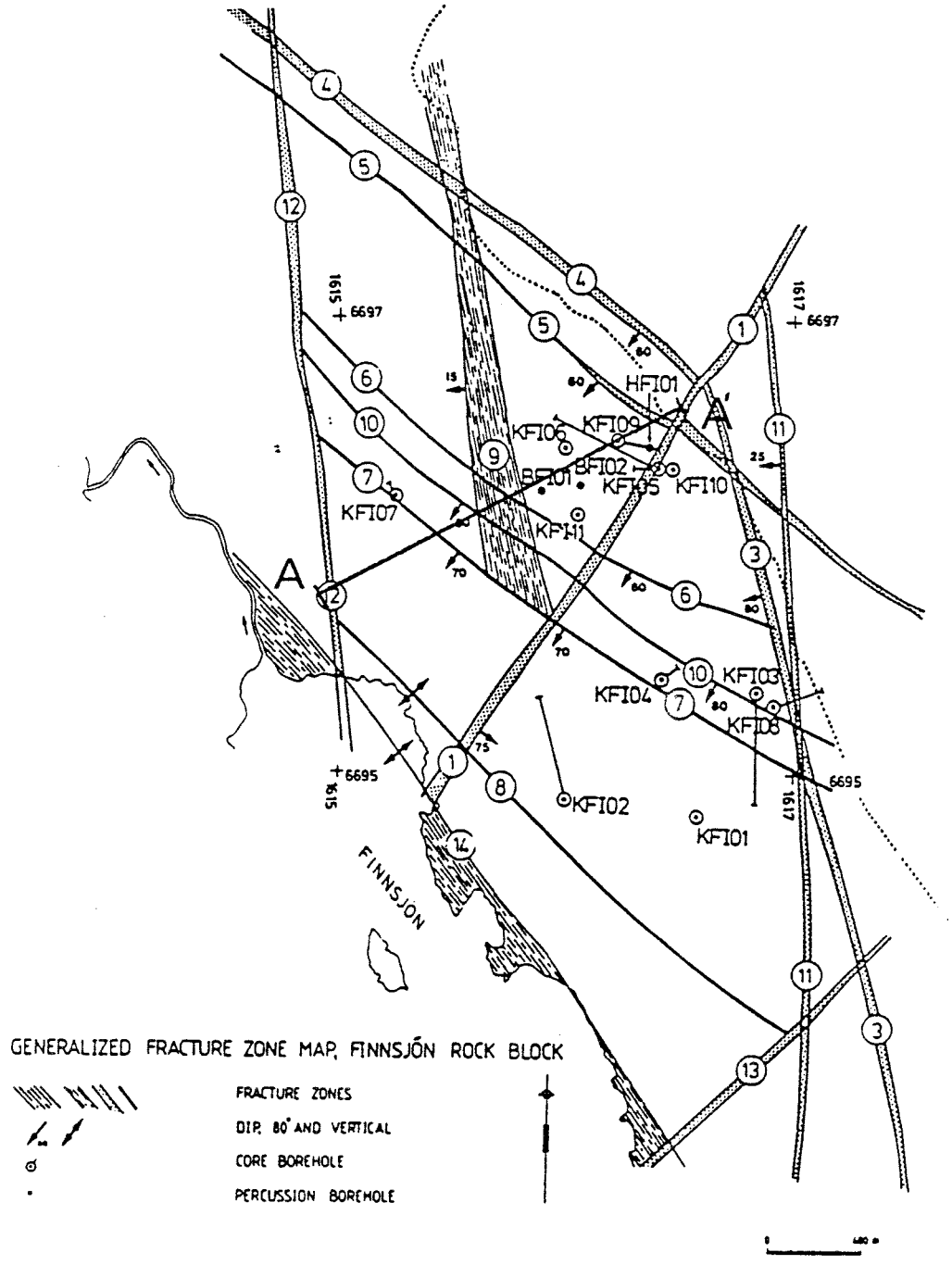


Figure 4. Areal coverage of the local area with the fracture zones indicated (From Lindbom [1991]).

The sub-horizontal zone 2 starts below the surface and is intersected by fracture zones 1, 3, 4 and 12 (see Figure 5 for a vertical projection of fracture zone 2). Because of its high hydraulic conductivity ($2 \cdot 10^{-5}$ - $4 \cdot 10^{-5}$ m/s) and location in the flow domain, it is believed that fracture zone 2 is of particular importance to the flow conditions in the flow domain.

It was stated in the previous study (Lindbom et al. 1991), that a large amount of groundwater discharges through fracture zone 2 to the eastern boundary. This implies that the physical properties, such as the permeability, of fracture zone 2 should have a significant influence over the flow pattern in the flow domain.

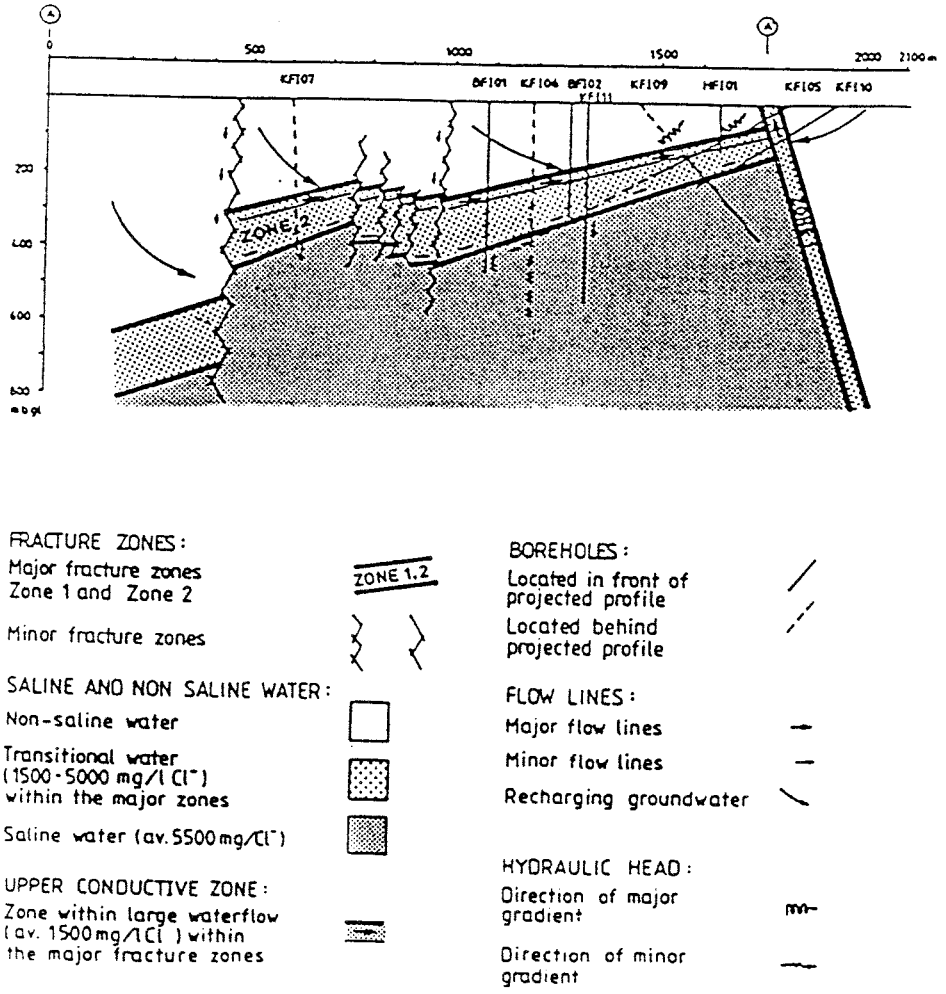


Figure 5. Vertical view of zone 2 (From Lindbom [1991]).

The local fracture zones 5, 6, 7, 8, 9, 10 and 11 (see Figure 4) were modelled implicitly according to a method presented in the Lindbom study (1991). Apart from the boundary fracture zones, only the sloping fracture zone 1, the sub-horizontal fracture zone 2 and the deep-horizontal fracture zone H1 were explicitly modelled. Figure 6 shows a perspective view of zone 2 and zone H1.

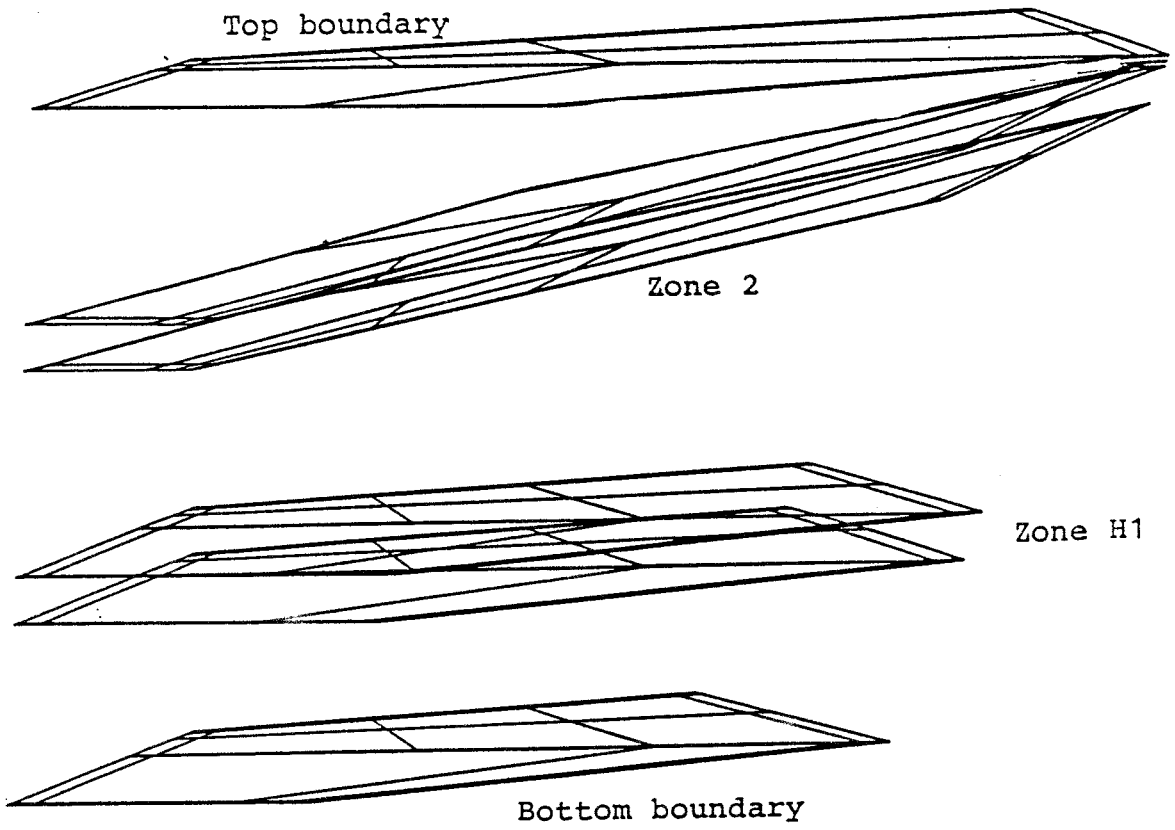


Figure 6. Perspective view of zone 2 and zone H1.

The input data in the present study were the same as in the Lindbom study (see Table 1).

Table 1: Input parameter values

| Parameter | Value | Unit |
|---|---|---|
| Porosity | 0.0001 | - |
| Density of water | 998 | $kgm^{-3}$ |
| Dynamic viscosity | $1.15 \cdot 10^{-3}$ | Pas |
| Compressibility | 0 | $Pa^{-1}$ |
| Acceleration of gravity | 9.81 | $ms^{-2}$ |

The hydraulic conductivity (K) was assumed to obey a power function of the form

$$K = a \cdot z^{(-b)} \qquad (2-1)$$

where z is the z-coordinate, and a and b are two coefficients chosen according to the assumed depth dependent variation of the hydraulic conductivity (see Lindbom et al. [1991], p.13).

# 3 MATHEMATICAL STATEMENT OF THE FLOW PROBLEM

## 3.1 Flow Model

The flow is assumed to be governed by Darcy's law

$$q_i = -\frac{k_{ij}}{\mu}(p_{,j} - \rho g_j) \tag{3-1}$$

Substitution of the above equation into the continuity equation yields the following flow equation (Thunvik and Braester, 1988)

$$\phi\rho^f[S(c^f + c^r) + S']p_{,t} - \phi S\rho^f\beta T^f_{,t} - \left[\rho^f\frac{k_{ij}}{\mu}(p_{,j} - \rho^f g_j)\right]_{,i} + Q = 0 \tag{3-2}$$

The boundary and initial conditions are

$$p(x_i, t) = \hat{p}(x_i, t) \qquad x_i \in \Gamma_1 \tag{3-3a}$$

$$-\frac{k_{ij}}{\mu}(p_{,j} - \rho g_j)n_i = \hat{q}(x_i, t) \qquad x_i \in \Gamma_2 \tag{3-3b}$$

$$p(x_i, 0) = p_0(x_i, 0) \qquad x_i \in \Omega \tag{3-3c}$$

where $p$ is pressure, $k_{ij}$ is the permeability tensor, $c^f$ is the compressibility of the fluid, $c^r$ is the compressibility of the rock, $\rho^f$ is density of water, $\phi$ is porosity, $S$ is the saturation of the fluid, $S'$ is $dS/dp$, $\beta$ is the coefficient for the thermal volume expansion of the fluid, $T$ is the fluid temperature, $\mu$ is the dynamic viscosity of the fluid, $g$ is the acceleration of gravity, $Q$ is a known source-sink term, $x$ (i= 1,2 or 3) are space variables, t is time, $\hat{p}$ is prescribed pressure on boundary $\Gamma_1$, $\hat{q}$ is prescribed flux normal to boundary $\Gamma_2$ (as designated by the components of the unit inward normal), $n_i$ is an inward normal vector, $\Gamma = \Gamma_1 + \Gamma_2$ represents the external boundary of the flow domain $\Omega$, and $p_0$ is the initial pressure over the flow domain $\Omega$.

## 3.2 Sensitivity Analysis Methods

### 3.2.1 Direct method of sensitivity analysis

Sensitivity analysis of the piezometric heads

The sensitivities of pressure to specified parameter changes, *the so-called state sensitivities*, are solved by the following equation (Bao [1990])

$$\phi\rho^f(c^f + c^r)\psi_{,t} - \left[\rho^f\frac{k_{ij}}{\mu}\psi_{,j}\right]_{,i} + D = 0 \tag{3-4}$$

where

$$D = \frac{\partial Q}{\partial\alpha_k} - \left[\frac{\partial\left(\rho^f\frac{k_{ij}}{\mu}\right)}{\partial\alpha_k}(p_{,j} - \rho^f g_j)\right]_{,i} + \frac{\partial\{\phi\rho^f(c^f + c^r)\}}{\partial\alpha_k}p_{,t} \tag{3-4a}$$

The initial and boundary conditions associated with equation (3-4) are:

$$\psi(\Omega,0)=p_0 \qquad \in \Omega, t=0 \qquad (3-5a)$$

$$\psi(\Gamma_1)=0 \qquad \in \Gamma_1 \qquad (3-5b)$$

$$-\frac{\partial\left(\frac{k_{ij}}{\mu}\right)}{\partial\alpha_k}(p_{,j}-\rho^f g_j)n_i-\left(\frac{k_{ij}}{\mu}\right)\psi_{,j}n_i=\frac{\partial\hat{q}}{\partial\alpha_k} \qquad \in \Gamma_2 \qquad (3-5c)$$

where $\psi=\partial p/\partial\alpha_k$ is the sensitivity of the pressure ($p$) to the parameter $\alpha_k$. In the present study $\alpha_k$ represents permeabilities ($k$) or prescribed pressure values ($p$) at various regions of significance. Solution of equation (3-4 gives a direct measure of the "state sensitivities" for each point in the domain.

Sensitivity analysis of the Darcy flux across a surface

The total normal flux across the surface ($\Gamma$), which may be an exterior or an interior boundary depending upon the problem of interest, is obtained by integrating the scalar product of Darcy's law and the outward normal vector to the boundary along the boundary and we obtain the following relationship:

$$Q_\Gamma=\int_\Gamma -\frac{k_{ij}}{\mu}(p_{,j}-\rho^f g_j)n_i d\Gamma \qquad (3-6)$$

For axisymmetric flow the previous expression may be written as follows

$$Q_\Gamma=2\pi\int_\Gamma -\frac{k_{ij}}{\mu}(p_{,j}-\rho^f g_j)r n_i dr \qquad (3-7)$$

The sensitivity of the integrated flux $Q_\Gamma$ may be obtained by the following relationship (in a Cartesian system)

$$\frac{\partial Q_\Gamma}{\partial\alpha_k}=-\int_\Gamma\left(\frac{1}{\mu}\frac{\partial k_{ij}}{\partial\alpha_k}(p_{,j}-\rho^f g_j)+\frac{k_{ij}}{\mu}\psi_{,j}\right)n_i d\Gamma \qquad (3-8)$$

and similarly for an axisymmetric flow domain, we obtain

$$\frac{\partial Q_\Gamma}{\partial\alpha_k}=-2\pi\int_\Gamma\left(\frac{1}{\mu}\frac{\partial k_{ij}}{\partial\alpha_k}(p_{,j}-\rho^f g_j)+\frac{k_{ij}}{\mu}\psi_{,j}\right)r n_i dr \qquad (3-8)$$

where $p$ is pressure and $\psi$ is the "state sensitivity" obtained from equation (3-4).

### 3.2.2 Adjoint method

General performance function

In the adjoint sensitivity analysis we consider a performance function of the following general form as (See Bao, [1990])

$$P = \int_R f(\{\alpha\}, p) dR \qquad (3-10)$$

where $f(\{\alpha\}, p)$ is a function of the system state selected in order to define the parameters and region of interest in the sensitivity analysis.

Adjoint equation

The "adjoint state sensitivity" $\psi^*$ is obtained by solving the following equation:

$$\phi \rho^f (c^f + c^c)\psi^*_{,t} - \left[\left(\rho^f \frac{k_{ij}}{\mu}\right)\psi^*_{,j}\right]_{,i} + \frac{\partial f(\{\alpha\}, p)}{\partial p} = 0 \qquad (3-11)$$

$$\psi^*(\Omega, \tau) = 0 \qquad \in \Omega, t = \tau \qquad (3-12a)$$

$$\psi^*(\Gamma_1, t) = 0 \qquad \in \Gamma_1 \qquad (3-12b)$$

$$\frac{k_{ji}}{\mu}\psi^*_{,i} n_j = 0 \qquad \in \Gamma_2 \qquad (3-12c)$$

Sensitivity of the pressure performance function

The "system state function" $f(\{\alpha\}, p)$ for the pressure performance function may be written as follows

$$f(\{\alpha\}, p) = w(x_i)p(x_i) \qquad (3-13)$$

and the pressure performance function becomes

$$P = \int_R w(x_i)p(x_i) dR \qquad (3-14)$$

The state function above is used typically when the piezometric head is used to define the performance measure with $w(x_i)$ being an arbitrary weighting function used to identify the region of importance.

Alternatively, if for example, the pressure is sought at only some selected nodal points $l$ in the domain, one may choose to define the "system state function" as follows

$$f(\{\alpha\},p)=\sum_{l}\{p(x_i^l)\delta(x_i-x_i^l)\} \qquad (3-15)$$

where $x_i$ is a location vector $x_i=(x_1,x_2,x_3)$. In this case the performance measure $P$ becomes $P=\{w\}^T\{p\}$, where $w=\delta(x_i-x_i^l)$ are dimensionless weights designated to the nodal points, implying that $w_i=1$ at the nodal points 1 and $w_i=0$ at all other nodal points.

The marginal sensitivities of the previous performance measures are calculated by the following equation:

$$\frac{\partial P}{\partial\alpha_k}=-\int_R \psi_{,i}^{*}\frac{\partial\left(\rho^f\frac{k_{ij}}{\mu}\right)}{\partial\alpha_k}(p_{,j}-\rho^f g_j)dR \qquad (3-16)$$

Sensitivity of the flux performance function

In defining the flux performance function the following "system state function" was chosen

$$f(\{\alpha\},p)=\sqrt{\sum_{m=1}^{3}q_m^2}\,\delta(x_i-x_i^c) \qquad (3-17)$$

which defines the magnitude of the Darcy velocity at a point $x_i^c$ corresponding to the centroid of the selected element for which the sensitivity is sought.

The flux performance function then becomes

$$P=\int_R\sqrt{\sum_{m=1}^{3}q_m^2}\,\delta(x_i-x_i^c)dR \qquad (3-18)$$

The marginal sensitivity of this performance function is obtained by the following relationship:

$$\frac{\partial P}{\partial\alpha_k}=\int_{R_e}\left[-\frac{1}{\mu\sqrt{\sum_{m=1}^{3}q_m^2}}q_i\frac{\partial k_{ij}}{\partial\alpha_k}p_{,j}-\psi_{,i}^{*}\frac{\partial\left(\rho\frac{k_{ij}}{\mu}\right)}{\partial\alpha_k}(p_{,i}-\rho g_j)\right]dR_e \qquad \forall x_i=x_i^c \qquad (3-19)$$

where $\psi^*$ is called the adjoint state sensitivity obtained from equation (3-13). The first term of equation (3-19) is non-zero only when $\alpha_k$ represents the value of $k_{ij}$ within the selected element $e$. Since $f=\sqrt{\sum_{m=1}^{3}q_m^2}\cdot\delta(x_i-x_i^c)$ for this performance function the third term of the adjoint equation (3-11) can be calculated by the following equation:

$$\frac{\partial f}{\partial p_e}=-\frac{1}{\mu\sqrt{\sum_{m=1}^{3}q_m^2}}q_i\frac{\partial(k_{ij}p_{,j})}{\partial p_e} \qquad \forall \quad e \text{ on the element} \qquad (3-20)$$

$$\frac{\partial f}{\partial p_e} = 0 \qquad \forall \quad e \; not \; on \; the \; element \qquad (3-21)$$

where pressure $p$ is obtained from equation (3-2).

## 3.3 Sensitivity Analysis of Perturbations of Permeability in Major Fracture Zones

### 3.3.1 Sensitivity of pressure to perturbation of permeability

The sensitivities of the pressure to permeability changes, *the state sensitivity*, is solved by following equations.

$$\phi\rho^f(c^f + c^r)\psi_{,t} - \left[\left(\rho\frac{k_{ij}}{\mu}\right)\psi_{,j}\right]_{,i} + D = 0 \qquad (3-22)$$

where $\psi = \partial p/\partial k_l$ and $k_l$ is the permeability of the perturbed fracture zone and

$$D = -\left[\frac{\partial\left(\rho^f\frac{k_{ij}}{\mu}\right)}{\partial k_l}(p_{,j} - \rho g_j)\right]_{,i} \qquad (3-22a)$$

The initial and the boundary conditions associated with Eq (3.22) are:

$$\psi(\Omega, 0) = p_0 \qquad \in \Omega, t = 0 \qquad (3-23a)$$

$$\psi(\Gamma_1) = 0 \qquad \in \Gamma_1 \qquad (3-23b)$$

$$-\frac{\partial\left(\frac{k_{ij}}{\mu}\right)}{\partial k_l}(p_{,j} - \rho g_j)n_i - \left(\frac{k_{ij}}{\mu}\right)\psi_{,j}n_i = 0 \qquad \in \Gamma_2 \qquad (3-23c)$$

Solution to equation (3-22) gives a direct measure of state sensitivities for each point in the domain.

### 3.3.2 Sensitivity of the total Darcy flux across a specified surface to perturbation in permeability

Sensitivity of the total flux across a specified surface to perturbation of permeability is calculated by following equations:

$$\frac{\partial Q_\Gamma}{\partial k_l} = -\int_\Gamma\left(\frac{1}{\mu}\frac{\partial k_{ij}}{\partial k_l}(p_{,j} - \rho^f g_j) + \frac{k_{ij}}{\mu}\psi_{,j}\right)n_i d\Gamma \qquad (3-24)$$

where $k_l$ is the permeability of the perturbed fracture zone.

## 3.4 Sensitivity Analysis of Perturbations of the Prescribed Pressure Boundary

### 3.4.1 Sensitivity of pressure to perturbations of the prescribed pressure boundary

The sensitivities of pressure with respect to prescribed pressure values ($\hat{p}$) on $\Gamma_1$ are solved by the following equation

$$\phi\rho(c^f + c^r)\psi_{,t} - \left[\rho\frac{k_{ij}}{\mu}(\psi_{,j})\right]_{,i} + D = 0 \qquad (3-25)$$

where

$$D = \frac{\partial Q}{\partial \hat{p}} - \left[\frac{\partial\left(\rho\frac{k_{ij}}{\mu}\right)}{\partial \hat{p}}(p_{,j} - \rho^f g_j)\right]_{,i} + \frac{\partial(\phi\rho^f(c^f + c^r))}{\partial \hat{p}}p_{,t} \qquad (3-25a)$$

and the initial and boundary conditions are:

$$\psi(\Omega, 0) = 0 \qquad \in \Omega, t = 0 \qquad (3-26a)$$

$$\psi(\Gamma_1) = 1 \qquad \in \Gamma_1 \qquad (3-26b)$$

$$-\frac{k_{ij}}{\mu}\psi_{,j}n_i = 0 \qquad \in \Gamma_2 \qquad (3-26c)$$

and $\psi = \partial p/\partial \hat{p}$ is the sensitivity of the pressure ($p$) with respect to $\hat{p}$, which are the prescribed pressure values on boundaries. Solution to equation (3-25) under the boundary conditions given in (3-26) yields a direct measure of the state sensitivity for each point in the domain.

### 3.4.2 Sensitivity of the Darcy flux to perturbation of the prescribed pressure boundary

The formulation of sensitivity of flux with respect to prescribed pressure in the flow domain can be obtained by differentiating Darcy's law :

$$\frac{\partial q_i}{\partial \hat{p}} = -\frac{\partial\left(\frac{k_{ij}}{\mu}\right)}{\partial \hat{p}}(p_{,j} - \rho^f g_j) - \frac{k_{ij}}{\mu}\psi_{,j} \qquad (3-27)$$

where, as defined previously, $\psi = \partial p/\partial \hat{p}$ which is obtained from equation (3-25) and (p) is pressure obtained from the primary equation (3-2). Solution to equation (3-27) gives a distribution of the sensitivity of flux for each point in the flow domain.

### 3.4.3 Sensitivity of the total Darcy flux across a surface to perturbation of the prescribed pressure boundary

The total flux across the surface ($\Gamma$), which may be an exterior or an interior boundary depending upon the problem of interest, is obtained by integrating the scalar product of Darcy's law and the outward normal vector to the boundary along the boundary:

$$Q_\Gamma = \int_\Gamma -\frac{k_{ij}}{\mu}(p_{,j} - \rho^f g_j) n_i d\Gamma \qquad (3-28)$$

The sensitivity of the integrated flux ($Q_\Gamma$) can be obtained by the following relationship.

$$\frac{\partial Q_\Gamma}{\partial \hat{p}} = \int_\Gamma \left[ -\frac{\partial\left(\frac{k_{ij}}{\mu}\right)}{\partial \hat{p}}(p_{,j} - \rho^f g_j) - \frac{k_{ij}}{\mu}\psi_{,j} \right] n_i d\Gamma \qquad (3-29)$$

where p is pressure and $\psi$ is the " state sensitivity" obtained from equation (3-25).

### 3.5 Normalized Sensitivity

Since the units and numerical scale of the output and input parameters are often different, it is useful to normalize the sensitivity coefficients by dividing the differentials $dP$ and $d\alpha_k$ by their nominal values so that the sensitivity values will be on a more comparable basis. The (dimensionless) normalized sensitivity is here defined as:

$$S_k = \frac{dP}{d\alpha_k}\frac{\alpha_k}{P} \qquad (3-30)$$

# 4 NUMERICAL SOLUTIONS

## 4.1 General Description

Two of the cases that were analysed in the Lindbom study [1991], viz. the cases 3DSLR and 3DSLB, were analysed here using the sensitivity method developed previously (Bao [1990]). Case 3DSLR is referred to as a reference case and 3DSLB as a base case in the Lindbom study. The main characteristics of the two cases are summarized in Table 2.

Table 2: Main characteristics of the two cases studied

| Case | Major fracture zones | Local fracture zones | Lateral boundaries | Top boundaries |
|---|---|---|---|---|
| 3DLSR | Included | Non-Included | Transferred | Regional topography |
| 3DLSB | Included | Included | Transferred | Regional topography |

As can be seen in Table 2 the difference between the two cases is that in case 3DSLR only the major fracture zones were included, while in case 3DSLB also minor fracture zones were implicitly modelled by using a special averaging technique (See Appendix D in the Lindbom study [1991]). Therefore it was considered to be of interest to check whether a sensitivity analysis could indicate any difference in the behaviour of the two model approaches.

All input data in the present study were the same as in the Lindbom study. Subsequently the element grid used was also the same as that used for the local study areas at Finnsjön described in the Lindbom study. The flow domain was discretized into 24 layers and the resulting element grid consisted of 39000 nodes and about 35000 eight noded brick-elements. The RAK-coordinate system with offset in y = 1600000 m and x = 6600000 m was used. The horizontal discretization of the flow domain is illustrated in Figure 7.

The results are for convenience presented in piezometric head instead of pressure. The piezometric head (h) is defined as

$$h = \frac{p}{\rho g} + (x_3 - x_3^{ref}) \qquad (4-1)$$

where $p$ is pressure, $\rho$ is the fluid density, $g$ is the acceleration of gravity, $x_3$ is the elevation and $x_3^{ref}$ is the reference datum.

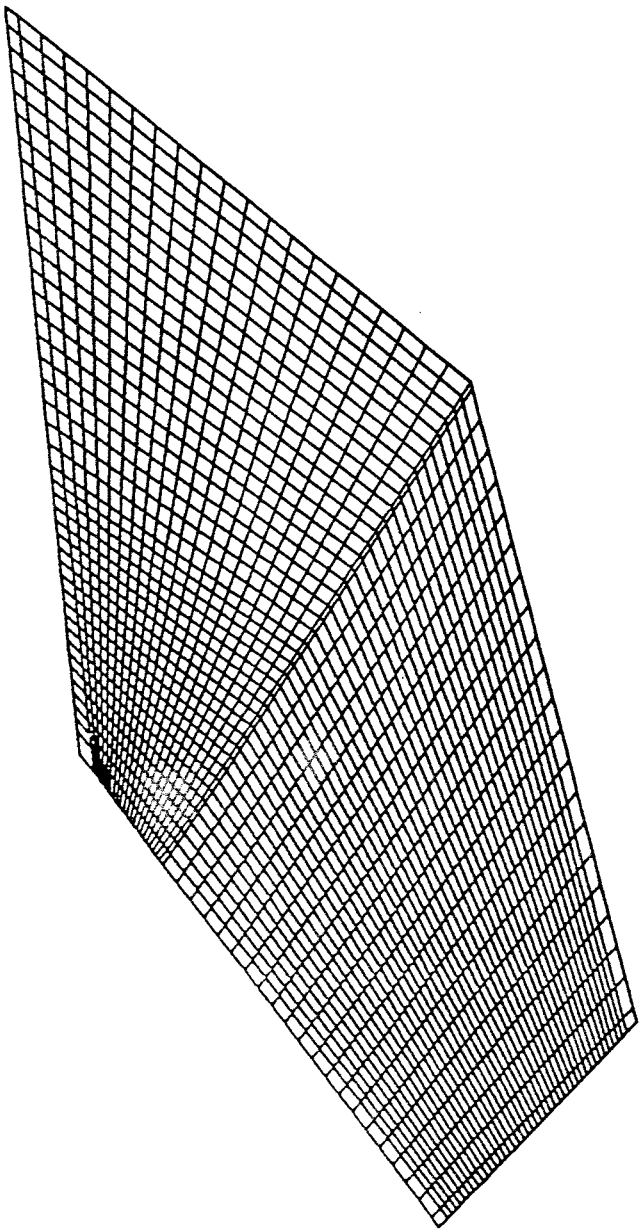

Figure 7. The discretization of the flow domain for the local model (from Lindbom et al. [1991]).

The flow domain is a three-dimensional one and the results are presented in the form of contour plots at various relevant vertical and horizontal sections through the flow domain. The selected sections are schematically depicted in Figure 8. The following sections were considered:

(a) Vertical profiles at selected points in the horizontal plane. (The profiles were defined as: $P_1$ x=15682 m, y=96362 m, $-1500 \leq z \leq 0$ m and $P_2$ x=15500 m, y=95725, $-1500 \leq z \leq 0$ m in Figure 8a).

(b) A horizontal section at z = -500 (corresponding to a typical repository level, marked by G-H-I-J in Figure 8b).

(c) A vertical section through the centre of the imaginary repository (marked by the line L1 (x = 15203, y = 95429) - L2 (x = 16125, y = 96893) in Figure 8c).

(d) A vertical section crossing the fracture zones 2, 4 and 1 at the north-eastern corner (marked by the line L3 (x = 15600, y = 95704)- L4 (x = 15800, y = 97400) in Figure 8d), through the three-dimensional flow domain.

The motivation for choosing the last-mentioned vertical section was that the natural groundwater discharge was estimated through part of this particular area of zone 2 in previous studies (Andersson et al. [1989]). Although the section does not coincide exactly with that of the previous studies it remains useful for comparative analysis.

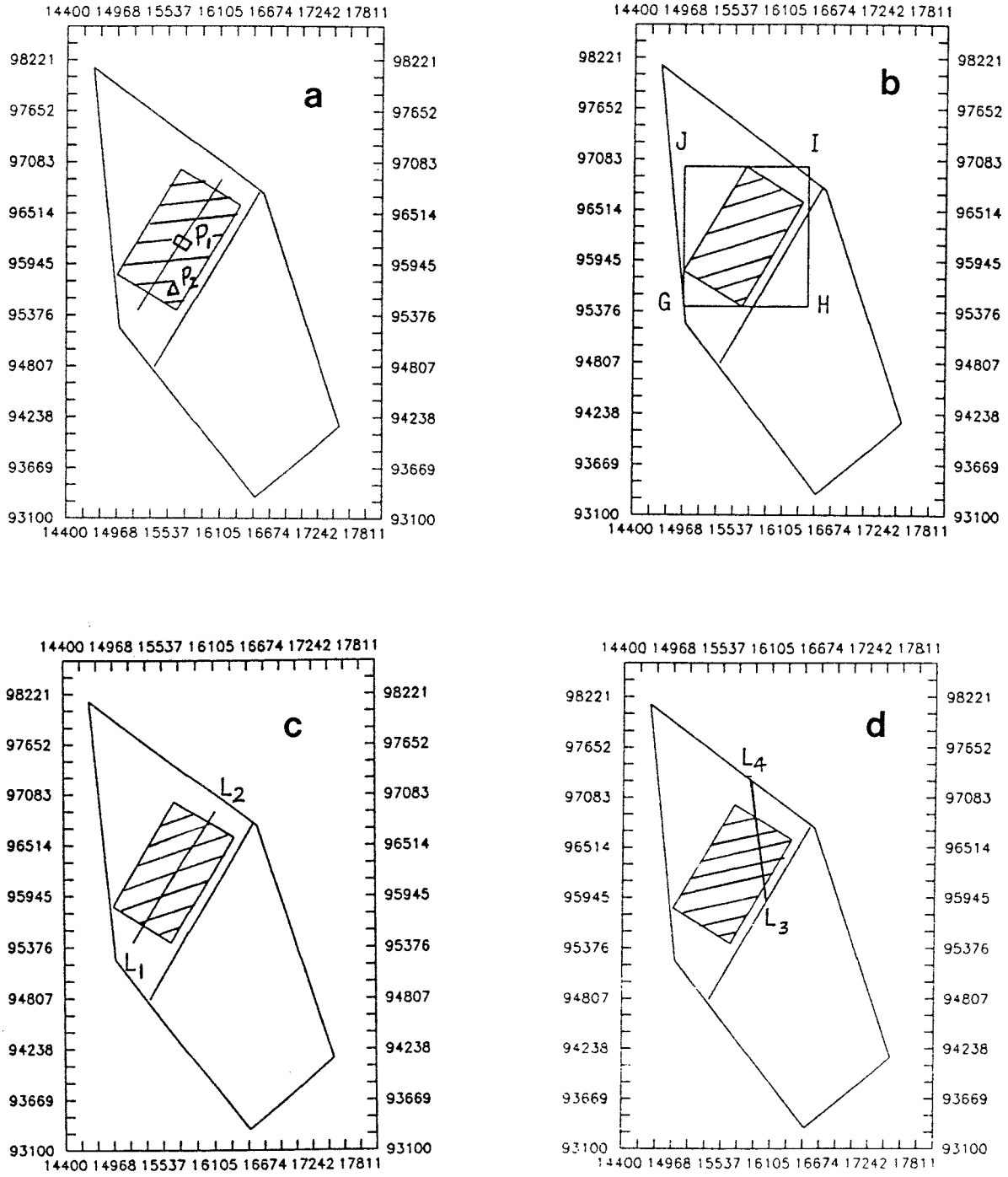


Figure 8: Schematic view of the flow domain showing the sections selected for the sensitivity analysis: (a) vertical profiles for the point $P_1$ and $P_2$ (b) horizontal section at z = -500 m (c) vertical section through the imaginary repository (shaded area) and (d) vertical section through discharge region.

### 4.2 Primary Solutions

The numerical solutions were achieved using the Galerkin finite element method. The piezometric head in both the 3DLSR and 3DLSB cases is depicted in vertical sections through the flow domain in Appendix Figures A1 and A2, also in horizontal sections through the flow domain in Figures A3 (z = -500 m), A4 (z = -200 m), A5 (z = -500 m) and A6 (z = -200 m), and vertical north-eastern sections through the flow domain in Figures A7 and A8, respectively.

The solutions for the piezometric head in the two cases are rather alike, qualitatively as well as quantitatively. It may be pointed out that the solutions presented here agree with the solutions presented in the Lindbom [1991] study.

The Darcy flux distributions in both the 3DLSR and 3DLSB cases are depicted in Figures A7, A8 and A9 for the same three sections mentioned above. The contour lines at the vertical sections show that high flux values are distributed around fracture zone 2.

Contour lines of the Darcy flux values are shown at vertical cross-section for the case 3DLSR (Figure A12). As one can see in Figure A12, the high flux contour lines are located in fracture zone 2 as well as along fracture zone 4 (the northern inclined lateral boundary). A comparison between the contour lines of Figure A9 and Figure A12 show the effect of the local fracture zones on the flow conditions.

### 4.3 Sensitivity to Perturbation of Permeability ($k$)

In this section, the sensitivity to permeability changes in either of two major fracture zones in the flow domain was calculated. The perturbed fracture zones were the sub-horizontal fracture zone 2 and the deep horizontal fracture zone H1 (see Figure 6).

As mentioned in the introduction the sensitivity of one variable to another is described by the partial derivatives of an output variable of interest versus the input variable of which the sensitivity (S) is sought. A positive value of S implies that the value of the output variable increases as the input variable increases. Conversely, a negative value of S implies that the value of the output variable decreases as the value of the input variable increases.

#### 4.3.1 Sensitivity of the piezometric head to perturbation of permeability

Piezometric head sensitivity to perturbation of permeability of fracture zone H1

In case 3DLSR, sensitivity of the piezometric head to perturbation of the hydraulic conductivity in zone H1 is depicted in a vertical section through the flow domain in Figure B1, for vertical profiles in Figure B2 (defined as: X = 15862 m, Y = 96362 m, $-1500 \leq Z \leq 0$ m and X = 15500 m, Y = 95725 m, $-1500 \leq Z \leq 0$ m, respectively), and in horizontal sections, at Z = -500 m and Z = -200 m, through the flow domain in Figures B3 and B4, respectively.

In case 3DLSB, sensitivity of the piezometric head to perturbation of the hydraulic conductivity in zone H1 is depicted for a vertical section through the flow domain in Figure B5, for vertical profiles in Figure B6. (defined as: X = 15682 m, Y = 96362 m, $-1500 \leq Z \leq 0$ m and X = 15500 m, Y = 95725 m, $-1500 \leq Z \leq 0$ m, respectively), and in horizontal sections, at Z = -500 m and Z = -200 m, through the flow domain in Figures B7 and B8, respectively.

The contour lines showing the distribution of the sensitivity of the piezometric head versus the hydraulic conductivity in the horizontal fracture zone H1 differ significantly from each other in the two cases (Figures B1 and B5). As one may see in case 3DLSR (Figure B1) the sensitivity coefficients are drastically changing from positive values below the fracture zone to negative values above the zone.

Case 3DLSB (Figure B7) exhibits a much more complex pattern of sensitivity coefficients than that of case 3DSLR, reflecting the differences in the fracture modelling concepts of the rock mass in the two cases. As can be observed in case 3DLSB (Figure B7), the sensitivity coefficients vary in a cyclic-like manner in the direction along the horizontal fracture zone (H1), while in case 3DLSR the sensitivity contour lines are oriented horizontally along the fracture zone.

Both solutions to the piezometric head sensitivity indicate that the region located between the upper boundary of the flow domain down to a depth of about 400 m is practically unaffected by changes of the hydraulic conductivity of zone H1. This fact is also confirmed by the vertical sensitivity profiles shown in Figures B2 and B6. It should be pointed out, however, that the vanishing sensitivities on top and bottom boundaries are due to the fact that the piezometric head values are prescribed along these boundaries.

The piezometric head contour lines for a horizontal section at z = -500 m show that the piezometric head values in case 3DLSR (Figure B3) are slightly higher than that in case 3DSLB (Figure B7). However, the large scale flow patterns are rather similar to each other in the two cases.

The corresponding graphical representations of the piezometric head sensitivity values show that the two different model approaches will lead to significantly different flow behaviour predictions. In case 3DLSB the high sensitivity values are limited to a certain region around the lower left corner, while in case 3DLSR the sensitivity values are distributed practically all over the depicted flow domain. Moreover, the sensitivity values in case 3DLSR are considerably higher (about 10 times).

The piezometric head values at the horizontal sections at z = -200 m are largely the same for case 3DLSR (Figure B4) and 3DLSB (Figure B8). The piezometric head sensitivity to changes of the hydraulic conductivity of the horizontal fracture zone are also rather similar. As can be observed in Figures B4 and B8, the sensitivity contour lines are limited to about a quarter (South-West region) of the depicted part of the flow domain.

Piezometric head sensitivity to perturbation of permeability of fracture zone 2

The contour line patterns, showing the distribution of the sensitivity of the piezometric head to perturbation of the hydraulic conductivity in sub-horizontal zone 2, for a vertical cross section through the hypothetical repository, appear to be rather alike in the two cases (Figures B9 and B10). The highest sensitivity value is on the western edge of fracture zone 2.

In the horizontal cross-section the distributions of sensitivity values differ significantly from each other in the two cases (Figures B11 (z = -500m 3DLSR) and B12 (z = -500m 3DLSB) ). In case 3DLSR, the contour lines correspond to the pattern of topography and in case 3DLSB the contour lines coincide with the strike of local fracture zones 5, 6, 7, 8, and 10. It may be observed that the sensitivity values in case 3DLSB are higher than that in case 3DLSR. This is due to the fact that the local fracture zones interact with zone 2. It may be noticed that there was a contrary result in the case with perturbation of the deep horizontal fracture zone H1.

### 4.3.2 Darcy flux sensitivity to perturbation of permeability

Darcy flux sensitivity to perturbation of permeability of fracture zone H1

The sensitivity of the total normal flux across an imaginary repository plane with an area of $1.5085 \cdot 10^6 m^2$ was analyzed for the two cases.

Table 3: Sensitivity of the total flux across the hypothetical repository region located at a depth of 500 m

| Case | Total flux | Sensitivity | Sensitivity (normalized) |
|---|---|---|---|
| 3DLSR | $-3.813 \cdot 10^{-4}$ | $6.28 \cdot 10^{1}$ | 0.128% |
| 3DLSB | $-3.939 \cdot 10^{-4}$ | $1.54 \cdot 10^{1}$ | 0.031% |

A horizontal view of the repository region chosen for the calculation is presented in Figure 3. As can be observed in Table 3 the results show that the sensitivity value of the integrated normal flux across the repository region in case 3DLSR is about four times higher than that of case 3DLSB.

Darcy flux sensitivity to perturbation of permeability of fracture zone 2

The results of the Darcy flux sensitivity are presented in Table 4.

Table 4: Sensitivity of the total flux across the hypothetical repository region located at a depth of 500 m to perturbing fracture zone 2

| Case | Total flux | Sensitivity | Sensitivity (normalized) |
|---|---|---|---|
| 3DLSR | $-3.813 \cdot 10^{-4}$ | $2.167 \cdot 10^{-4}$ | 1.71% |
| 3DLSB | $-3.939 \cdot 10^{-4}$ | $2.366 \cdot 10^{-4}$ | 1.80% |

The results in Table 4 show that the sensitivity values of the integrated normal flux across the repository region to perturbations of fracture zone 2 are significantly higher than that of perturbations of fracture zone H1. The order of magnitude of the sensitivity values connected to perturbation of fracture zone 2 is about the same in the two cases 3DLSR and case 3DLSB. This means that the local fracture zones have little influence on the total flux sensitivity to perturbations of fracture zone 2.

Conversely, the local fracture zones have a certain influence on the flux sensitivity to perturbation of the deep horizontal fracture zone H1. However, the sensitivity to perturbation of zone H1 with regard to the presence of local fracture zones is negligible in comparison with the sensitivity to perturbation of zone 2 (the latter irrespective of the presence of local fracture zones). For example the difference between the cases 3DLSR and 3DLSB when perturbing zone 2 is about 0.09 per cent, a value which appears also in table 3, but is overwhelmed in comparison by the normalized sensitivity in Table 4.

Sensitivities of the Darcy flux distributions to perturbation of fracture zone 2 are depicted on the vertical cross-section for the cases 3DLSR (Figure B13) and 3DLSB (Figure A14), respectively. The contour pattern of the flux sensitivity is similar to that of the flux contour pattern. This implies that the high sensitivity values of the flux are located in regions with high flux.

### 4.4 Sensitivity to Perturbation of the Prescribed Pressure ($\hat{p}$) Boundary

The sensitivity of (i) the piezometric head, (ii) the flux at selected points, and (iii) the Darcy flux across specified surfaces were calculated with respect to perturbations of the prescribed pressure at specified parts of the exterior boundary. The areas subject to perturbation were: (i) Fracture zone 4, (ii) The top boundary at the north-eastern corner (perturbation area = $1.209 \cdot 10^6$ $m^2$), and (iii) The top boundary at the north-eastern corner including parts of the vertical boundaries (perturbation area = $1.991 \cdot 10^6$ $m^2$). The perturbation regions considered are schematically illustrated in the form of perspective plots in Figure 9.

The selection of the perturbation areas were based on the following considerations: (i) in the Lindbom study the prescribed pressure boundary conditions set to fracture zone 4 proved to have a significant effect on the flow patterns and especially on the water balance, (ii) on the top area at the north-eastern corner, as already mentioned above, a rather large deviation exists between the regional topography map and local scale topography map, and (iii) fracture zones 1, 3 and 4 intersect each other at the north-eastern area.

Moreover, zone 2 is located only about 10 metres below this intersection. Therefore the perturbation area is extended from the top downwards to a depth of 300 metres along the vertical boundaries to account for effects of the artificial gradients associated with the transferred vertical boundary conditions. In addition, this point was the major discharge area in the domain and considering the intersection between the water bearing structures mentioned in (iii) this area could be a source for numerical difficulties.

The results are graphically displayed in the form of contour lines showing the distribution of the parameters of interest over the flow domain. The results of the following parameters are presented: (i) the piezometric head and its sensitivity to the perturbations considered (ii) the point flux and its sensitivity to the perturbations considered, and (iii) the integrated flux and its sensitivity to the perturbations considered.

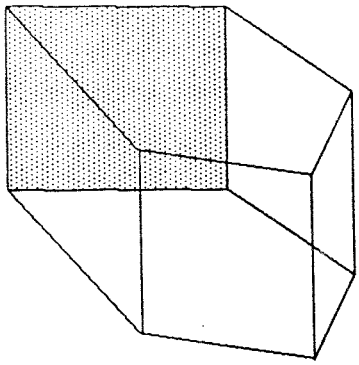

(a) Fracture zone 4

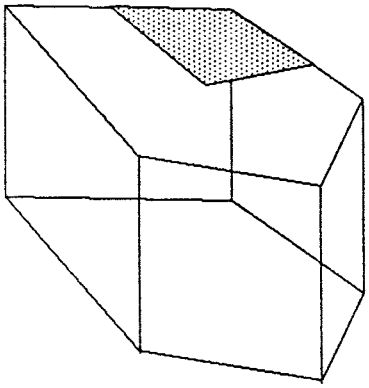

(b) The top boundary at the north-eastern corner

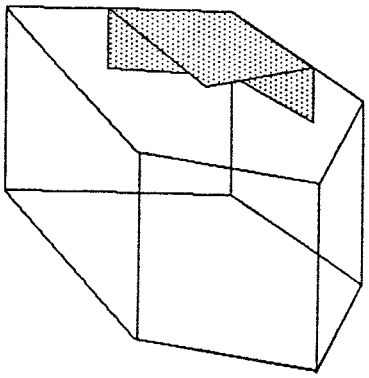

(c) The top boundary at the north-eastern corner including parts of the vertical (lateral) boundaries

Figure 9: Perspective plots showing the perturbation areas under consideration (shaded): (a) Fracture zone 4, (b) The top boundary at the north-eastern corner and (c) The top boundary at the north-eastern corner including parts of the vertical (lateral) boundaries.

### 4.4.1 Sensitivity of the piezometric head

Vertical section

The vertical section showing the distributions of the piezometric head sensitivity to perturbation of fracture zone 4, the north-eastern top area, and the north-eastern top with connected vertical parts are depicted in Figures C1, C2 and C3, respectively, for case 3DLSB and in Figures C4, C5 and C6, respectively, for case 3DLSR.

The sensitivity of the piezometric head to perturbation of fracture zone 4 is illustrated in Figure C1. The results show that the normalized piezometric head sensitivity approaches 1 towards the perturbed boundary fracture zone 4 and decreases gradually to 0 from the perturbed boundary to the (prescribed head) top and bottom boundaries.

The results of sensitivity to perturbation of the north-eastern top area and to perturbation of the top with parts of the vertical boundary included show quite similar patterns. The sensitivity value towards the perturbed boundaries approaches 1 and vanishes at the bottom and at the unperturbed part of the top boundary. But it should be noticed that the values of the sensitivity to perturbation of the top with the vertical parts are about 2.5 times higher than that of perturbing the top boundary only. As one may see from the figures the values of the piezometric head sensitivity in case 3DLSR are slightly higher than that of case 3DLSB, which is due to an interaction with the local fracture zones in the latter case. However, the overall patterns are rather similar to each other in the two cases.

Horizontal cross-section (z = -500 m)

The results of the piezometric head sensitivity to perturbation of fracture zone 4, the north-eastern top area and the north-eastern top with connected vertical parts are presented for a horizontal cross-section in Figures C7, C8 and C9, respectively, for case 3DLSB, and in Figures C10, C11 and C12, respectively, for case 3DLSR.

The contour lines of the piezometric head sensitivity to perturbation of fracture zone 4 are oriented parallel to the perturbed boundary (Figure C10). The value of the normalized sensitivity decreases from 1 to 0 from north-east to south-west. The contour lines of the piezometric head sensitivity to perturbation of the north-eastern top area show that the values of the sensitivity are relatively higher in the south-eastern region.

Along the north-east as well as the south-west boundaries the normalized sensitivity value approaches 0 (Figure C8). The results of the piezometric head sensitivity to perturbation of the north-eastern top area with the connected vertical parts has a pattern similar to that of perturbing the top area, but the values are about 2 times higher (Figure C9).

North-eastern vertical section

The north-eastern vertical section, showing the distribution of the piezometric head sensitivity to perturbation of fracture zone 4, the north-eastern top area and the north-eastern top with connected vertical parts, are depicted in Figures C13, C14 and C15, respectively, for case 3DLSB and in Figures C16, C17 and C18, respectively, for case 3DLSR. The results of the piezometric head sensitivity to perturbation of fracture zone 4 show that the value of the sensitivity is about 1 along the perturbed fracture zone 4, and nearly 0 along the top boundary (Figure C16).

The contour lines of the piezometric head sensitivity to perturbation of the top area show that the normalized sensitivity decreases from 1 to 0 from the top downward to fracture zone 4 and the bottom boundary (Figure C17). Perturbing the top area, with part of the vertical boundary included, shows a sensitivity pattern similar to that of perturbing the top area only. But the sensitive region extends closer to the bottom (Figure C18).

### 4.4.2 Sensitivity of the Darcy flux across specified horizontal surfaces

The sensitivity of the total normal flux across an imaginary repository plane (shown by the shaded area in Figure 3) with an area of $1.5085 \cdot 10^6\,m^2$ was analyzed. The results are displayed in Table 5. As can be observed in Table 5 the results show that the sensitivity value of the integrated normal flux across the repository region to perturbation of the north-eastern top area with connected vertical parts is about two and half times higher than that of perturbing the north-eastern top area only. The sensitivity value to perturbation of fracture zone 4 is between the values of the two above mentioned cases.

Table 5: Sensitivity of the total flux across the hypothetical repository region to three different perturbations in case 3DLSB.

| Perturbation Area | Total Flux | Sensitivity | Sensitivity (normalized) |
|---|---|---|---|
| Perturbation of fracture zone 4 | $3.94 \cdot 10^{-4}$ | $9.658 \cdot 10^{-6}$ | 2.45% |
| Perturbation of the north-eastern top area | $3.94 \cdot 10^{-4}$ | $6.790 \cdot 10^{-6}$ | 1.72% |
| Perturbation of the north-eastern top area with connected vertical parts | $3.94 \cdot 10^{-4}$ | $1.689 \cdot 10^{-5}$ | 4.29% |

As already mentioned, the natural groundwater discharge through a vertical section in the north-eastern part of the flow domain was estimated and used for calibration purposes in previous studies. Thus it was considered to be of interest to analyze the sensitivity of the total normal flux across this vertical section with an area of $1.457 \cdot 10^6\ m^2$. The results are displayed in Table 6.

The results of the calculations show that the integrated normal flux in the north-eastern vertical section is highly sensitive to perturbation of the lateral boundary fracture zone 4, but less sensitive (about half as much) to the two other perturbations, viz. the perturbation of the north-eastern top area and likewise with adjoining vertical parts.

From the above results the following conclusions may be drawn: (i) the normal total flux through the imaginary repository plane at 500 m depth is less sensitive to the perturbations of those selected boundary regions, and (ii) the total normal flux across the north-eastern vertical section is highly sensitive to perturbations of the selected boundary regions, especially to perturbation of the lateral boundary of fracture zone 4.

Table 6: Sensitivity of the total flux across the north-eastern vertical section with respect to the specified perturbation areas in case 3DLSB.

| Perturbation Area | Total Flux | Sensitivity | Sensitivity (normalized) |
|---|---|---|---|
| Perturbation of fracture zone 4 | $3.628 \cdot 10^{-2}$ | $3.232 \cdot 10^{-2}$ | 89.08% |
| Perturbation of the north-eastern top area | $3.628 \cdot 10^{-2}$ | $1.572 \cdot 10^{-2}$ | 43.33% |
| Perturbation of the north-eastern top and connected vertical parts | $3.628 \cdot 10^{-2}$ | $1.452 \cdot 10^{-2}$ | 40.02% |

### 4.4.3 Sensitivity of the Darcy flux distribution

Sensitivities of flux distributions to the three selected perturbation areas are depicted in the vertical cross-section in case 3DLSB in Figures C18, C20 and C21. As can be observed in the graphical displays, the contour lines of the flux sensitivity exhibit rather similar patterns in the three different perturbation cases. The high sensitivity values are concentrated to the region where sub-horizontal fracture zone 2 is located. However, in a horizontal cross-section the large scale of the flux sensitivity distribution is rather similar for the three selected perturbation cases (Figures C22, C23 and C24). The sensitivity values are mainly distributed in the regions where the fracture zones are located.

# 5 SUMMARY AND CONCLUSIONS

The object of the present study was to perform a sensitivity analysis of the previous groundwater flow modelling at the Finnsjön site. Sensitivity analysis may be characterized as a mathematical means for determining the relationships between the input and output variables of a mathematical model. The sensitivity of one variable to another in the mathematical model is described by the partial derivative of the output variable (or performance function) of interest versus the input variables. The performance functions considered in the study were: the piezometric head and the flux, both integrated and point-wise, at the region of an imaginary radioactive waste repository located at a depth of 500 metres below the ground surface.

Two different sensitivity methods were considered in the present study, one of which is called the direct method and the other the variational method. The direct sensitivity method was used to evaluate the sensitivity of the piezometric head at nodal points versus the hydraulic conductivity of a major fracture zone. The variational method was used to evaluate the sensitivity of the integrated Darcy flux across an imaginary repository region versus the hydraulic conductivity of a selected fracture zone. The numerical method for solving the primary flow equation and adjoint state equation are based on the Galerkin finite element method.

The study was divided into two main parts with regard to the types of perturbations, or say uncertainties, of the considered input. One type in which the uncertainty was associated with the permeability of some major fracture zones and the other type in which the uncertainty was associated with the specification of the prescribed pressure boundary conditions.

*Sensitivity to permeability of major fracture zones*

Two major fracture zones were analyzed viz. zone H1 and zone 2 at the Finnsjön site. Zone H1 is a horizontal fracture zone located at a depth of about 1100 m. Zone 2 is a sub-horizontal zone that was analyzed because of its high hydraulic conductivity ($2 \cdot 10^{-5}$ - $4 \cdot 10^{-5}$ m/s) and location in the flow domain, implying that it should be of particular importance to the flow conditions.

Zone H1 was included in the sensitivity study since the geometrical and physical properties of this zone are currently uncertain. Fracture zone H1 was unintentionally accounted for in the previous groundwater flow calculations at the Finnsjön study site. Therefore, it was found to be of interest to analyze the impact of this zone on the flow solutions.

The sensitivity of the selected performance functions selected was analyzed for different modelling concepts of the flow domain. The motivation for this part of the study was that in the previous groundwater flow calculations at the Finnsjön study site conducted by Kemakta (Lindbom et al. [1991]) a specific technique for averaging the hydraulic conductivities over large blocks was applied. It was considered relevant to perform a comparative sensitivity analysis between a flow domain conceptualized in a conventional manner and a flow domain described using the above mentioned technique.

Although the solutions to the primary problem (ie. pressure or piezometric head values) were rather alike, the present study shows that the two alternative flow domain conceptualization of the Finnsjön study site lead to significantly different flow systems with regard to perturbations of the permeability of the fracture zone considered.

*Sensitivity to boundary conditions*

The objective of this part of the study was to analyze the sensitivity of the piezometric head and flux to perturbations of the boundary conditions assumed in the previous modelling of the groundwater flow conditions at the Finnsjön study site. The motivation for this part of the sensitivity study was that ambiguities, or say uncertainties, in the boundary conditions were introduced by the procedure used to specify the boundary conditions for the local model based on results from calculations performed at a regional scale. As a consequence, contradictions between the upper boundary conditions dictated by the topography and the interpolated lateral boundary conditions created artificial gradients.

The present sensitivity analysis was directed towards the following parts of the flow domain: (i) a horizontal region located at a depth of 500 m, considered representative for the location a hypothetical repository, (ii) a vertical cross-section through the centre of the imaginary repository and (iii) a vertical section through a natural discharge region for the groundwater flow in the flow domain. The last-mentioned case (iii) was chosen since the flow across this section was studied previously and was used for calibration purposes in these studies.

The sensitivity of the piezometric head and the sensitivity of the flux to three different perturbation areas were investigated in the present study. The areas subject to perturbation were: (i) fracture zone 4, (ii) the top boundary at the north-eastern corner (perturbation area = $1.209 \cdot 10^6$ m), and (iii) the top boundary at the north-eastern corner including parts of the vertical boundaries (perturbation area = $1.991 \cdot 10^6$ m).

In summary, the main conclusions from the analysis of the boundary conditions are that

(1) the piezometric head at the repository region proved to be highly sensitive to the boundary condition perturbations considered. The distribution of the sensitivity values showed that the piezometric head was most sensitive to perturbation of the north-eastern top area with the connected vertical parts, but less sensitive to perturbation only of the north-eastern top boundary. The magnitude of the sensitivity to perturbation of fracture zone 4 (i.e. the north-eastern vertical boundary) is between that of the two afore-mentioned perturbations. This implies that the hydraulic conductivity of zone 4 is of major importance and should be further investigated.

(2) the sensitivity of the total normal flux through the horizontal imaginary repository plane (z = -500) to perturbation of the boundary conditions was less than that across the north-eastern vertical section. The results show that the sensitivity of the normal flux through the vertical

section to perturbing the lateral boundary fracture zone 4 was about twice as high compared to perturbing the north-eastern top area and to the north-eastern area with parts of the vertical boundary included. The horizontal cross-section at 500 m depth shows that the sensitivity of the normal flux has the highest value to perturbation of the north-eastern top with connected vertical parts. The sensitivity to perturbing the north-eastern top boundary is only half as large compared to that of perturbing the north-eastern top with parts of the vertical boundary included. The sensitivity value of the total normal flux to perturbation of fracture zone 4 lies between that of the two afore-mentioned cases.

(3) it was found that the high flux sensitivity values were always situated around fracture zone 2, which is a major sub-horizontal zone of relatively high hydraulic conductivity. The contour lines of the horizontal cross-section (z = -500) below zone 2, show that the flux in the regions where the fracture zones are located is more sensitive to perturbations than that of the rock mass.

*General conclusions*

Among the general conclusions that may be drawn from the results of this study is that the flow conditions are more sensitive to uncertainties associated with the procedure of specifying the boundary conditions for the local model (on basis of results from a regional model) than to uncertainties due to inadequacies in the description of the topography. This means that it is unsuitable to let the lateral boundaries coincide with vertical fracture zones as was the case in the previous studies. In conclusion, this suggests that the model area should be extended beyond the fracture zones in the future groundwater flow modelling.

## 6 REFERENCES


1. Alsmiller, R.G., J. Barhen, J.E. Horwedel, J.L. Lucius and J.D. Drischler, 1984,
The application of adjoint sensitivity theory to a liquid fuels supply model, Energy, 9(3), 239-253.

2. Andersson, J-E., Nordqvist R., Nyberg, G., Smellie, J., Tirén, S. 1989,
Hydrogeological conditions on the Finnsjön area - Compilation of data and conceptual model, Swedish Nuclear Fuel and Waste Management company, SKB AR 89-24.

3. Bao, Yung-Bing., 1990,
Sensitivity analysis of groundwater flow, Licentiate thesis at dept. Land and Water Resources, KTH, Swedish Nuclear Fuel and Waste Management company, SKB TR 90-36.

4. Bao, Y-B. and Thunvik, R., 1990,
Demonstrative sensitivity analysis of the flow conditions at the Finnsjön study site, SKB AR 90-43.

5. Cacui, D.G., C.F. Weber, E.M. Oblow and J.H. Marable, 1980,
Sensitivity theory for general systems of nonlinear equations, Nuclear Science & engineering, 75, 88-110.

6. Carrera, J and S.P.Neuman, 1986,
Estimation of aquifer parameters under transient and steady state conditions: 2. Uniqueness, stability, and solution algorithms, Water Resour. Res., Vol. 22, No. 2, 211-227.

7. Carter, R.D., L.F., Kemp, Jr. and A.C. Pearce, 1982,
Discussion of comparison of sensitivity coefficient calculation methods in automatic history matching, Soc. Pet. Eng. J., 22(2), 205-208.

8. Carter, R. D.,Kemp, L.F., Pierce, A.C. and Williams. D.L., 1974,
Performance Matching with Constraints, Soc. Pet. Eng. J. 187-196, April 1974.

9. David, P.A., John, M.M., George, F.P. and Eric, F.W., 1988,
Contaminated groundwater remediation design using simulation, optimization, and sensitivity theory 1. Model development, Water Resour. Res., Vol. 24, No. 3, 431-441.

10. Grundfelt, B., A. Boghammar and H. Lindberg, 1989,
HYPAC User's Guide, SKB-Arbetsrapport 89-22, SKB, Box 5864, S-102 48 Stockholm.

11. Jacquard, P. and Jain, C., 1965,
Permeability distribution from field pressure data, Soc. Pet. Eng. J., 5(6), 281-294.

12. Li, L-S., Sun, N-Z. and Yeh, W.W-G., 1987,
A comparative study of sensitivity coefficient circulation method in groundwater flow, RHO-BW-SA-586 P, January.

13 Lindbom, B., A., Boghammar, H., Lindberg and J. Bjelkås, 1991,
Numerical groundwater flow calculations at the Finnsjön study site, SKB TR 91-12, SKB, Box 5864, S-102 48 Stockholm.

14. Neuman, S.P., 1980,
A statistical approach to the inverse problem of aquifer hydrology, 3, Improved solution method and added perspective, Water Resour. Res., 16(2), 331-346.

15. Oblow, E.M., 1978,
Sensitivity theory for general nonlinear algebraic equations with constraints, Nucl. Sci. Eng., 65, 187-191.

16. Sun, N-Z, and Yeh, W. W-G., 1985,
Identification of parameters structure in groundwater inverse problem, Water Resour. Res., 21(6), 869-883.

17. Sykes, J.F., and J.L. Wilson, 1984,
Adjoint sensitivity analysis for the finite element method, in Proceeding of the 5th International Conference on Finite Elements in Water Resources, pp. 777-790, Springer-Verlag, New York.

18. Sykes, J.F., J.L. Wilson and R.W. Andrews. 1985,
Sensitivity analysis for steady-state groundwater flow using adjoint operators. Water Resour.Res., 21(3), 359-371.

19. Thunvik, R. and Braester, C., 1988,
GWHRT - A flow model for coupled groundwater and heat flow, Swedish Nuclear Fuel and Waste Management company, SKB TR 88-10.

20. Thunvik, R. and Bao, Y-B., 1988,
GWHRT-S - Documentation of computer program for sensitivity analysis of groundwater flow. Swedish Nuclear Fuel and Waste Management company, SKB AR 88-55.

# APPENDIX A Graphical display of the primary solutions

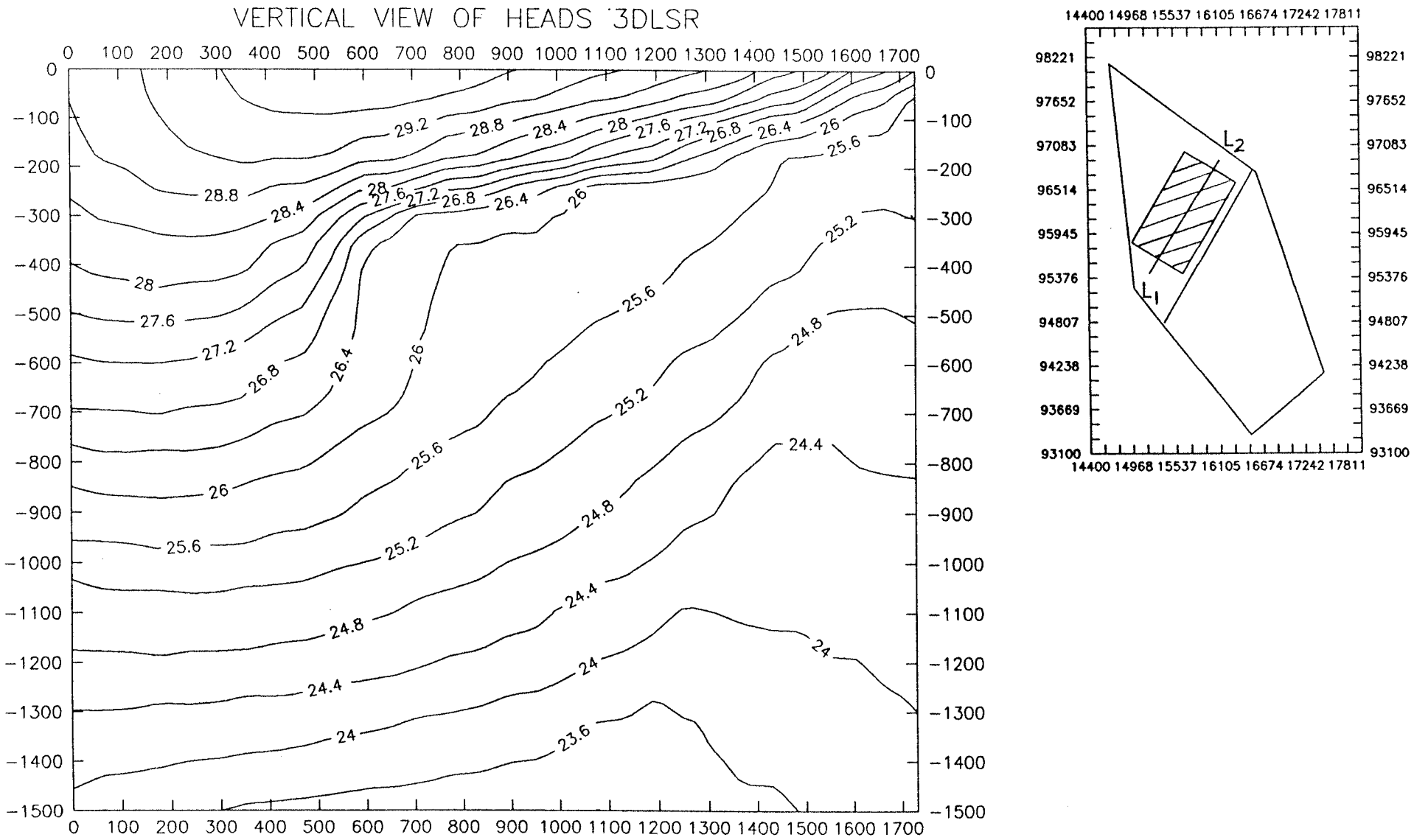


Figure A1. Contour lines showing the distribution of the piezometric head (m) in a vertical section through the imaginary repository in case 3DLSR.

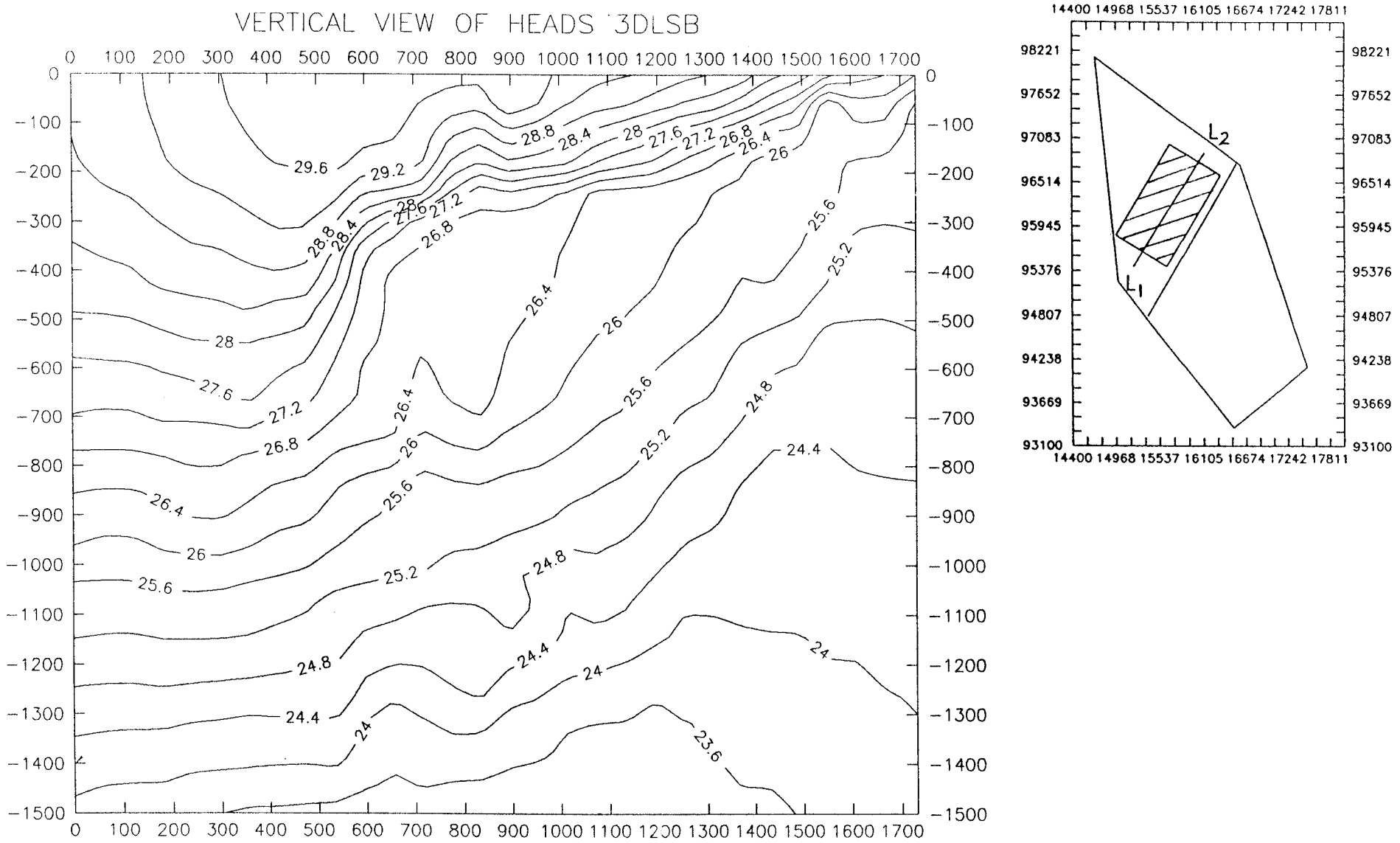


Figure A2. Contour lines showing the distribution of the piezometric head (m) in a vertical section through the flow domain in case 3DLSB.

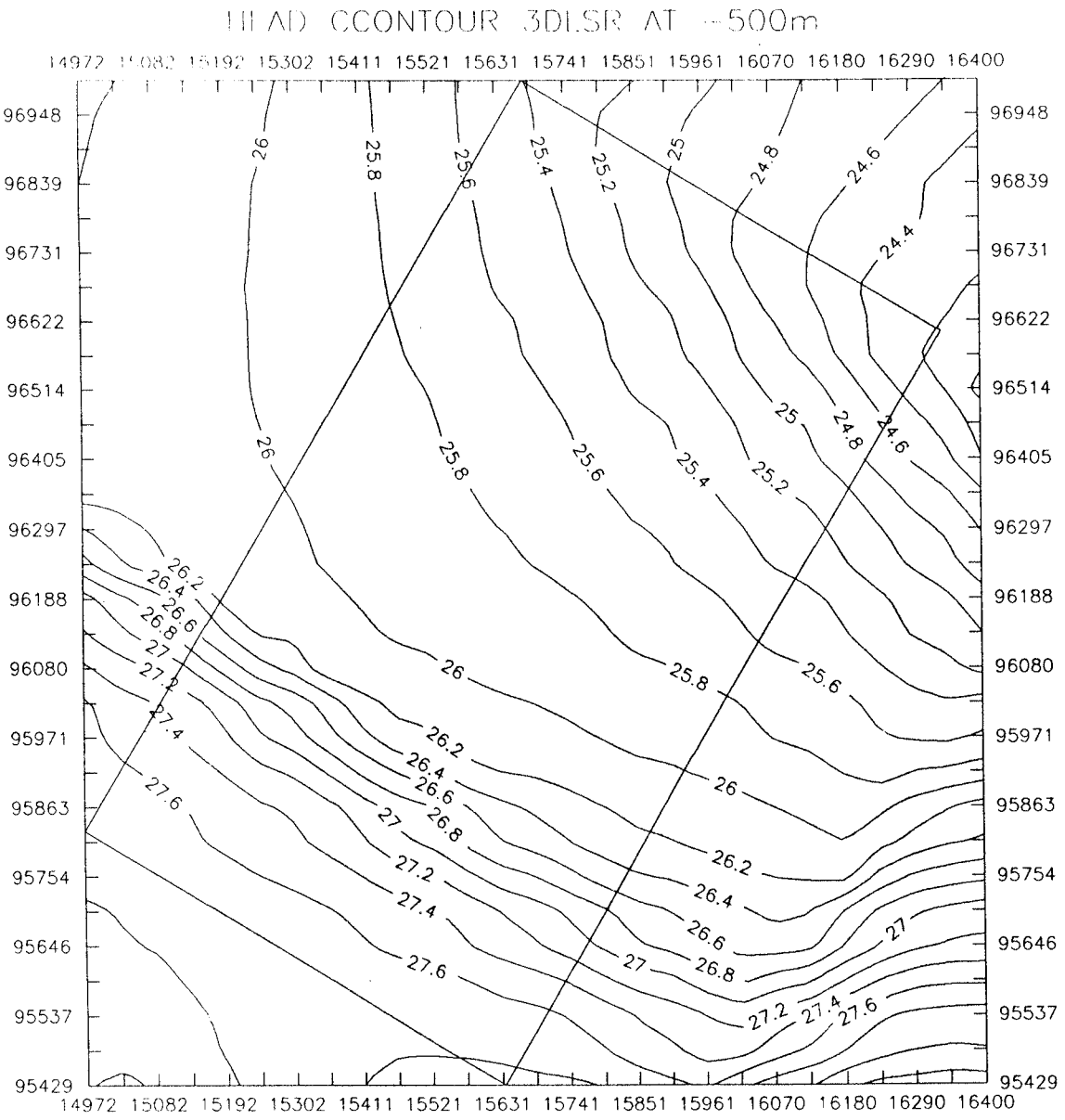


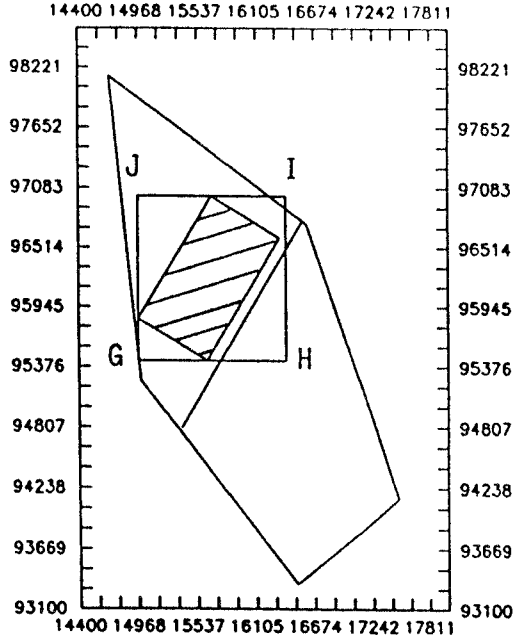


Figure A3. Contour lines showing the distribution of the piezometric head in a horizontal section (z = -500 m) through the flow domain in case 3DLSR.

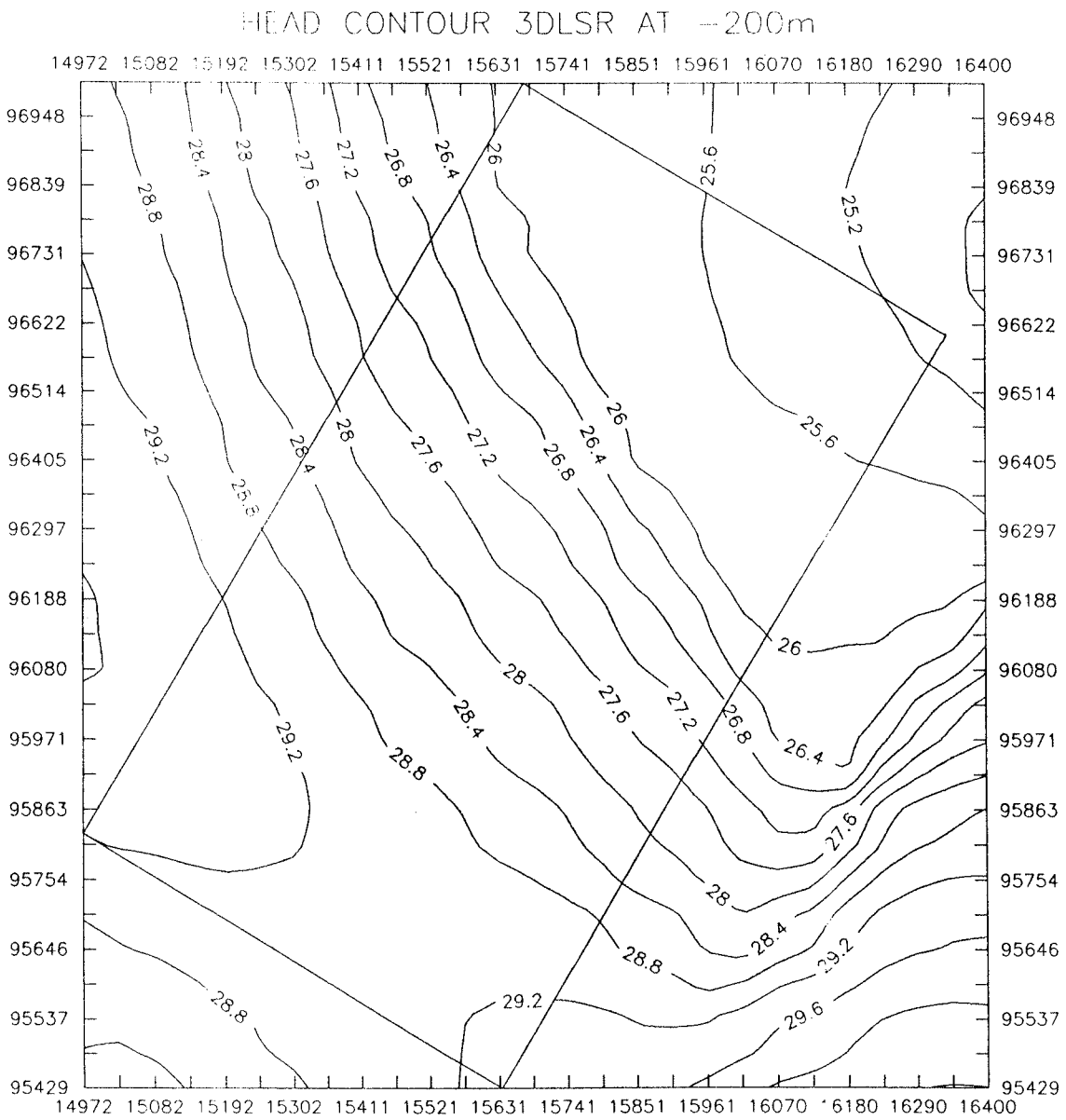


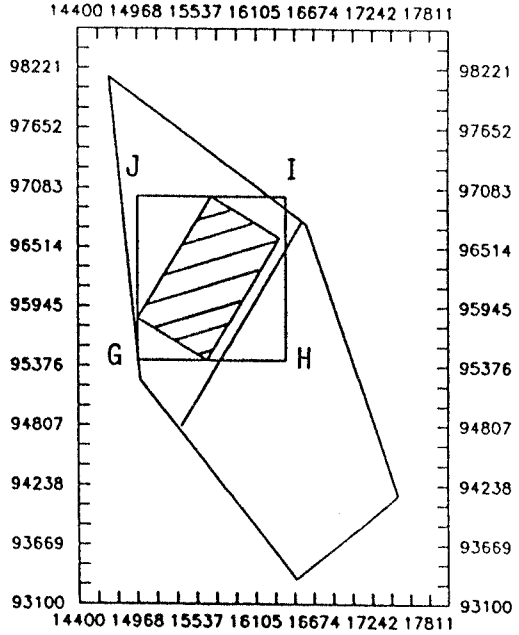


Figure A4. Contour lines showing the distribution of the piezometric head in a horizontal section (z = -200 m) through the flow domain in case 3DLSR.

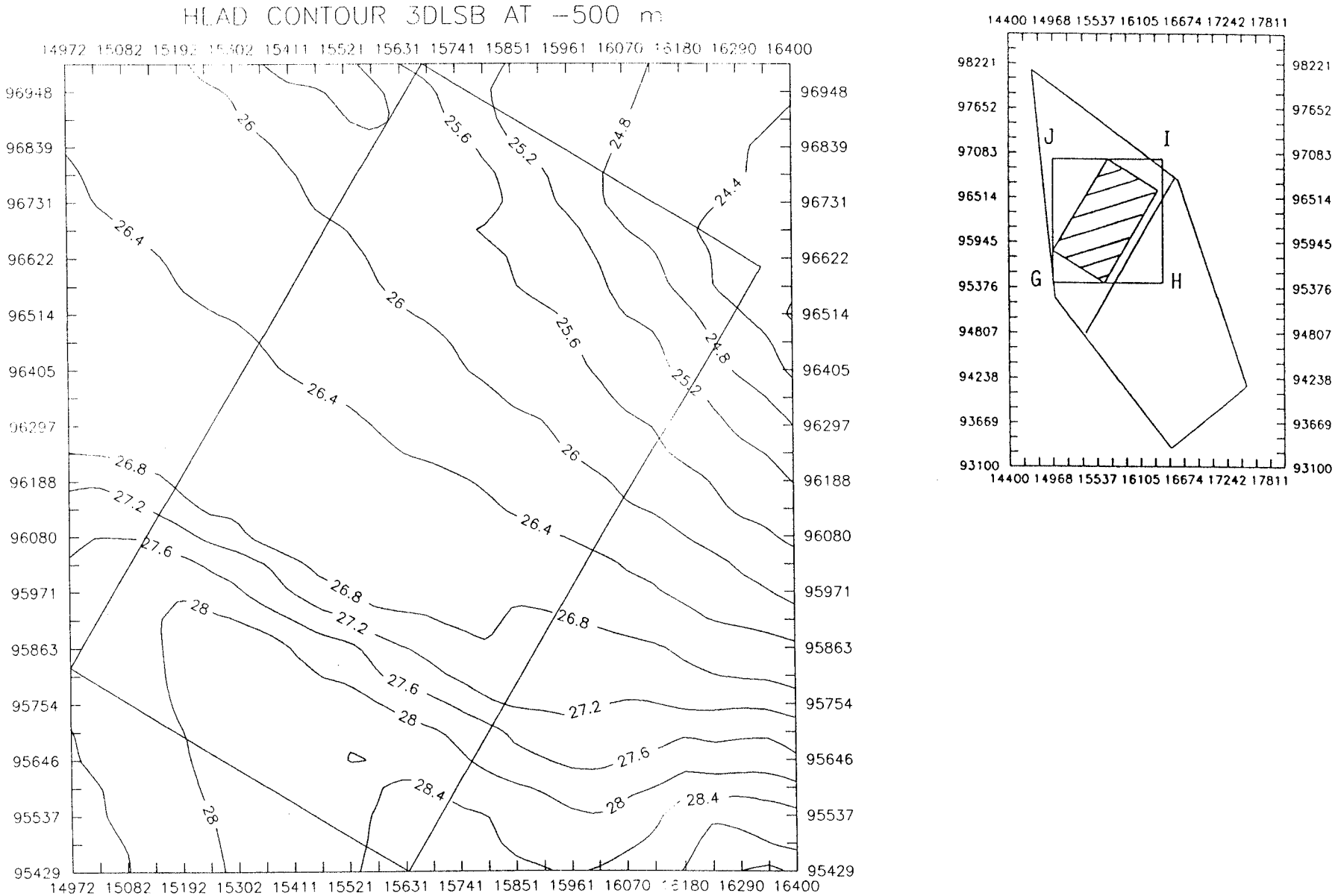


Figure A5. Contour lines showing the distribution of the piezometric head (m) in a horizontal section (z = -500 m) through the flow domain in case 3DLSB.

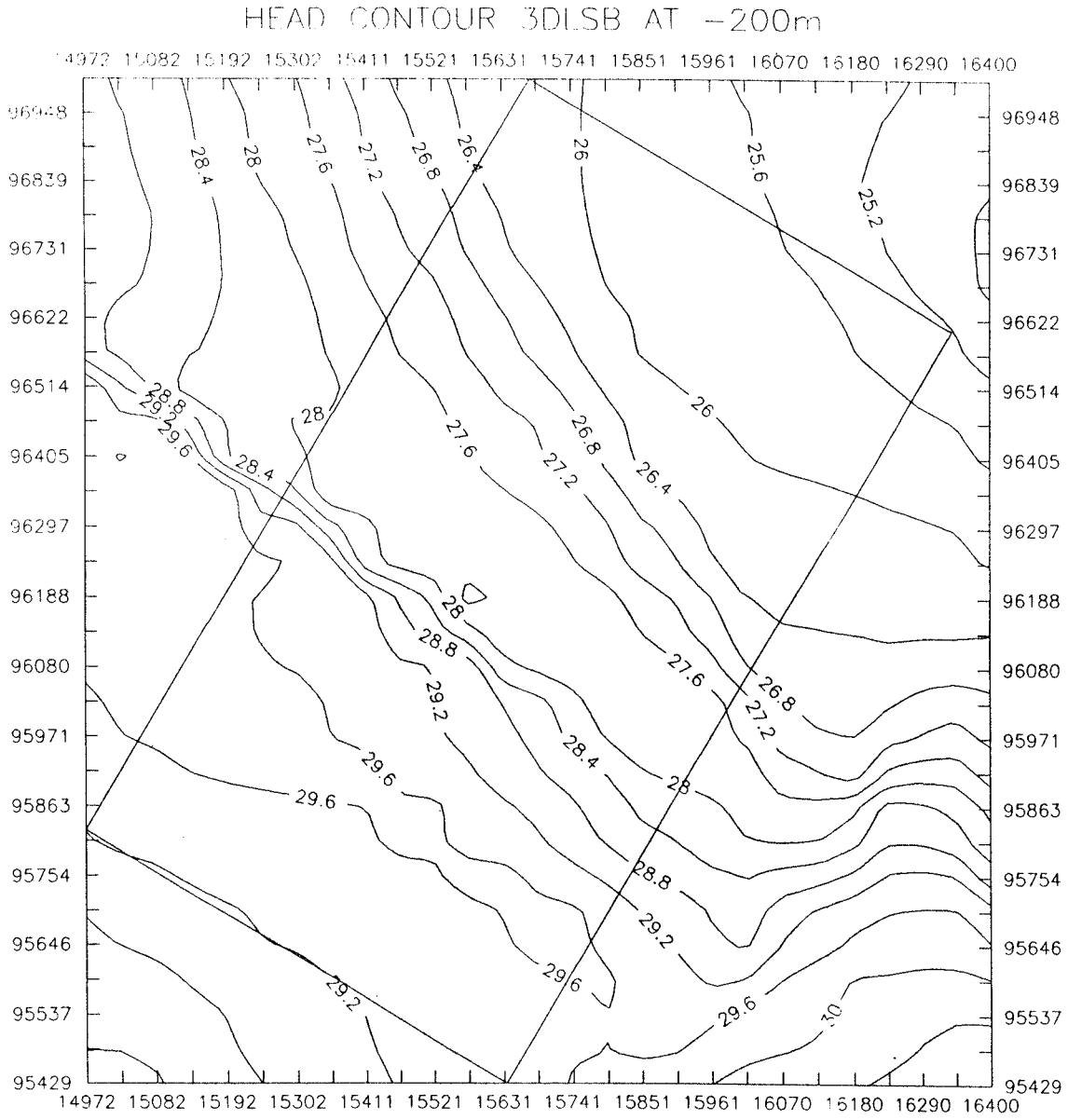


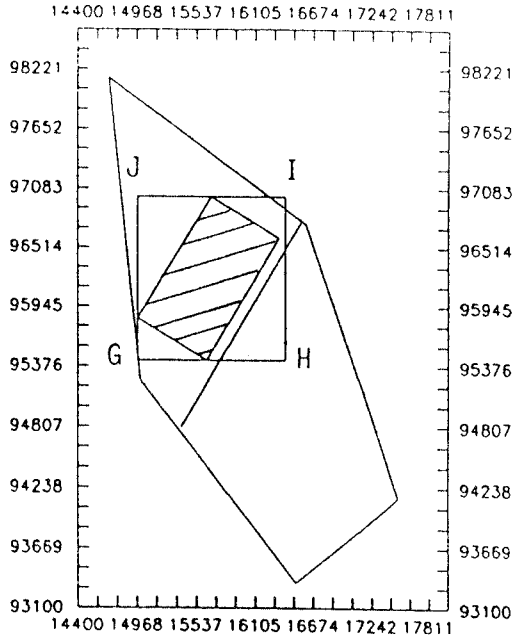


Figure A6. Contour lines showing the distribution of the piezometric head (m) in a horizontal section (z = -200 m) through the flow domain in case 3DLSB.

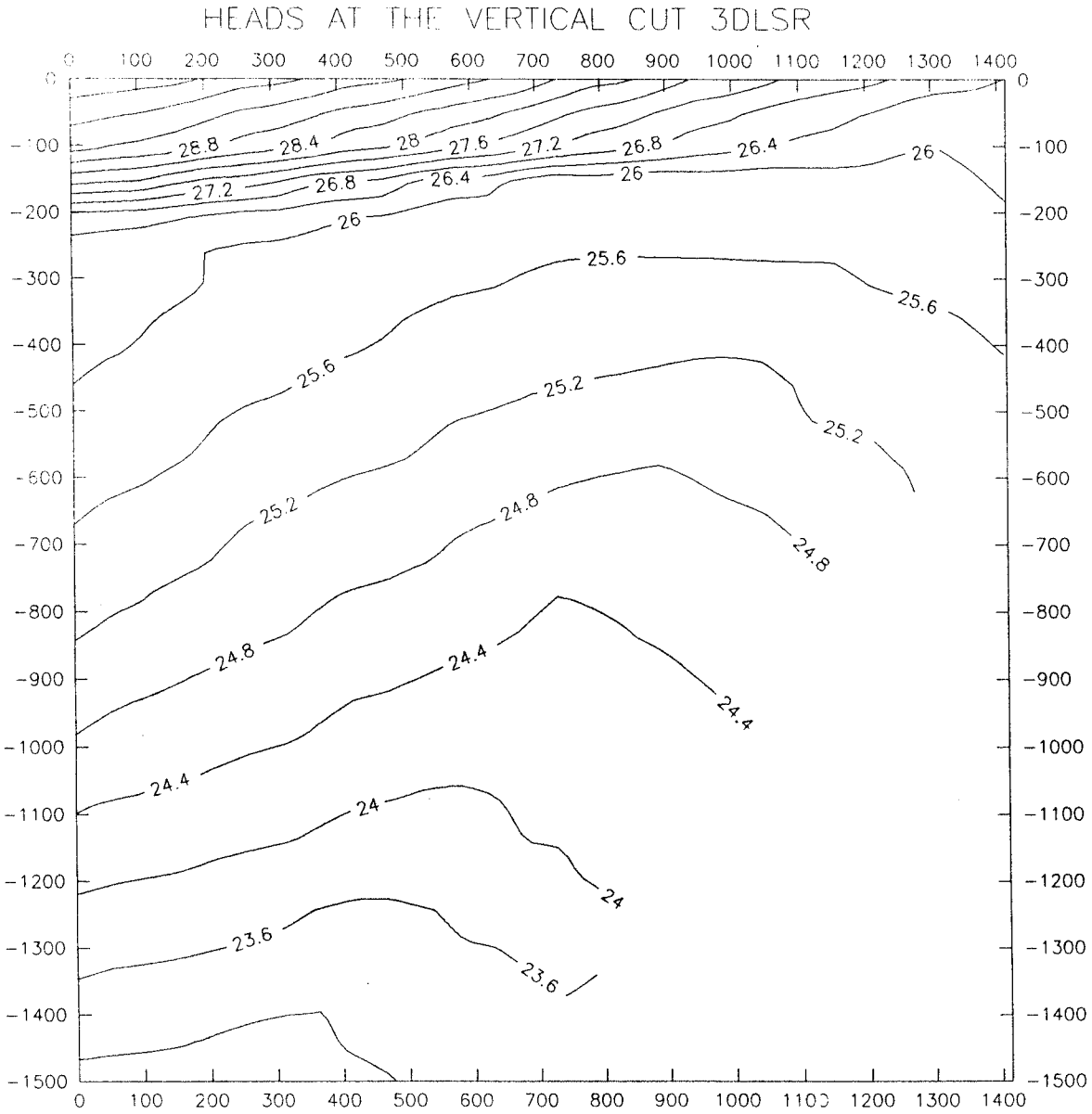


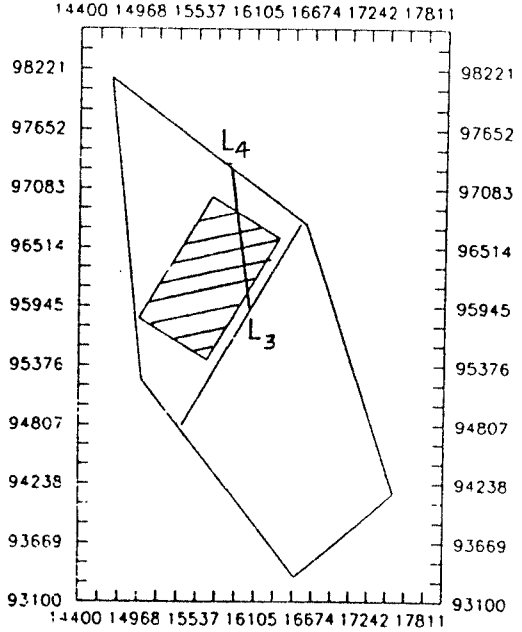


Figure A7. Contour lines showing the distribution of the piezometric head (m) in a vertical section through the north-eastern corner of flow domain in case 3DLSR.

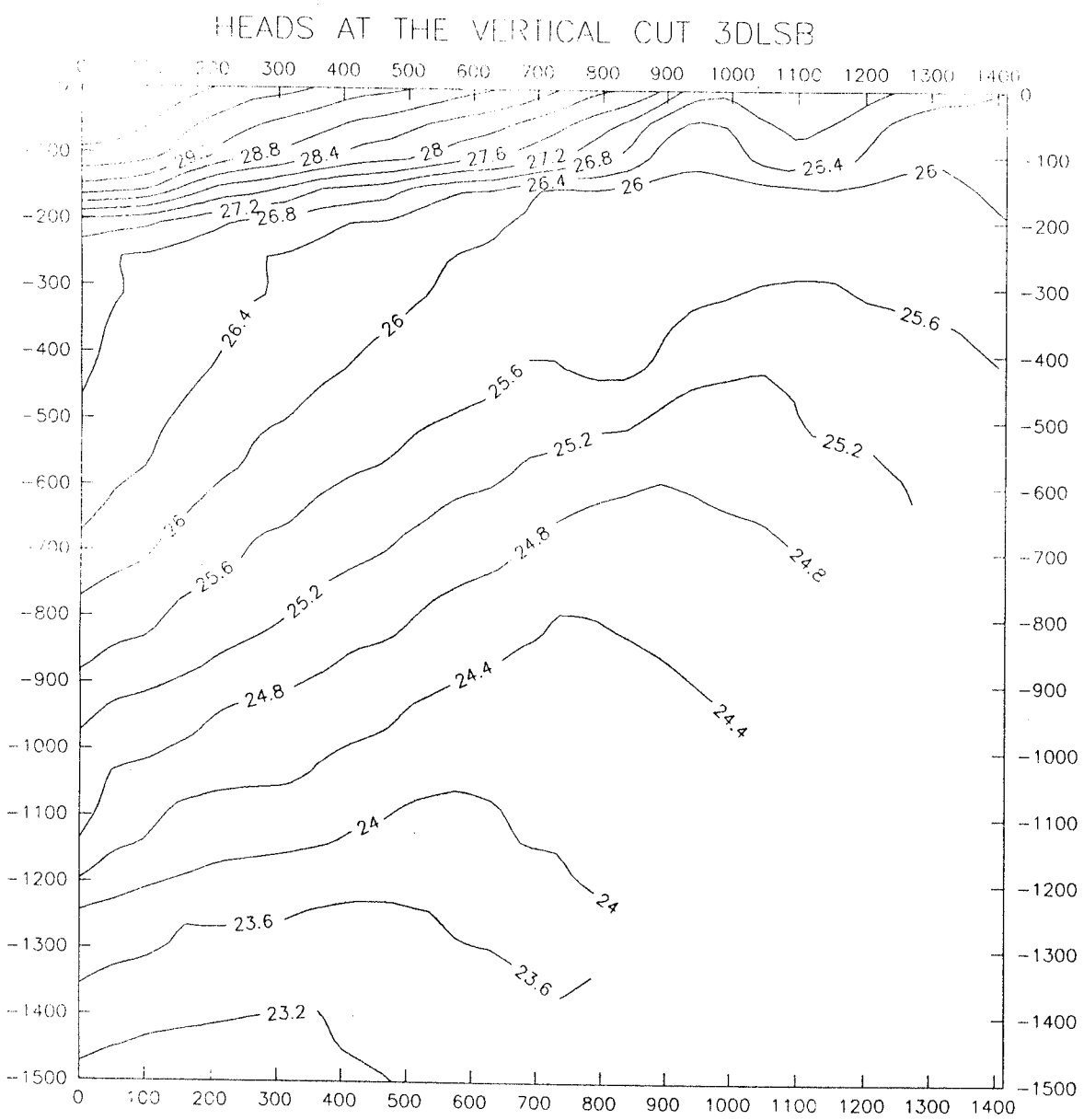


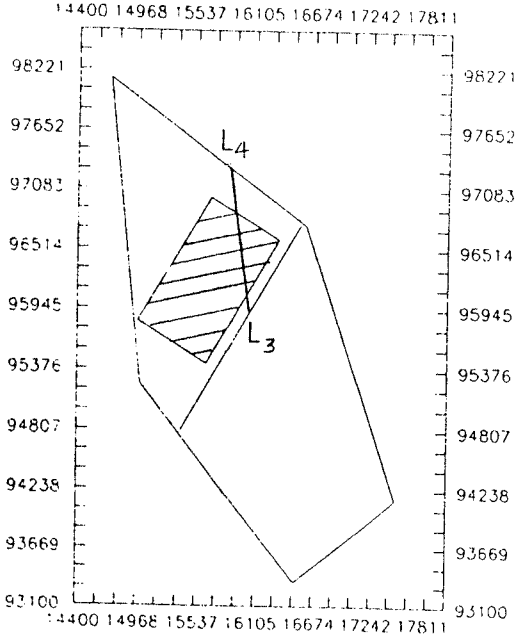


Figure A8. Contour lines showing the distribution of the piezometric head (m) in a vertical section through the north-eastern corner of flow domain in case 3DLSB.

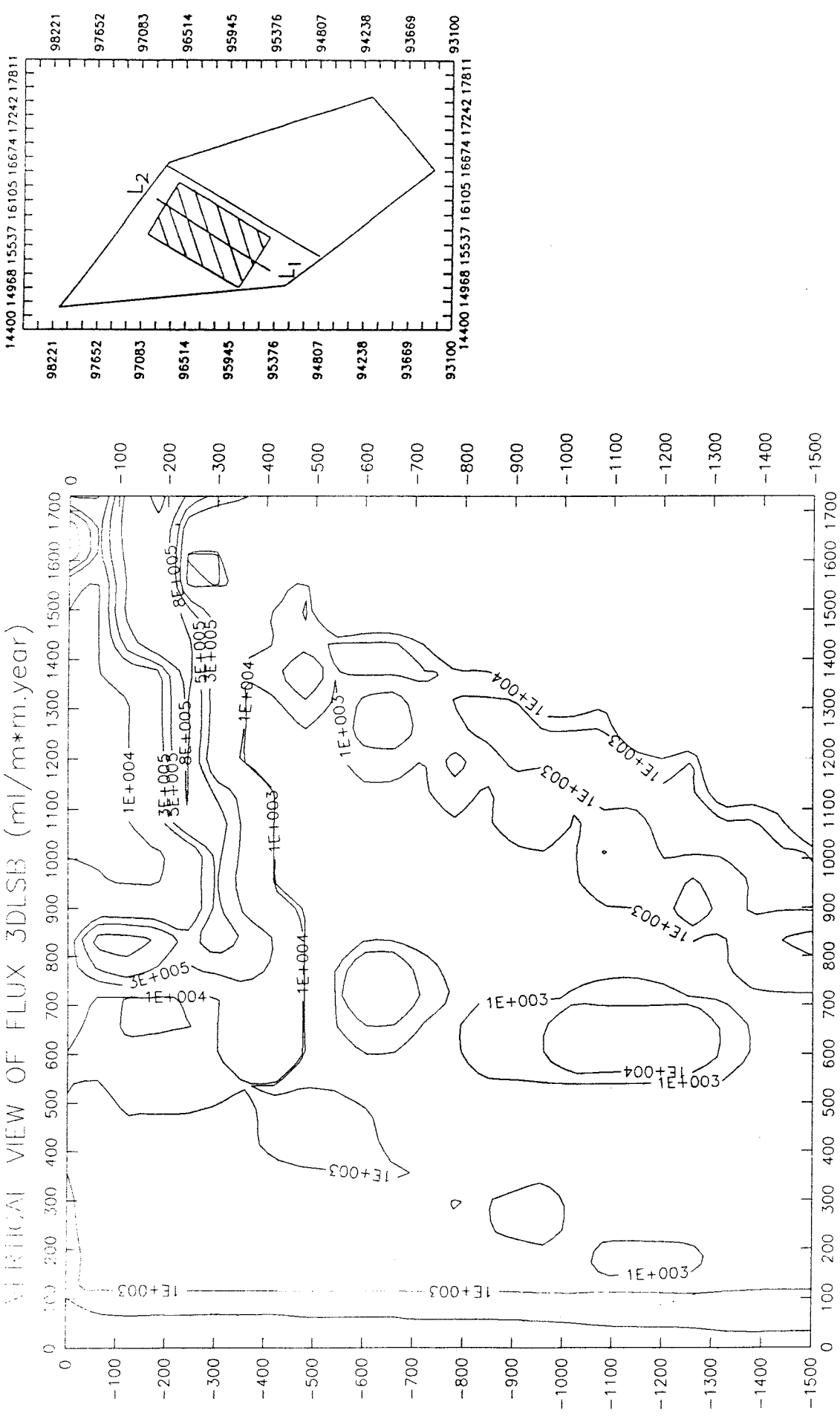


Figure A9. Contour lines showing the distribution of the Darcy flux (ml/m$^2$.year) in a vertical section through the flow domain in case 3DLSB.

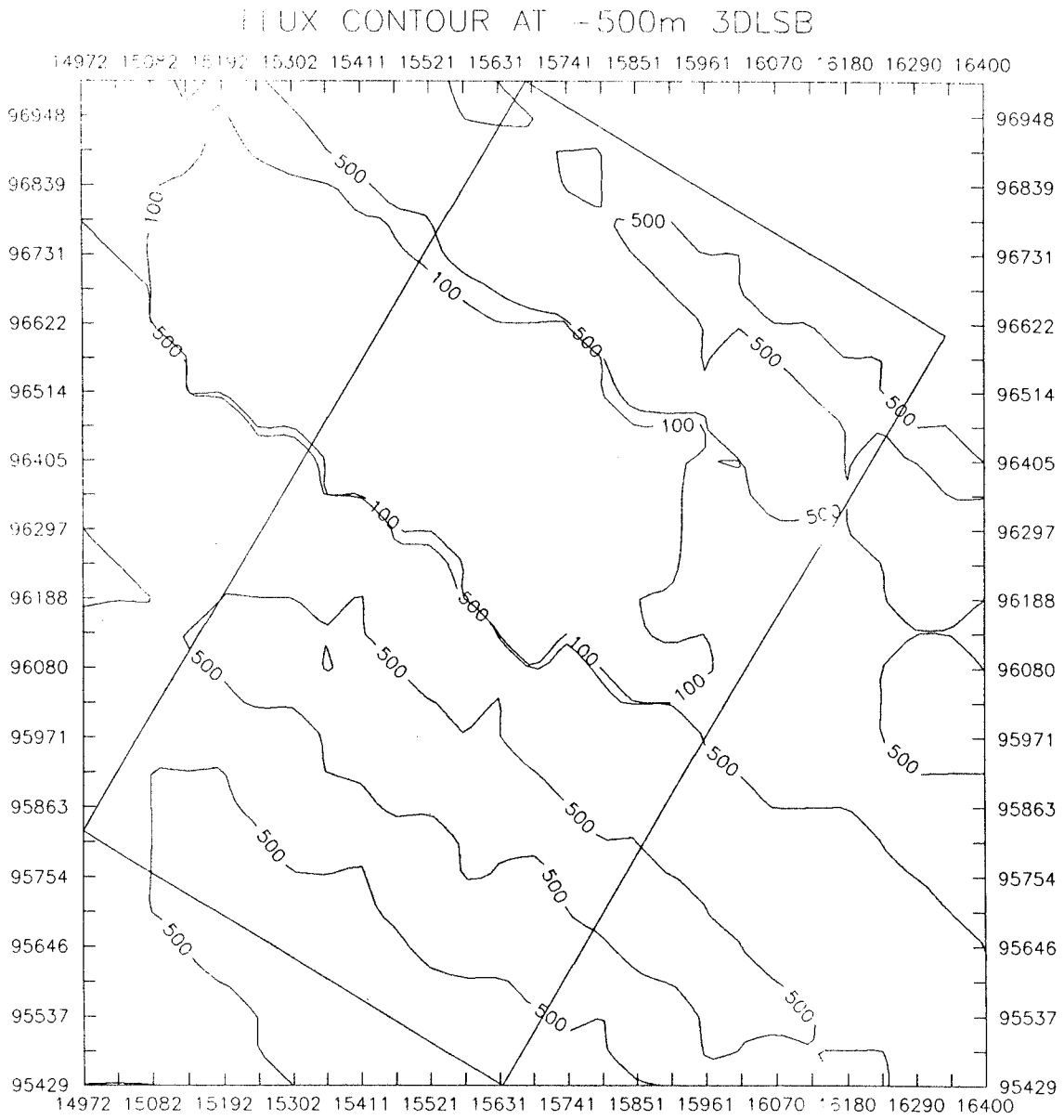


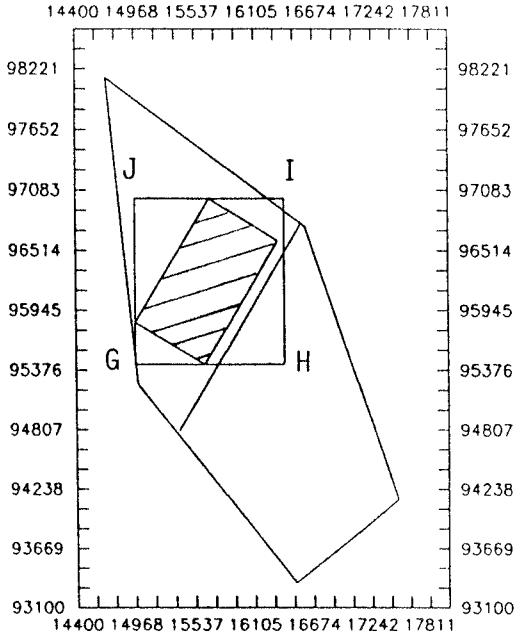


Figure A10. Contour lines showing the distribution of the Darcy flux (ml/m$^2$.year) in a horizontal section (z = -500 m) through the flow domain in case 3DLSB.

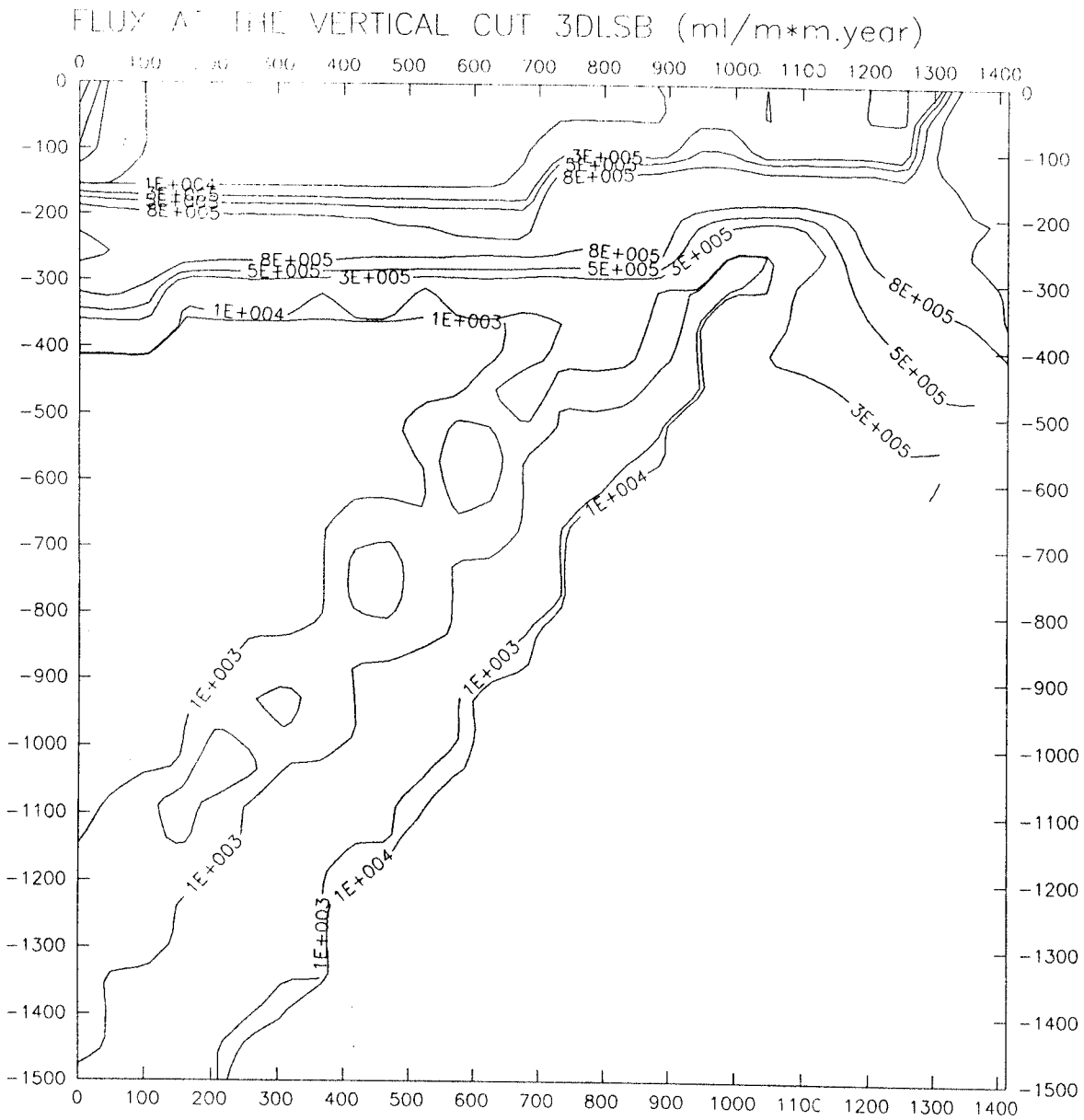


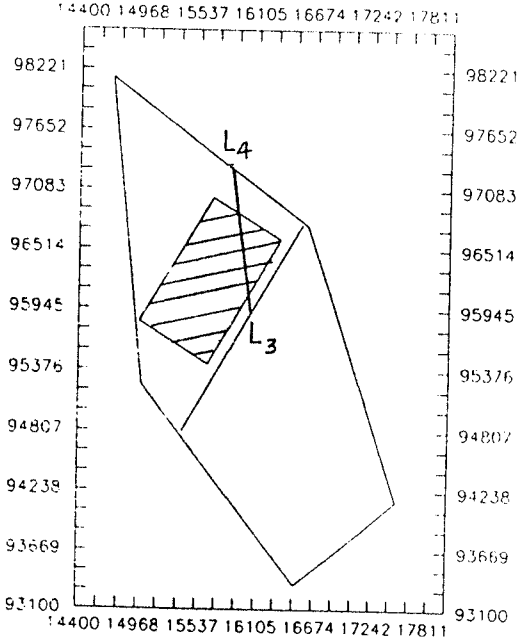


Figure A11. Contour lines showing the distribution of the Darcy flux (ml/m$^2$.year) in a vertical section through the north-eastern corner of in case 3DLSB.

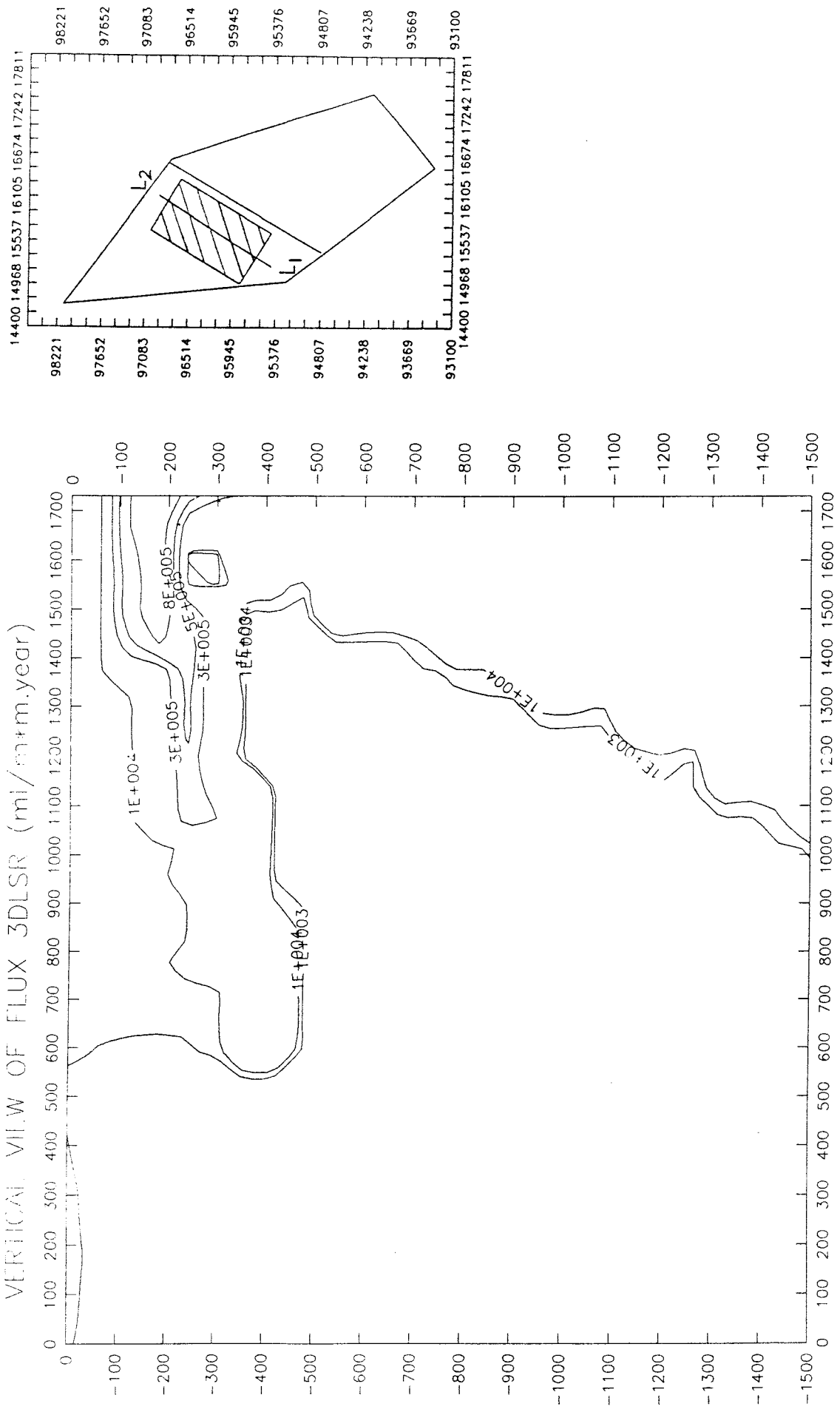


Figure A12. Contour lines showing the distribution of the Darcy flux (ml/m$^2$.year) in a vertical section through the flow domain in case 3DLSR.

# APPENDIX B Graphical display of sensitivity to permeability perturbations

Figure B1. Contour lines in a vertical section through the flow domain in case 3DLSR, showing distribution of the piezometric head sensitivity to perturbation of the hydraulic conductivity in zone H1.

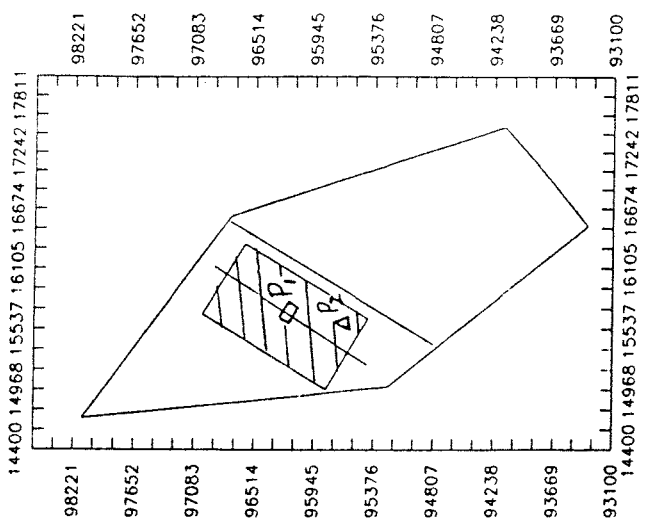


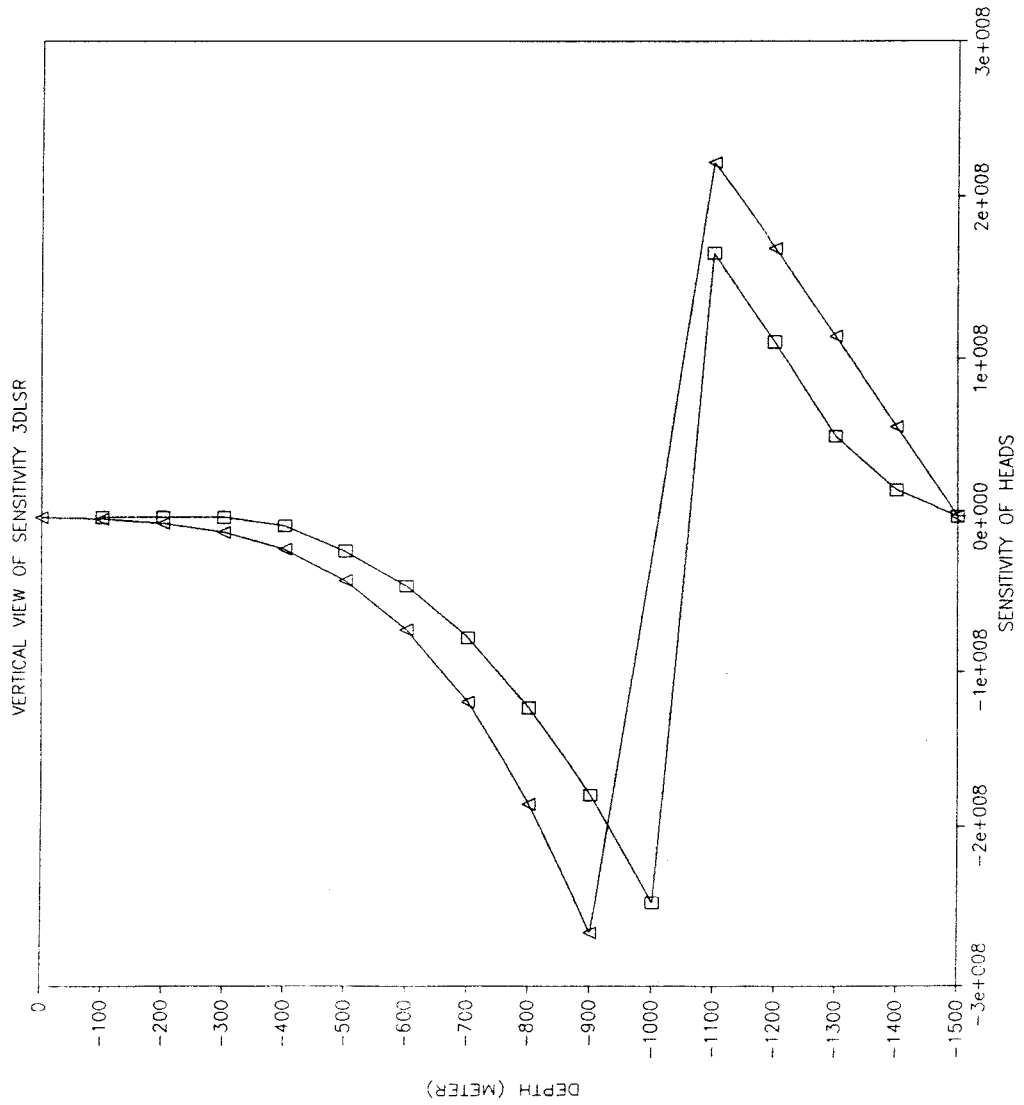


Figure B2. Vertical profiles of the piezometric head sensitivity to perturbation of the hydraulic conductivity in zone H1 in the case 3DLSR. (The profiles were defined as: X = 15682 m, Y = 96362 m, -1500 < Z < 0 m and X = 15500 m, Y = 95725 m, -1500 < Z < 0 m, respectively).

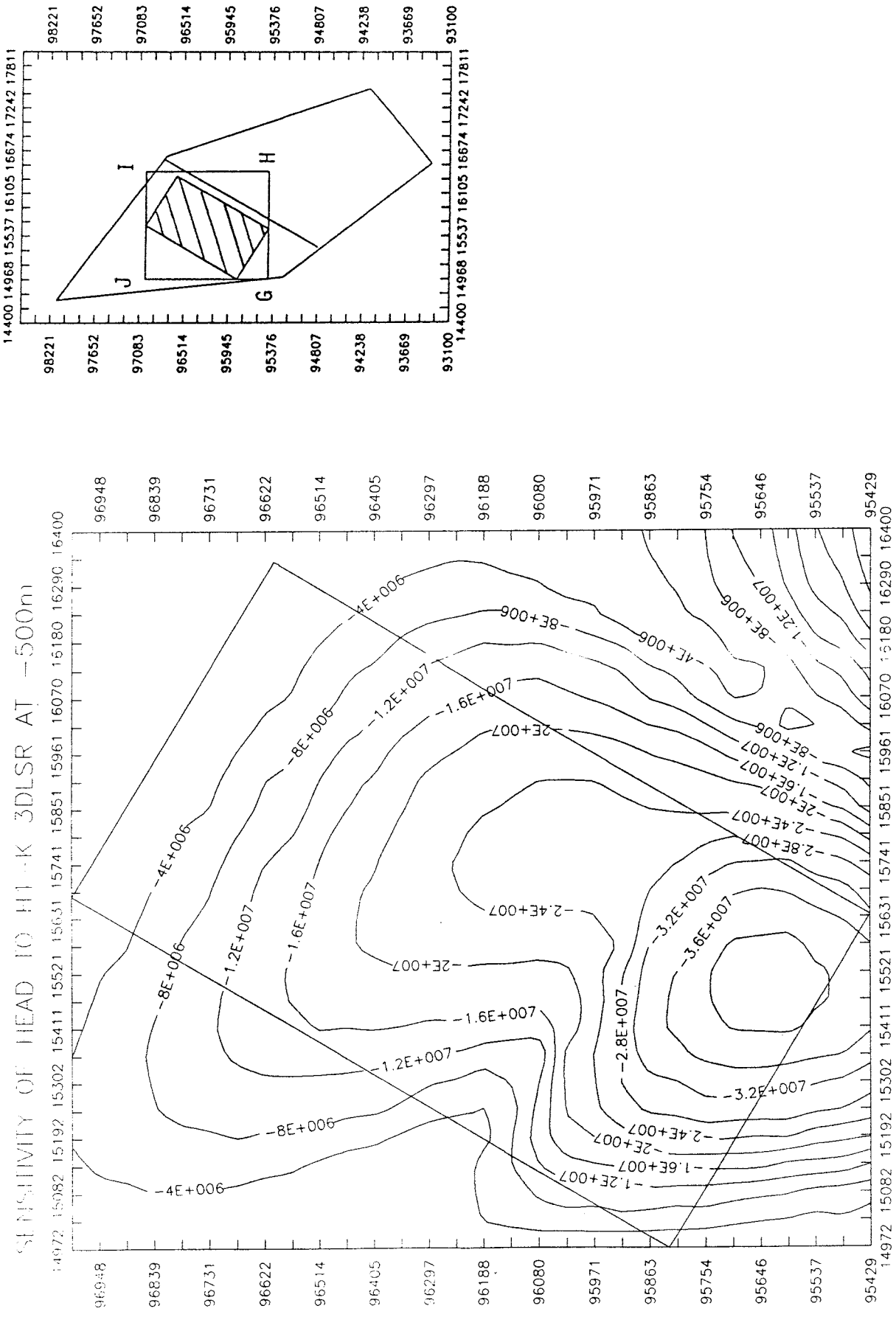


Figure B3 Contour lines in a horizontal cross-section (z = -500 m) through the flow domain in case 3DLSR, showing the distribution of the piezometric head sensitivity to perturbation of the hydraulic conductivity in zone H1.

Figure B4 Contour lines in a horizontal cross-section (z = -200 m) through the flow domain in case 3DLSR, showing the distribution of the piezometric head sensitivity to perturbation of the hydraulic conductivity in zone H1.

Figure B5. Contour lines in a vertical cross-section through the flow domain in case 3DLSB, showing distribution of the piezometric head sensitivity to perturbation of the hydraulic conductivity in zone H1.

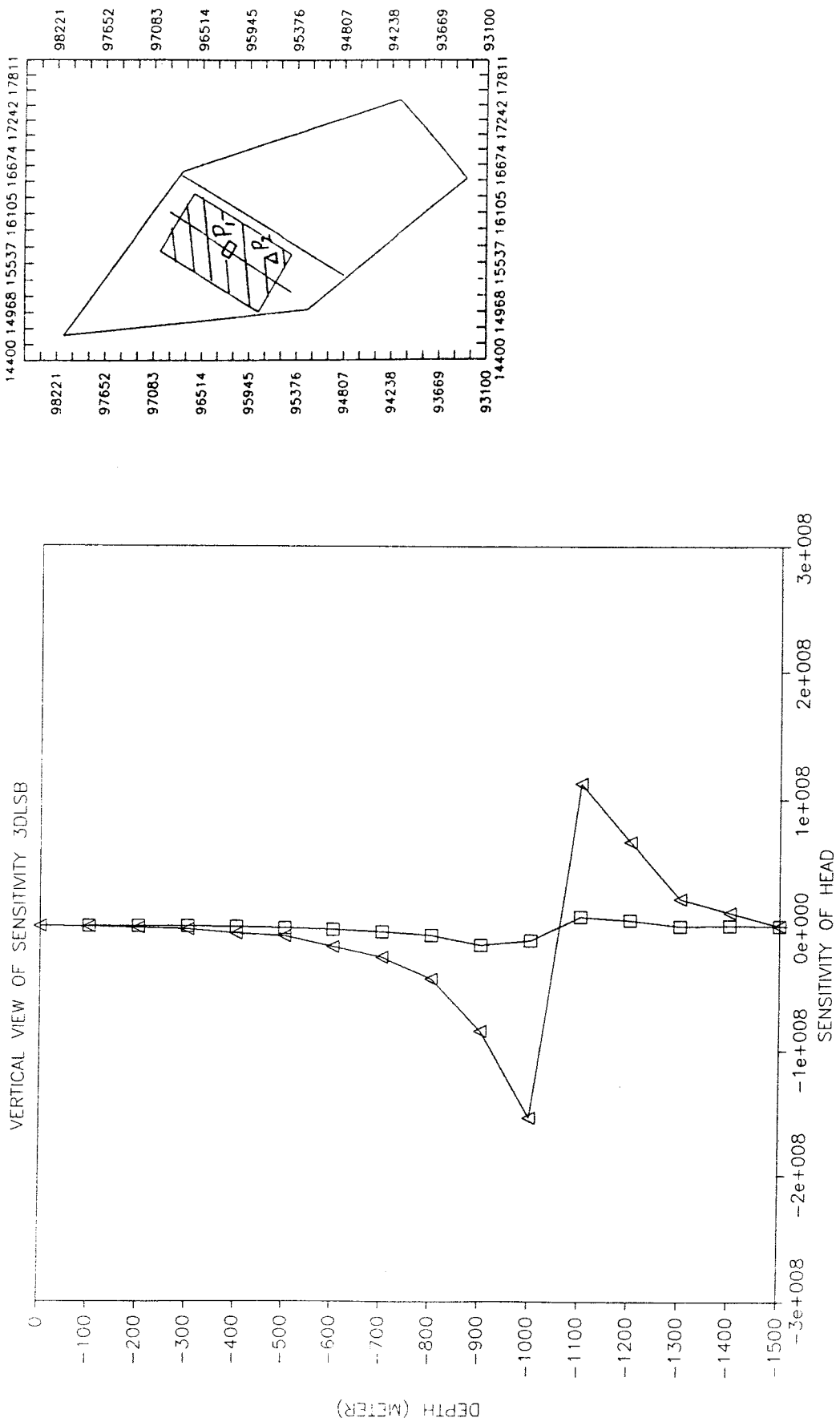


Figure B6. Vertical profiles of the piezometric head sensitivity to perturbation of the hydraulic conductivity in zone H1 in the case 3DLSB. (The profiles were defined as: X = 15682 m, Y = 96362 m, -1500 < Z < 0 m and X = 15500 m, Y = 95725 m, -1500 < Z < 0 m, respectively).

Figure B7 Contour lines in a horizontal cross-section (z = -500 m) through the flow domain of case 3DLSB, showing the distribution of the piezometric head sensitivity to perturbation of the hydraulic conductivity in zone H1.

Figure B8 Contour lines in a horizontal cross-section (z = -200 m) through the flow domain of case 3DLSB, showing the distribution of the piezometric head sensitivity to perturbation of the hydraulic conductivity in zone H1.

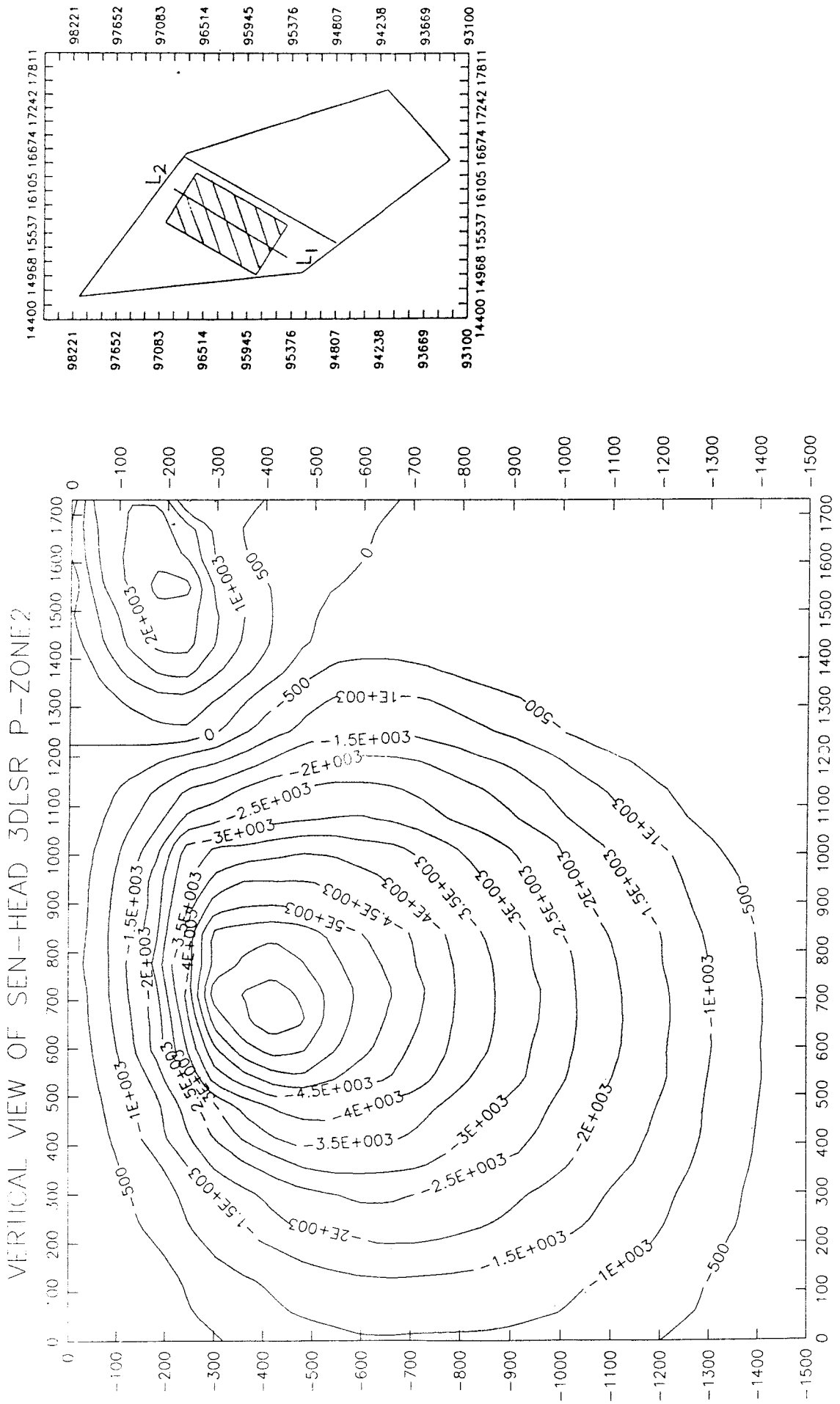


Figure B9. Contour lines in a vertical cross-section through the flow domain in case 3DLSR, showing distribution of the piezometric head sensitivity to perturbation of the hydraulic conductivity in zone 2.

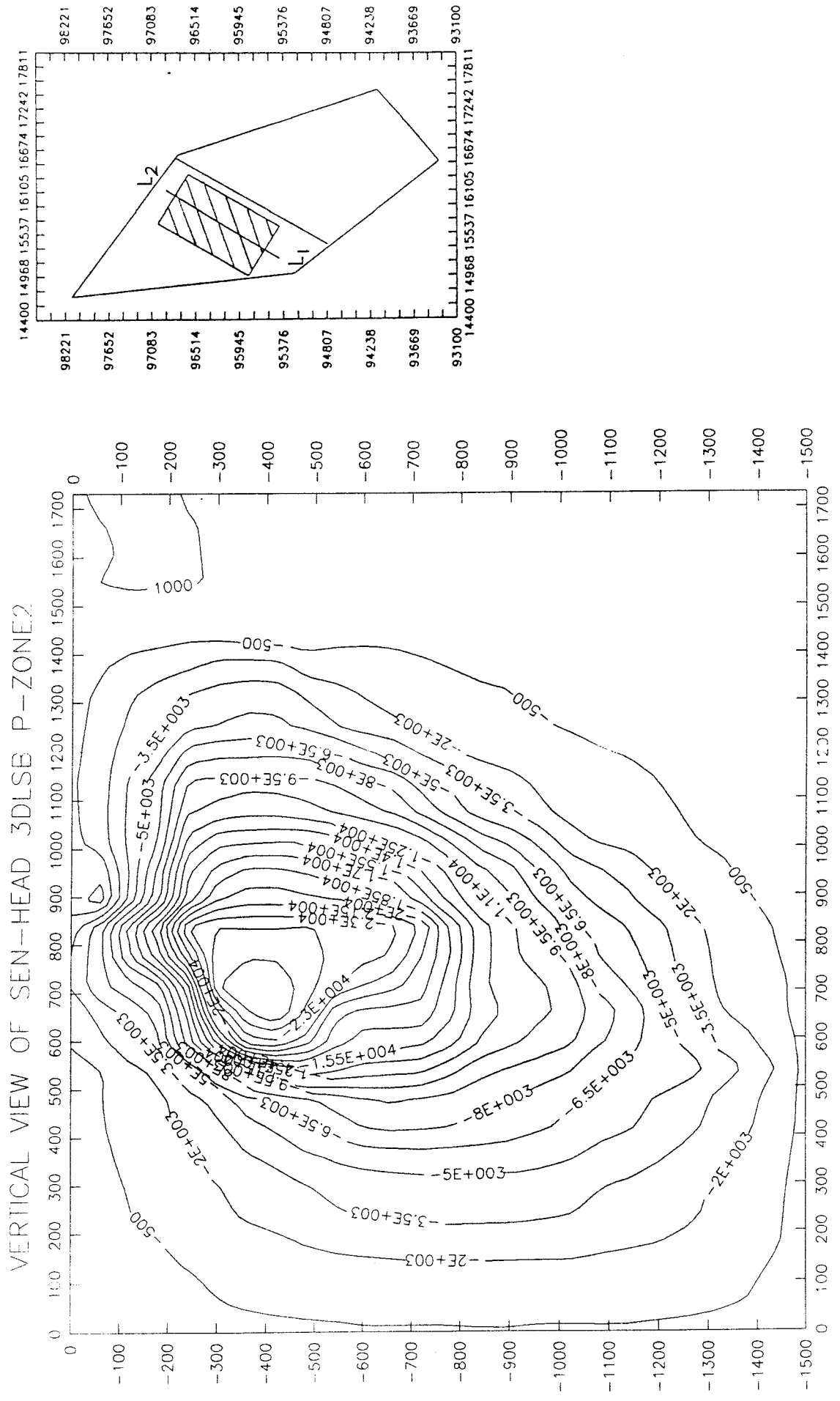


Figure B10. Contour lines in a vertical cross-section through the flow domain in case 3DLSB, showing distribution of the piezometric head sensitivity to perturbation of the hydraulic conductivity in zone 2.

Figure B11 Contour lines in a horizontal cross-section (z = -500 m) through the flow domain of case 3DLSR, showing the distribution of the piezometric head sensitivity to perturbation of the hydraulic conductivity in zone 2.

Figure B12 Contour lines in a horizontal cross-section (z = -500 m) through the flow domain of case 3DLSB, showing the distribution of the piezometric head sensitivity to perturbation of the hydraulic conductivity in zone 2.

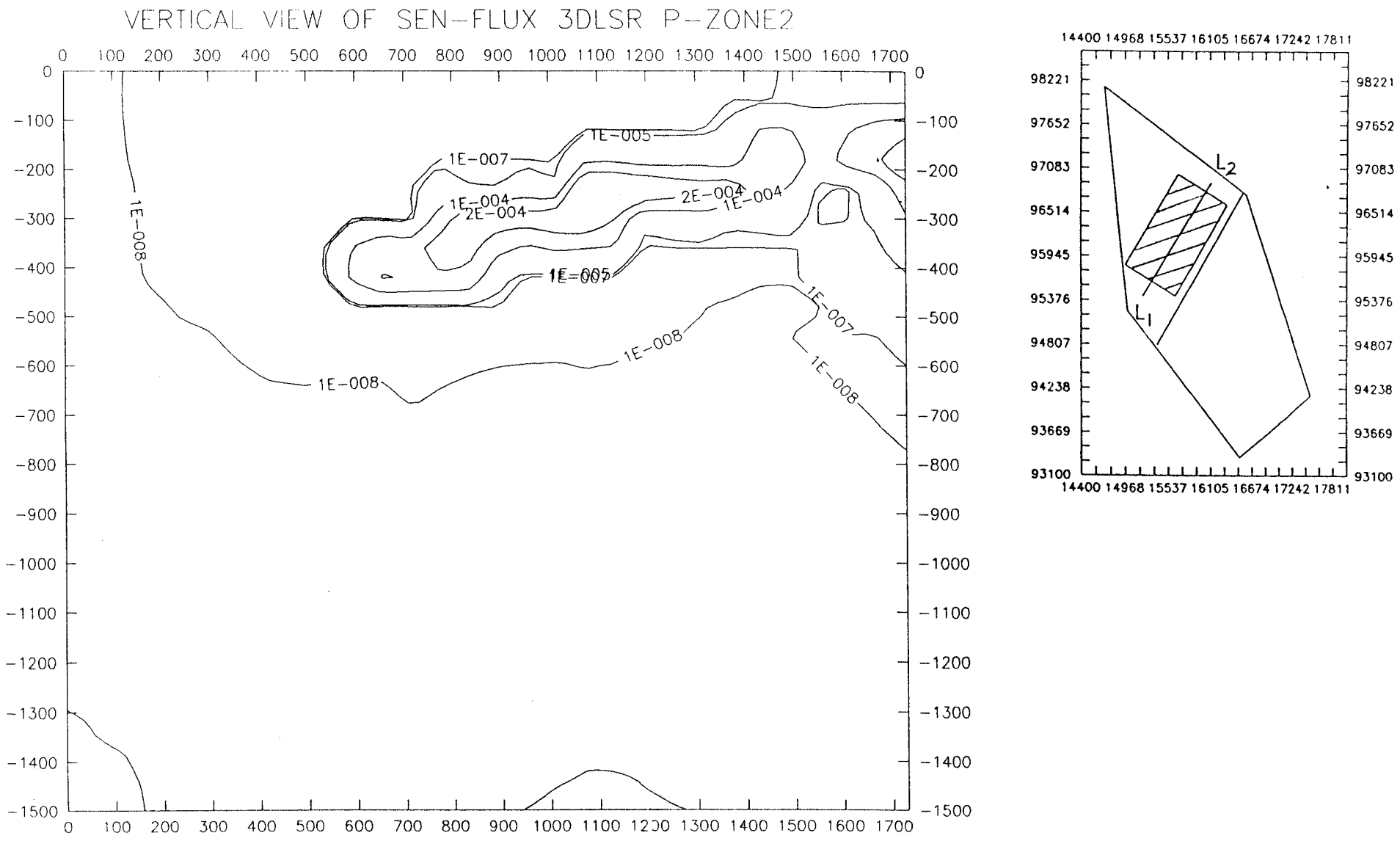


Figure B13 Contour lines showing the distribution of sensitivity of the Darcy flux across a vertical cross-section through the flow domain in case 3DLSR.

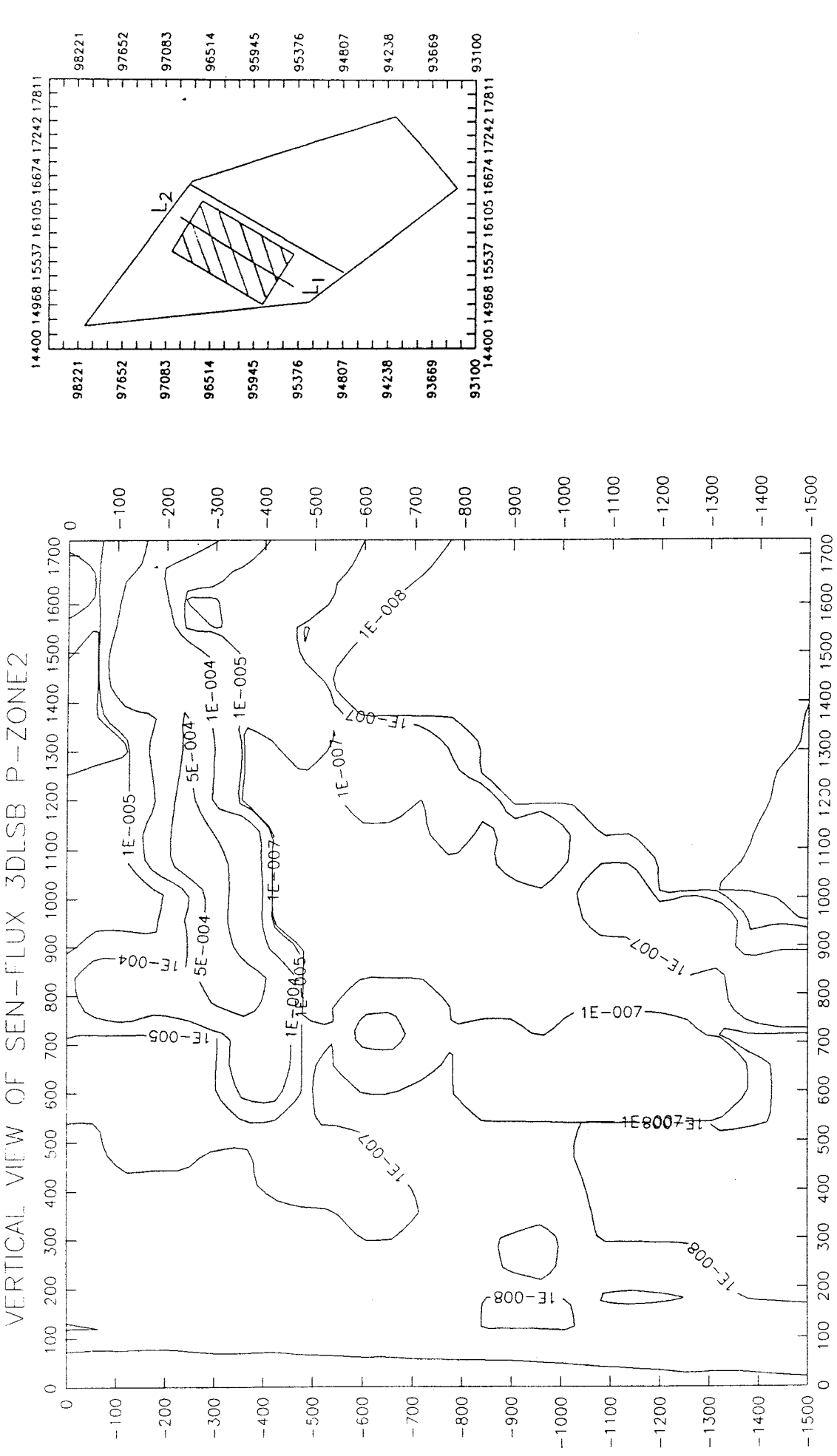


Figure B14 Contour lines showing the distribution of sensitivity of the Darcy flux across a vertical cross-section through the flow domain in case 3DLSB.

## APPENDIX C Graphical display of sensitivity to perturbations in the prescribed pressure boundary

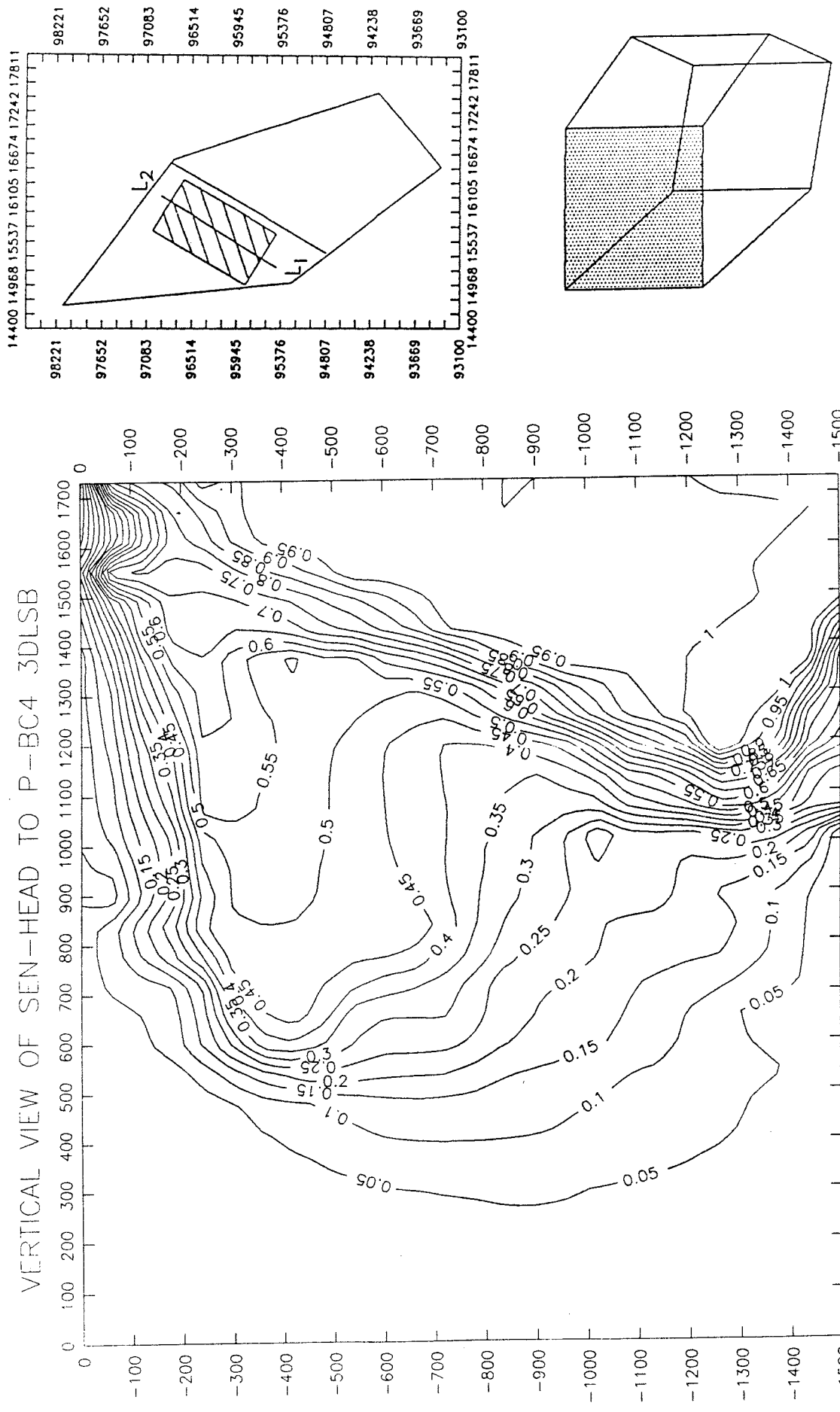


Figure C1. Contour lines in a vertical section through the flow domain in case 3DLSB, showing the distribution of the piezometric head sensitivity (normalized) to perturbation of the north lateral boundary (zone 4).

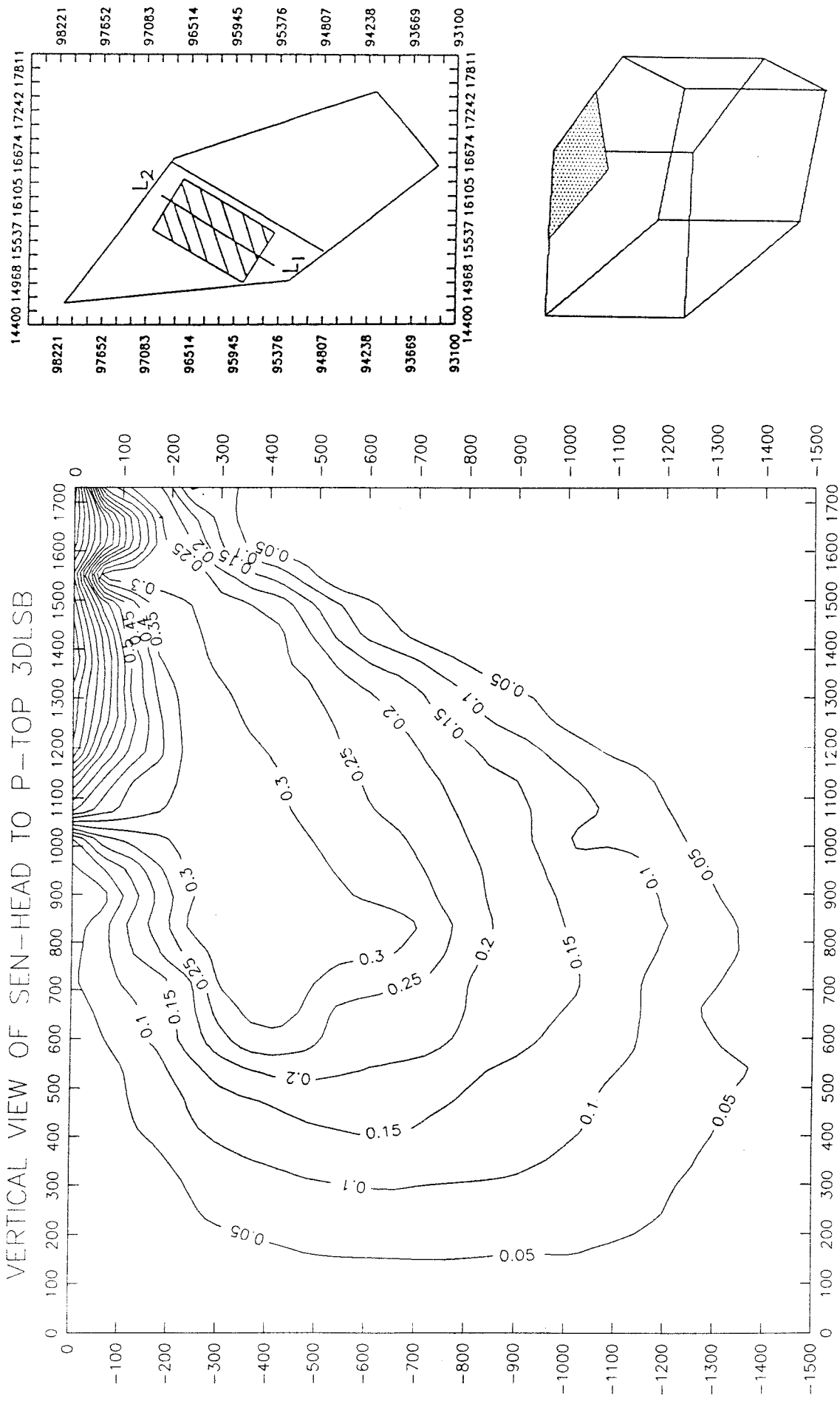


Figure C2. Contour lines in a vertical section through the flow domain in case 3DLSB, showing the distribution of the piezometric head sensitivity (normalized) to perturbation of the top boundary at the north-eastern corner.

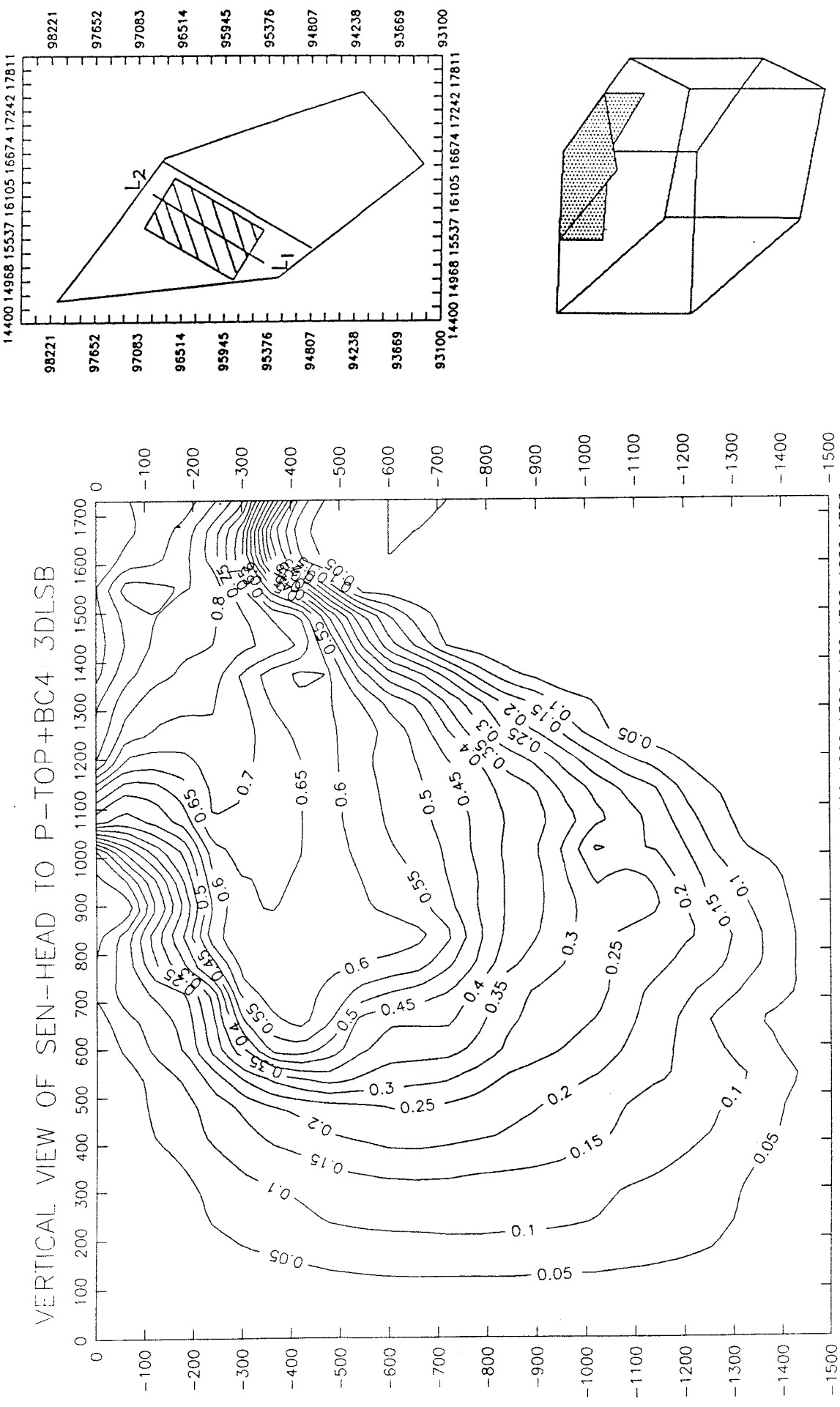


Figure C3. Contour lines in a vertical section through the flow domain in case 3DLSB, showing the distribution of the piezometric head sensitivity (normalized) to perturbation of the top boundary on north-eastern corner including parts of the lateral boundaries.

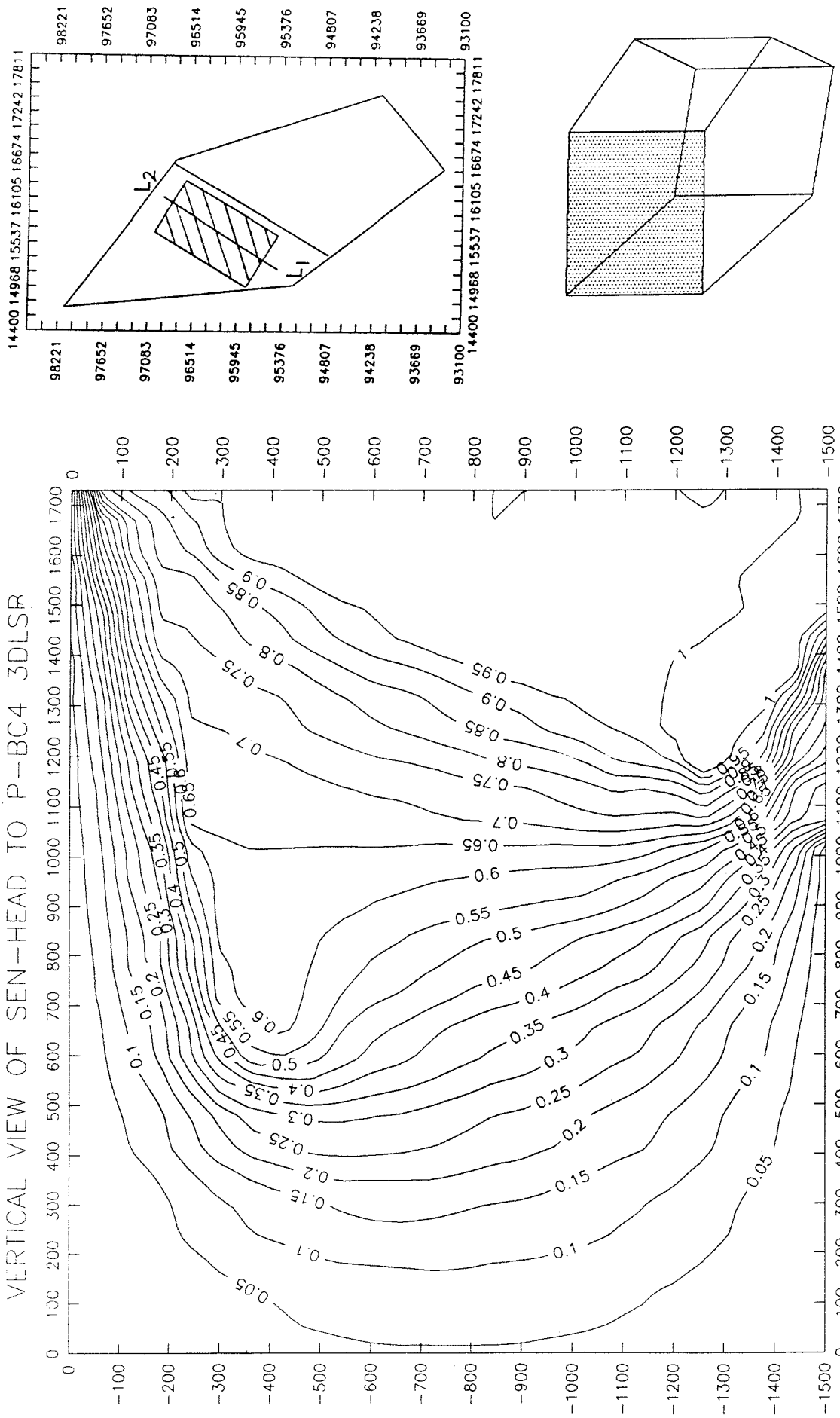


Figure C4 Contour lines in a vertical section through the flow domain in case 3DLSR, showing the distribution of the piezometric head sensitivity (normalized) to perturbation of the north lateral boundary (fracture zone 4).

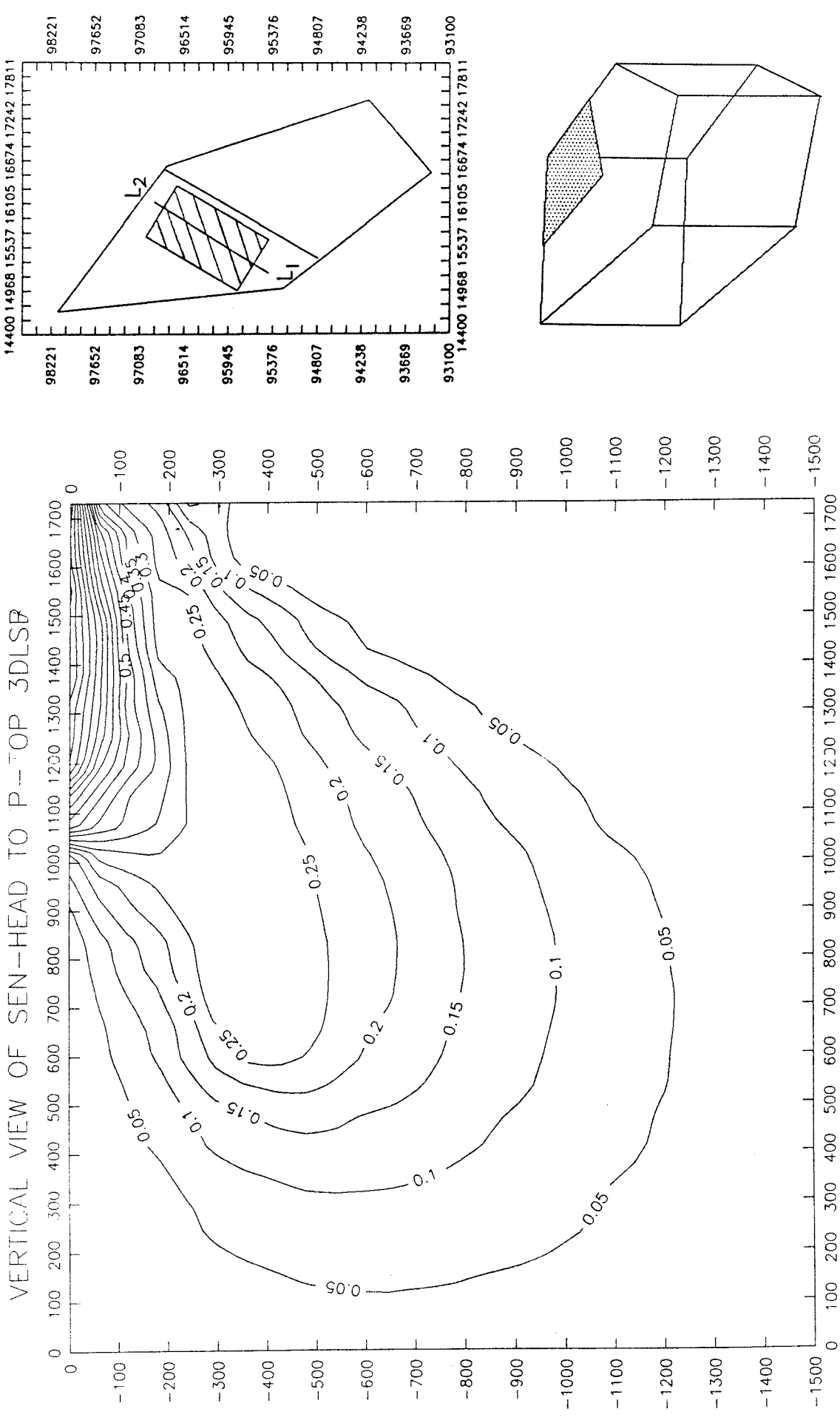


Figure C5. Contour lines in a vertical section through the flow domain in case 3DLSR, showing the distribution of the piezometric head sensitivity (normalized) to perturbation of the top boundary at the north-eastern corner.

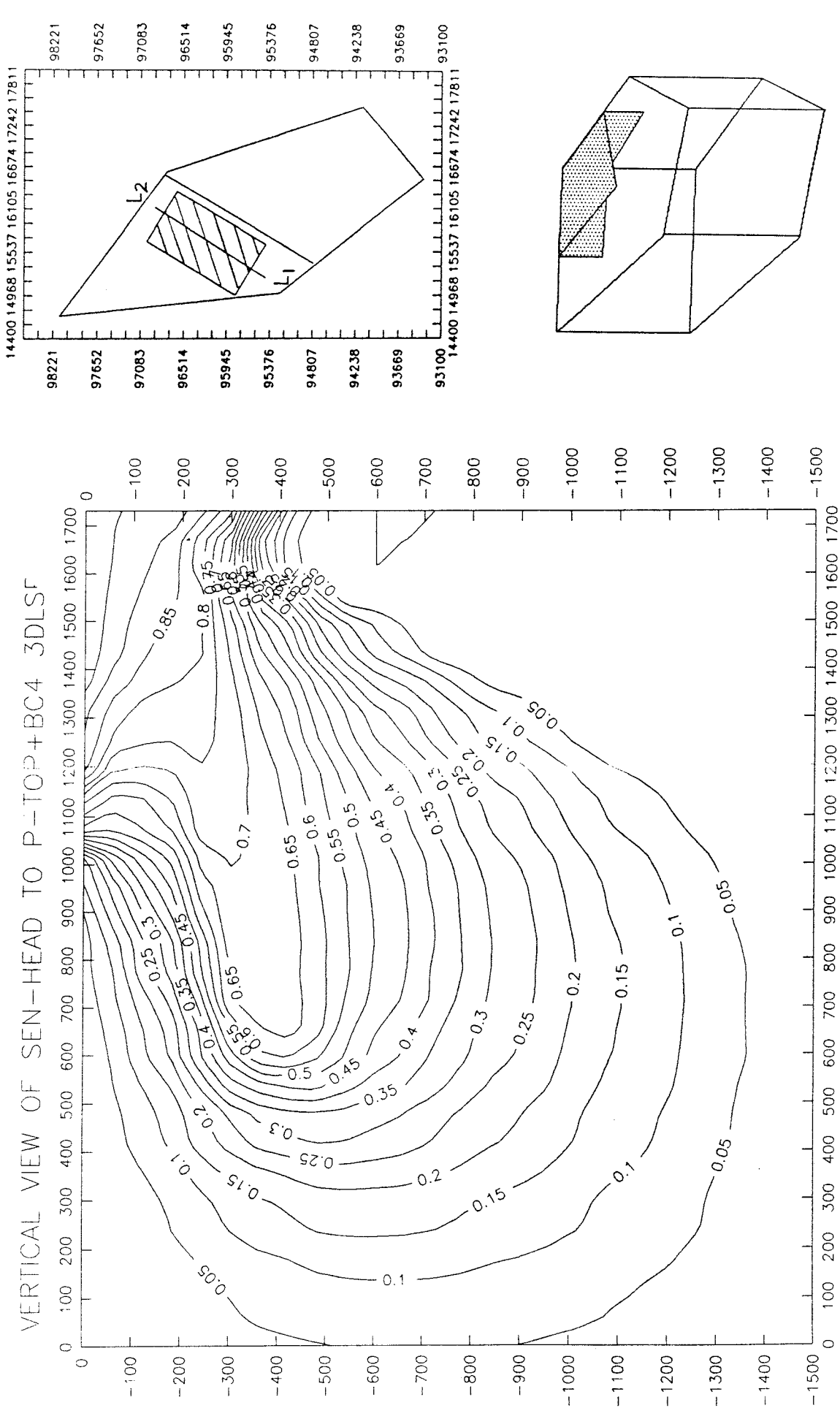


Figure C6. Contour lines in a vertical section through the flow domain in case 3DLSR, showing the distribution of the piezometric head sensitivity (normalized) to perturbation of the top boundary at the north-eastern corner including parts of the lateral boundaries.

Figure C7. Contour lines in a horizontal section (z = -500 m) through the flow domain in case 3DLSB, showing the distribution of the piezometric head sensitivity (normalized) to perturbation of the north lateral boundary ( zone 4).

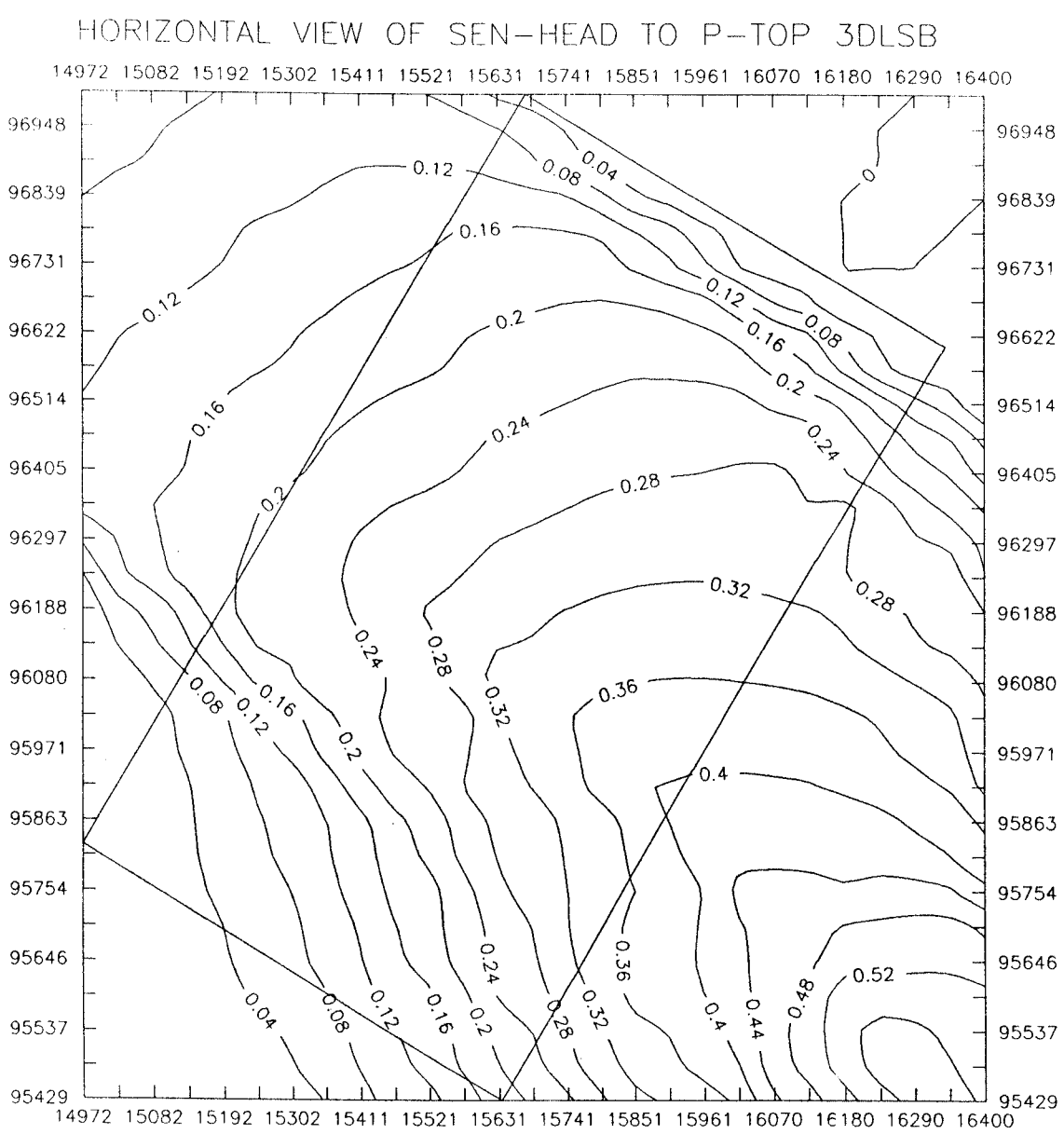


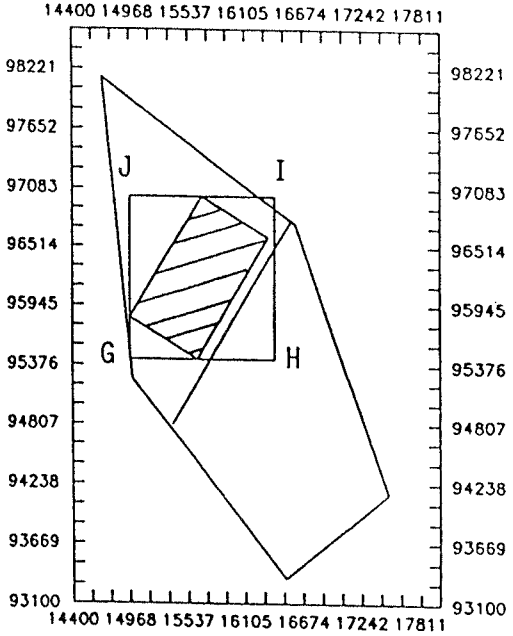


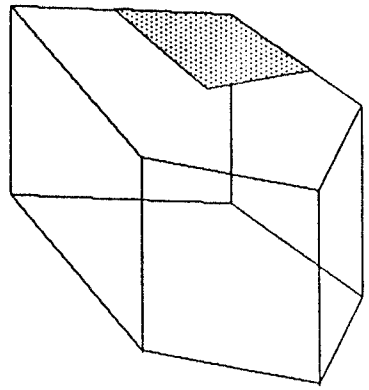

Figure C8. Contour lines in a horizontal section (z = -500 m) through the flow domain in case 3DLSB, showing the distribution of the piezometric head sensitivity (normalized) to perturbation of the top boundary at the north-eastern corner.

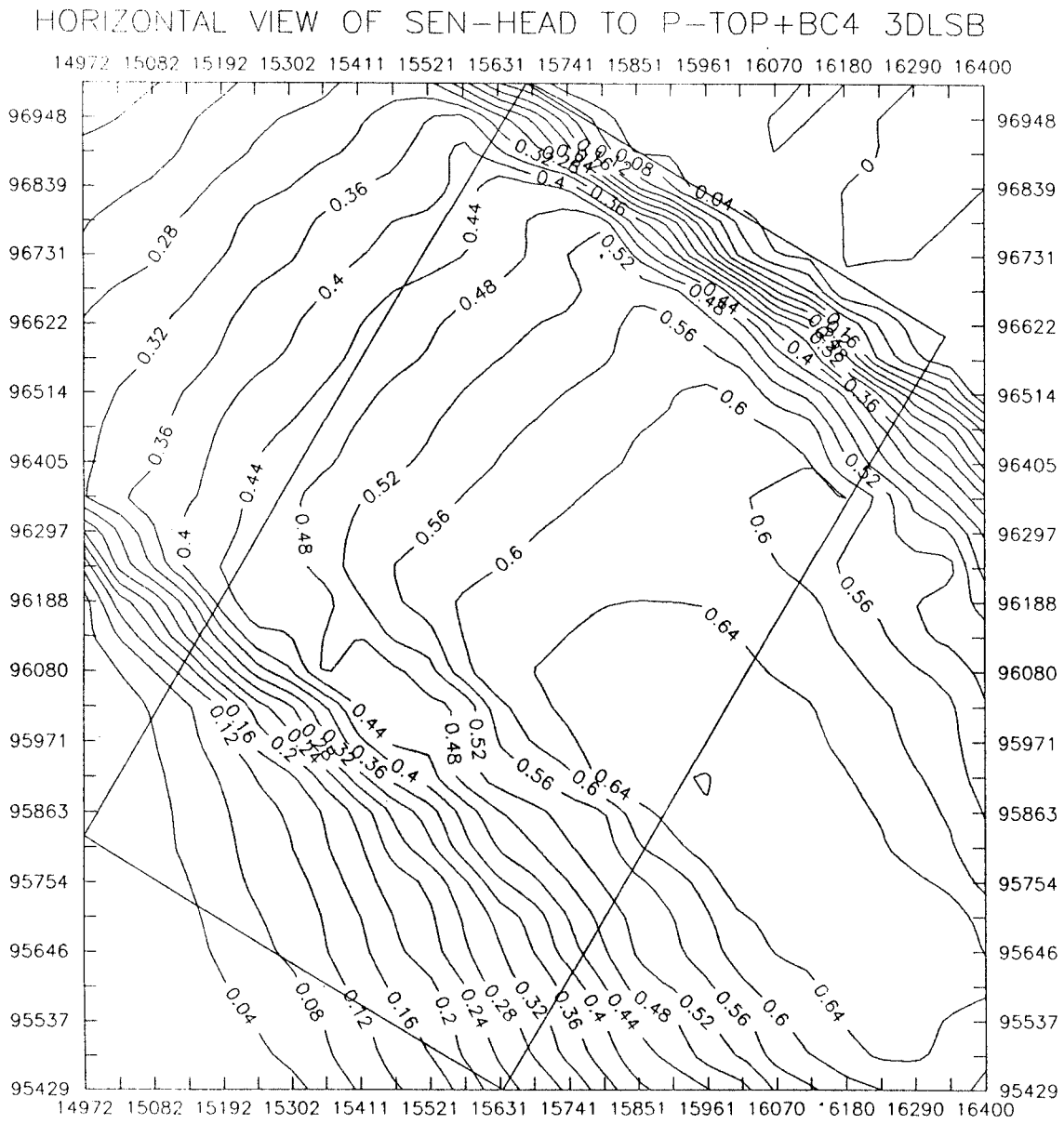


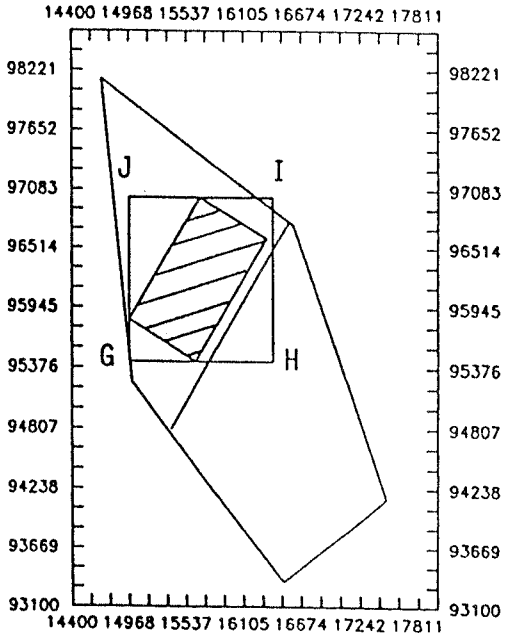


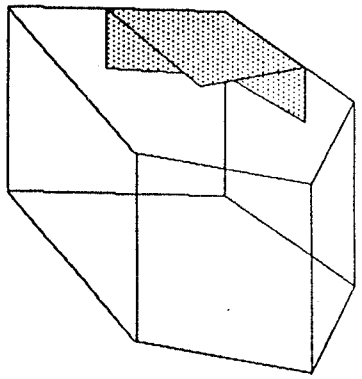

Figure C9. Contour lines in a horizontal section (z = -500 m) through the flow domain in case 3DLSB, showing the distribution of the piezometric head sensitivity (normalized) to perturbation of the top boundary at the north-eastern corner including parts of the lateral boundaries.

Figure C10. Contour lines in a horizontal section (z = -500 m) through the flow domain in case 3DLSR, showing the distribution of the piezometric head sensitivity (normalized) to perturbation of the north lateral boundary ( zone 4).

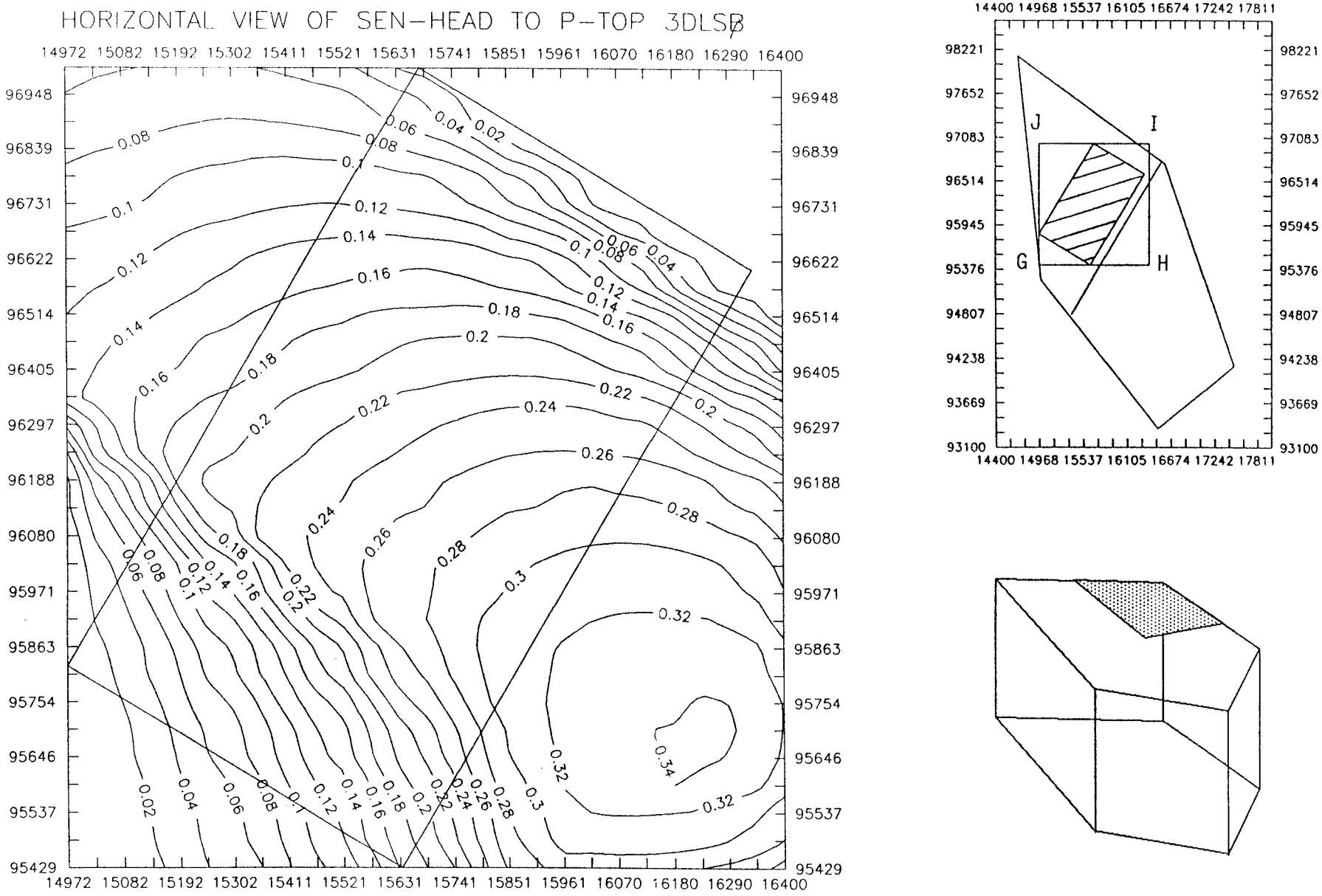







Figure C11. Contour lines in a horizontal section (z = -500 m) through the flow domain in case 3DLSR, showing the distribution of the piezometric head sensitivity (normalized) to perturbation of the top boundary at the north-eastern corner.

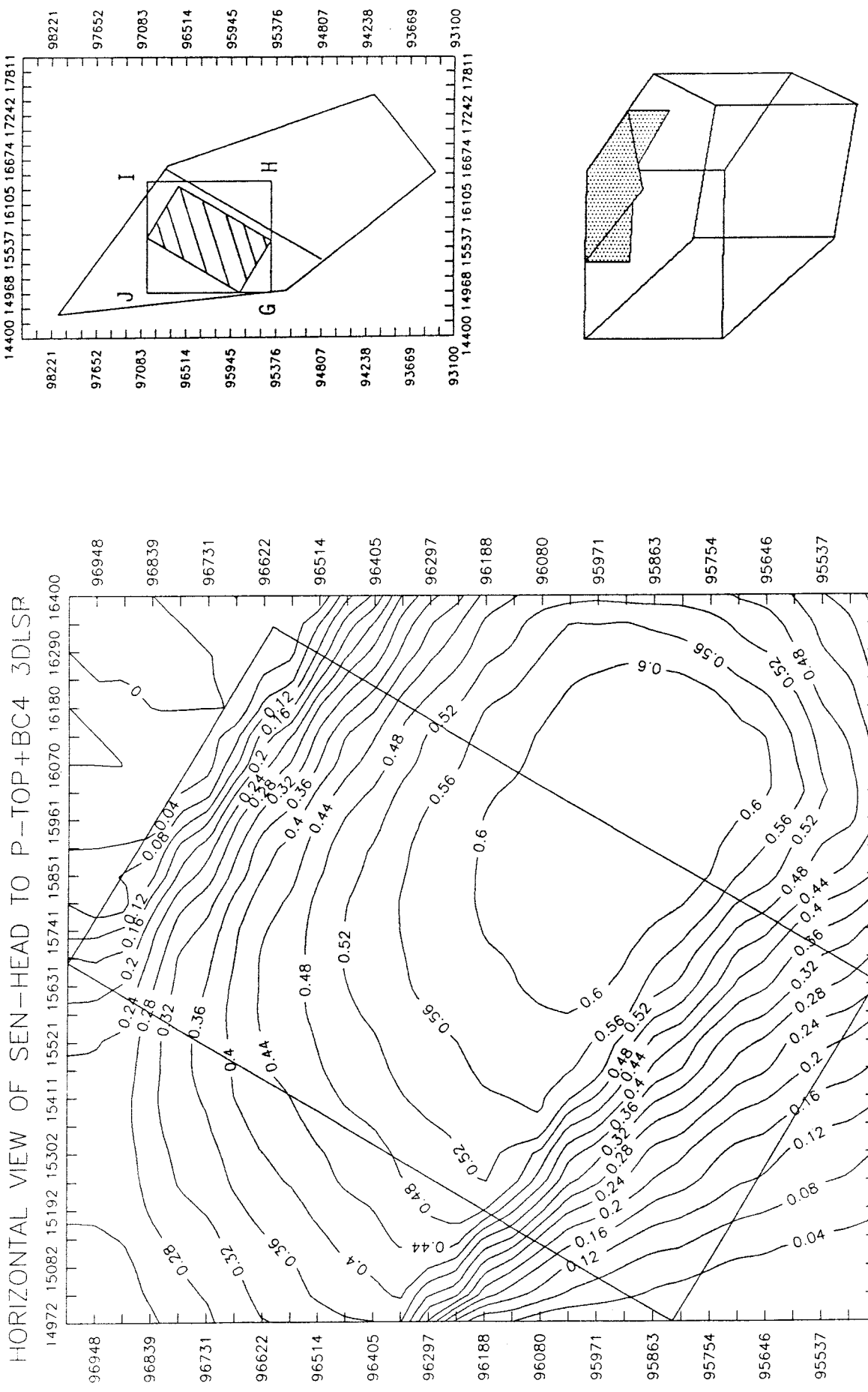


Figure C12. Contour lines in a horizontal section (z = -500 m) through the flow domain in case 3DLSR, showing the distribution of the piezometric head sensitivity (normalized) to perturbation of the top boundary at the north-eastern corner including parts of the lateral boundaries.

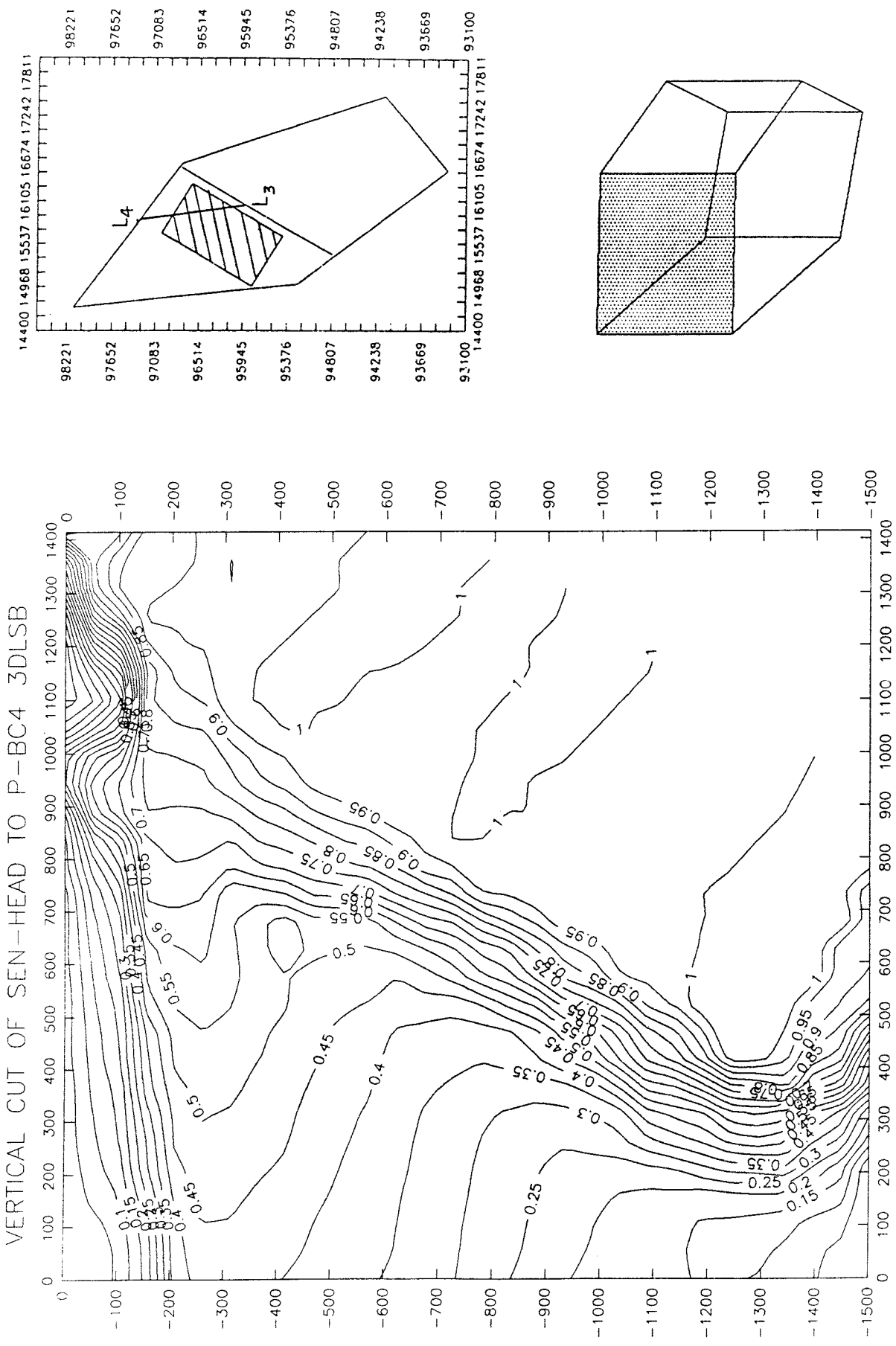


Figure C13. Contour lines in a vertical section through the north-eastern corner of flow domain in case 3DLSB, showing the distribution of the piezometric head sensitivity (normalized) to perturbation of the north lateral boundary (zone 4).

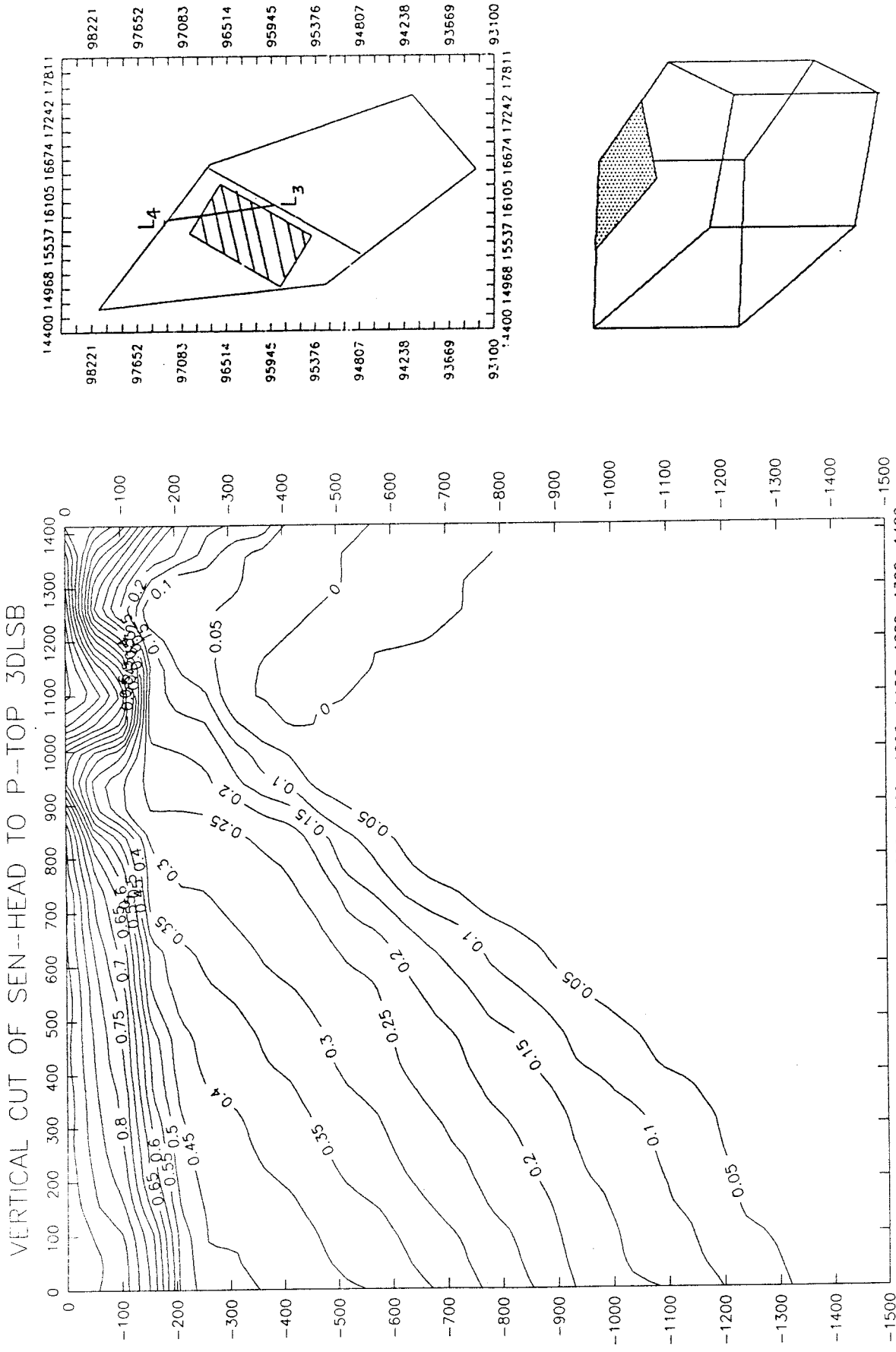


Figure C14. Contour lines in a vertical section through the north-eastern corner of flow domain in case 3DLSB, showing the distribution of the piezometric head sensitivity (normalized) to perturbation of the top boundary at the north-eastern corner.

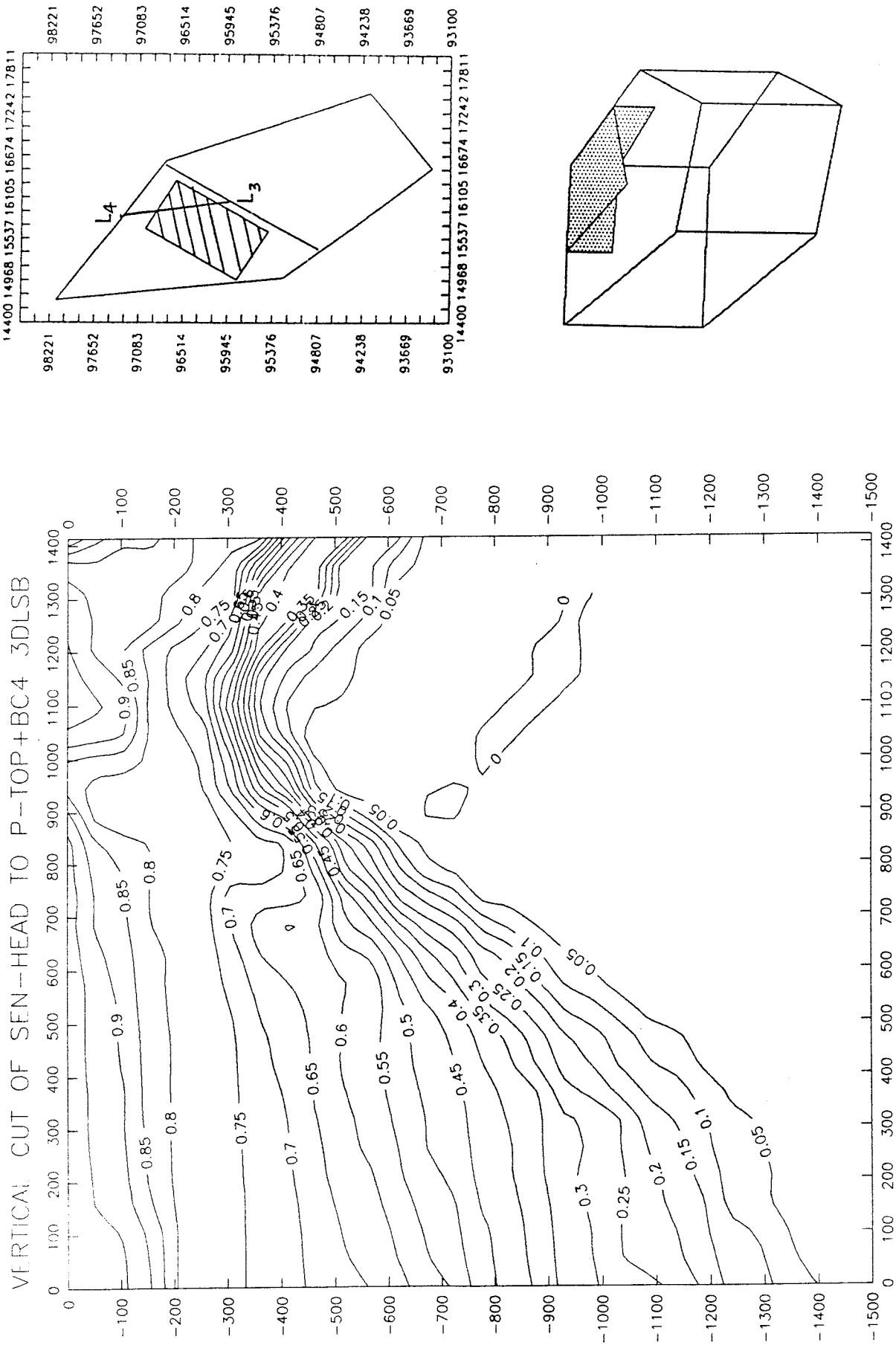


Figure C15. Contour lines in a vertical section through the north-eastern corner of flow domain in case 3DLSB, showing the distribution of the piezometric head sensitivity (normalized) to perturbation of the top boundary at the north-eastern corner including parts of the lateral boundaries.

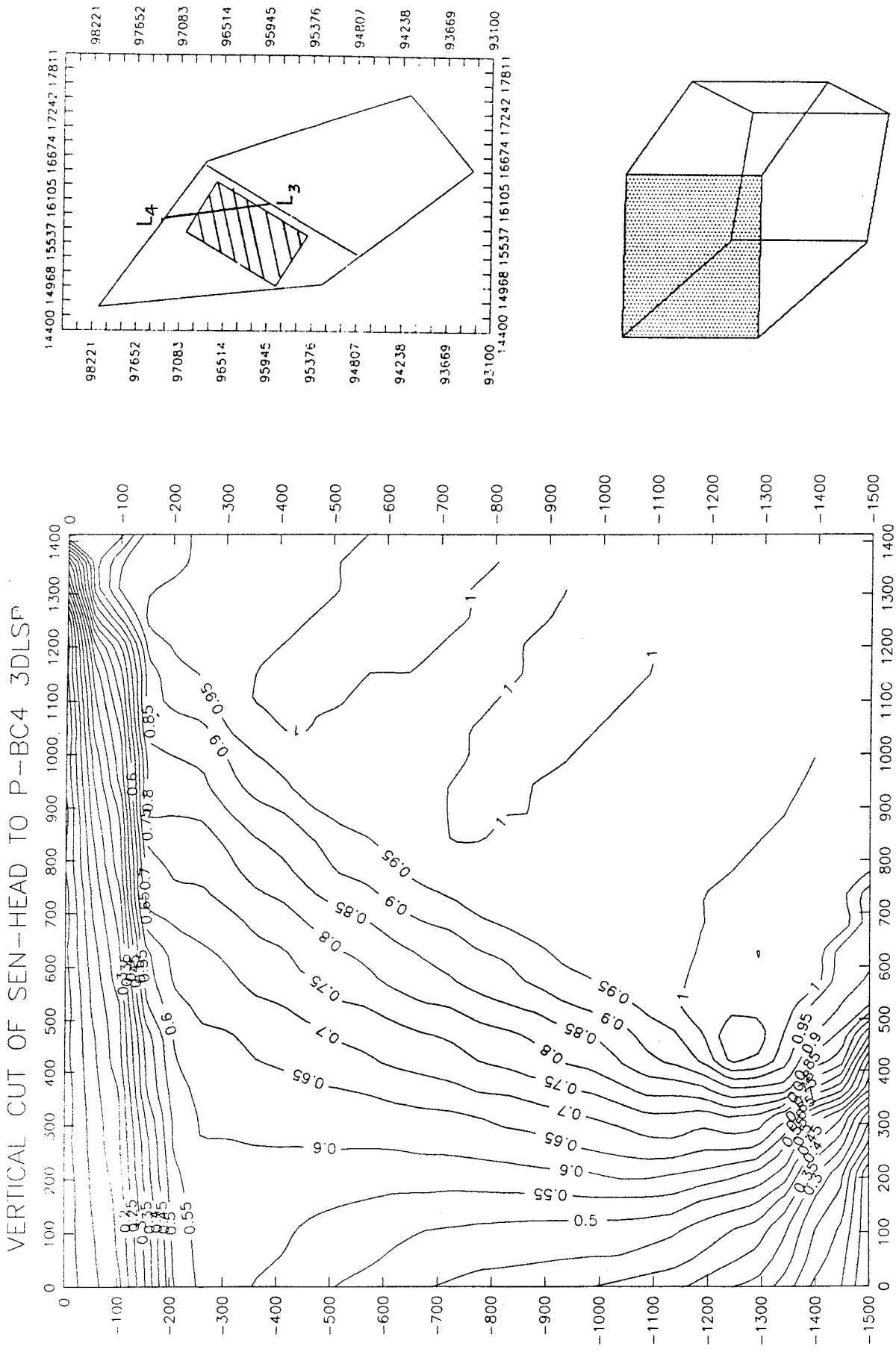


Figure C16. Contour lines in a vertical section through the north-eastern corner of flow domain in case 3DLSR, showing the distribution of the piezometric head sensitivity (normalized) to perturbation of the north lateral boundary (zone 4).

Figure C17. Contour lines in a vertical section through the north-eastern corner of flow domain in case 3DLSR, showing the distribution of the piezometric head sensitivity (normalized) to perturbation of the top boundary at the north-eastern corner.

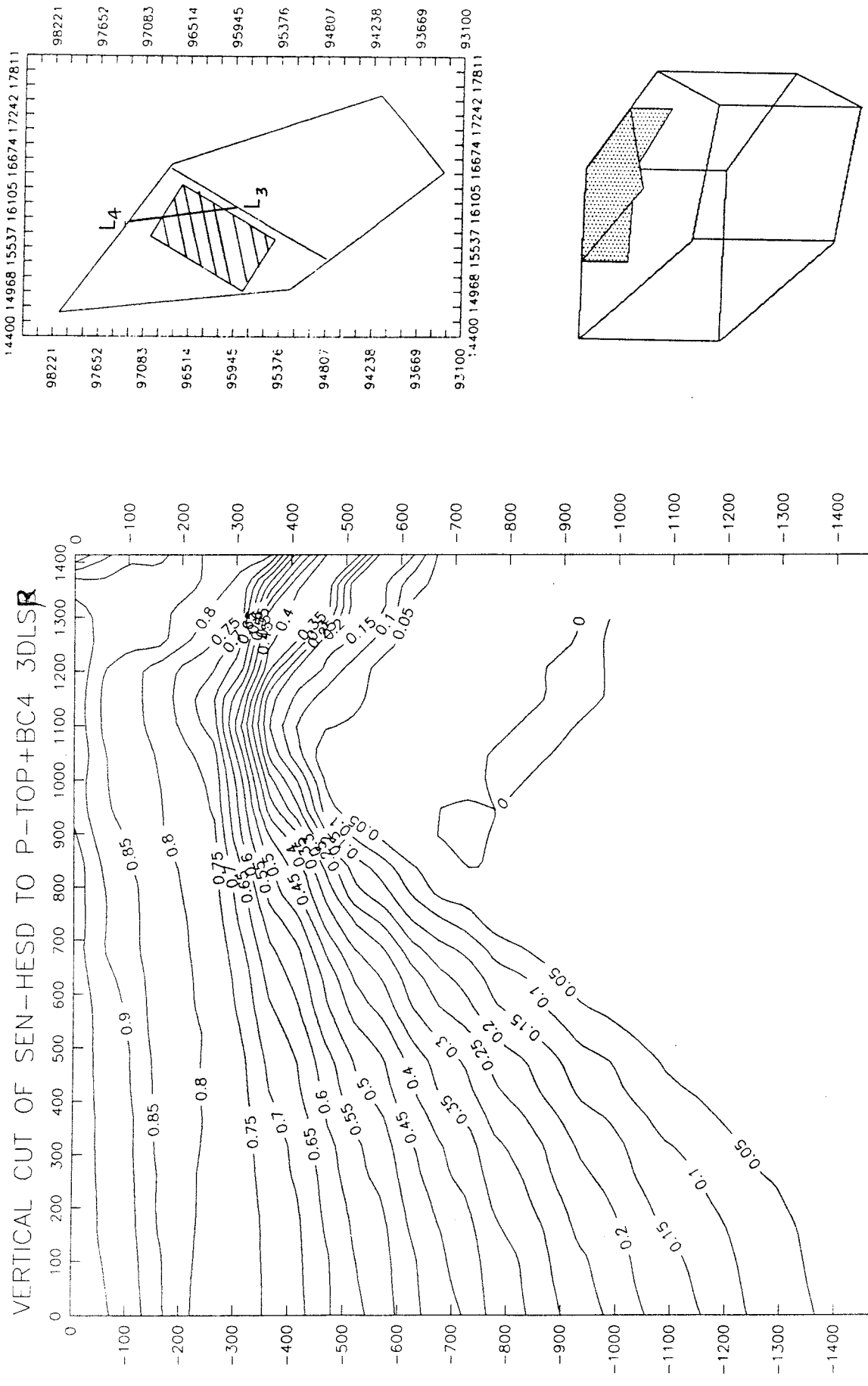


Figure C18. Contour lines in a vertical section through the north-eastern corner of flow domain in case 3DLSR, showing the distribution of the piezometric head sensitivity (normalized) to perturbation of the top boundary at the north-eastern corner including parts of the lateral boundaries.

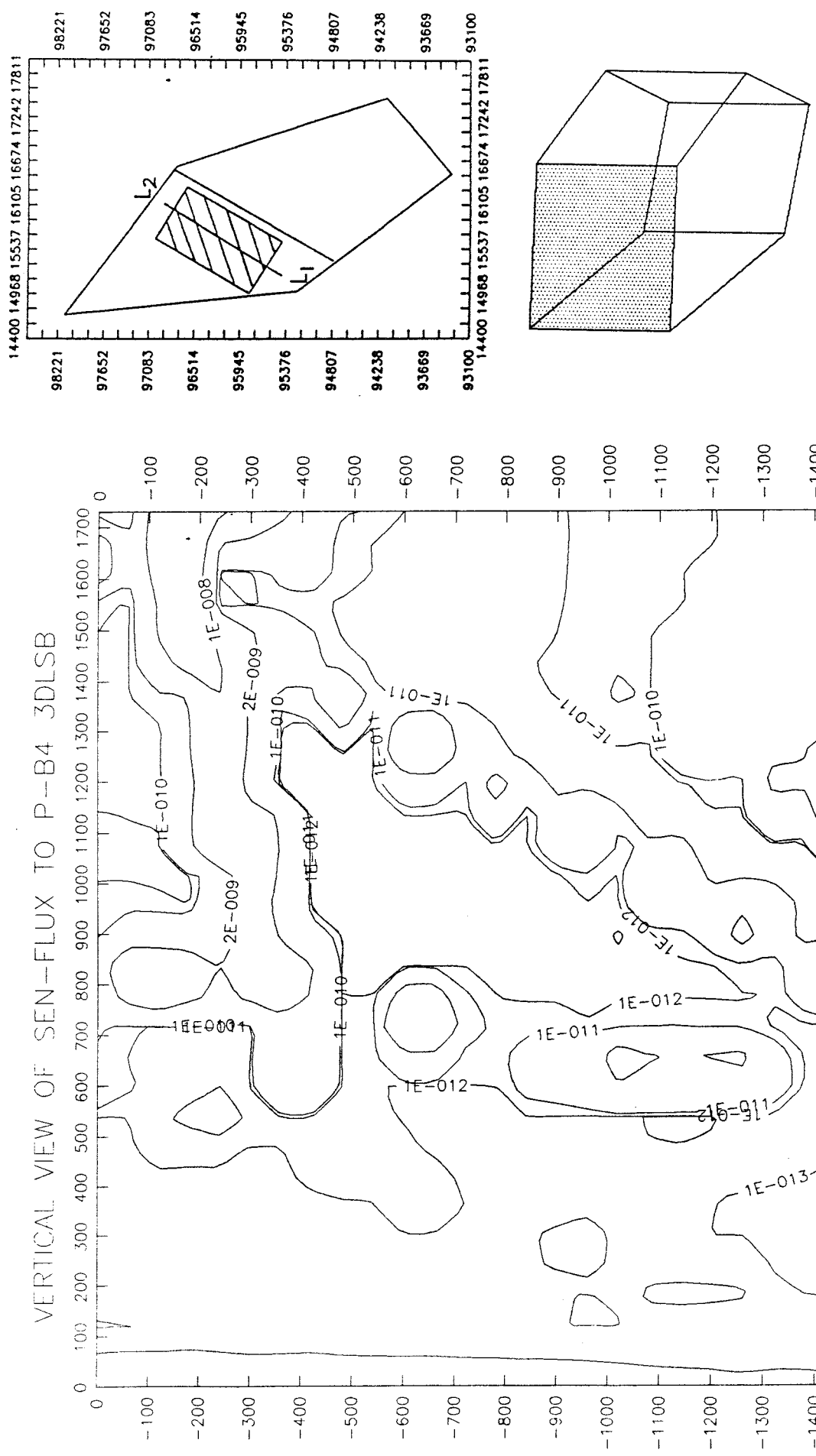


Figure C19. Contour lines in a vertical section through the flow domain in case 3DLSB, showing the distribution of the flux sensitivity (1/s) to perturbation of the north lateral boundary (zone 4).

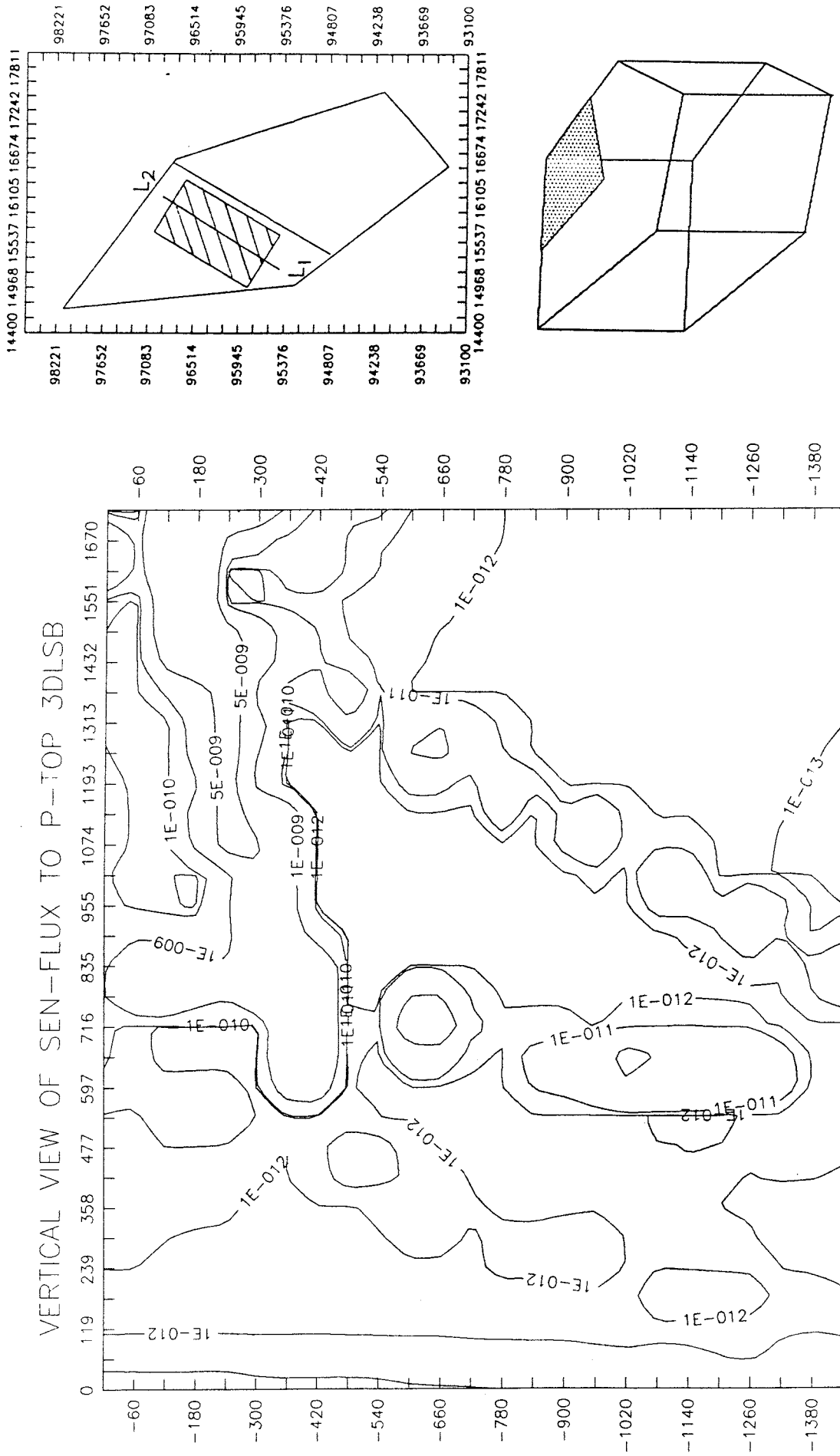


Figure C20. Contour lines in a vertical section through the flow domain in case 3DLSB, showing the distribution of the flux sensitivity (1/s) to perturbation of the top boundary at the north-eastern corner.

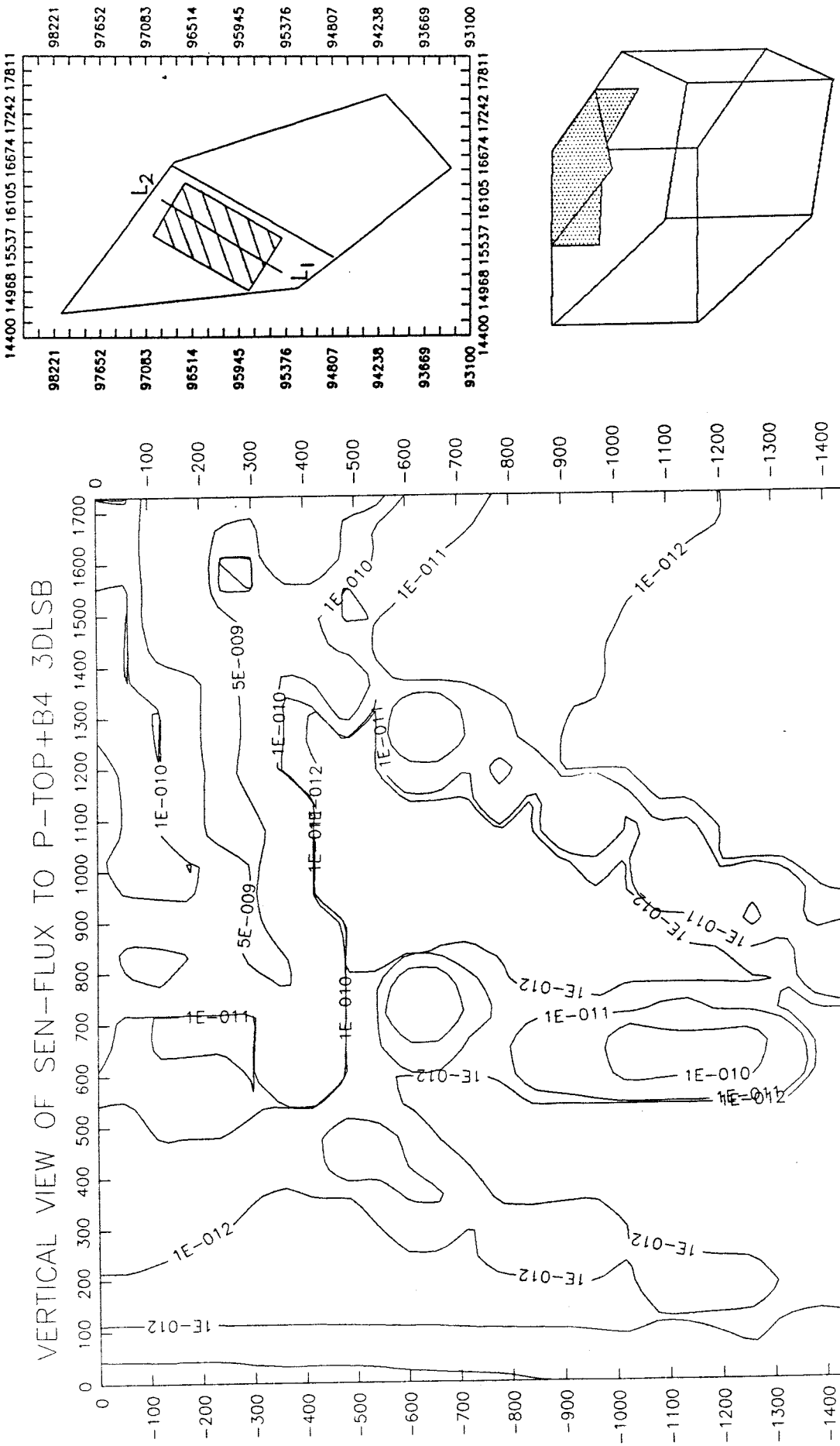


Figure C21. Contour lines in a vertical section through the flow domain in case 3DLSB, showing the distribution of the flux sensitivity (1/s) to perturbation of the top boundary at the north-eastern corner including parts of the lateral boundaries.

Figure C22. Contour lines in a horizontal section (z = -500 m) through the flow domain in case 3DLSB, showing the distribution of the flux sensitivity (1/s) to perturbation of the north lateral boundary (zone 4).

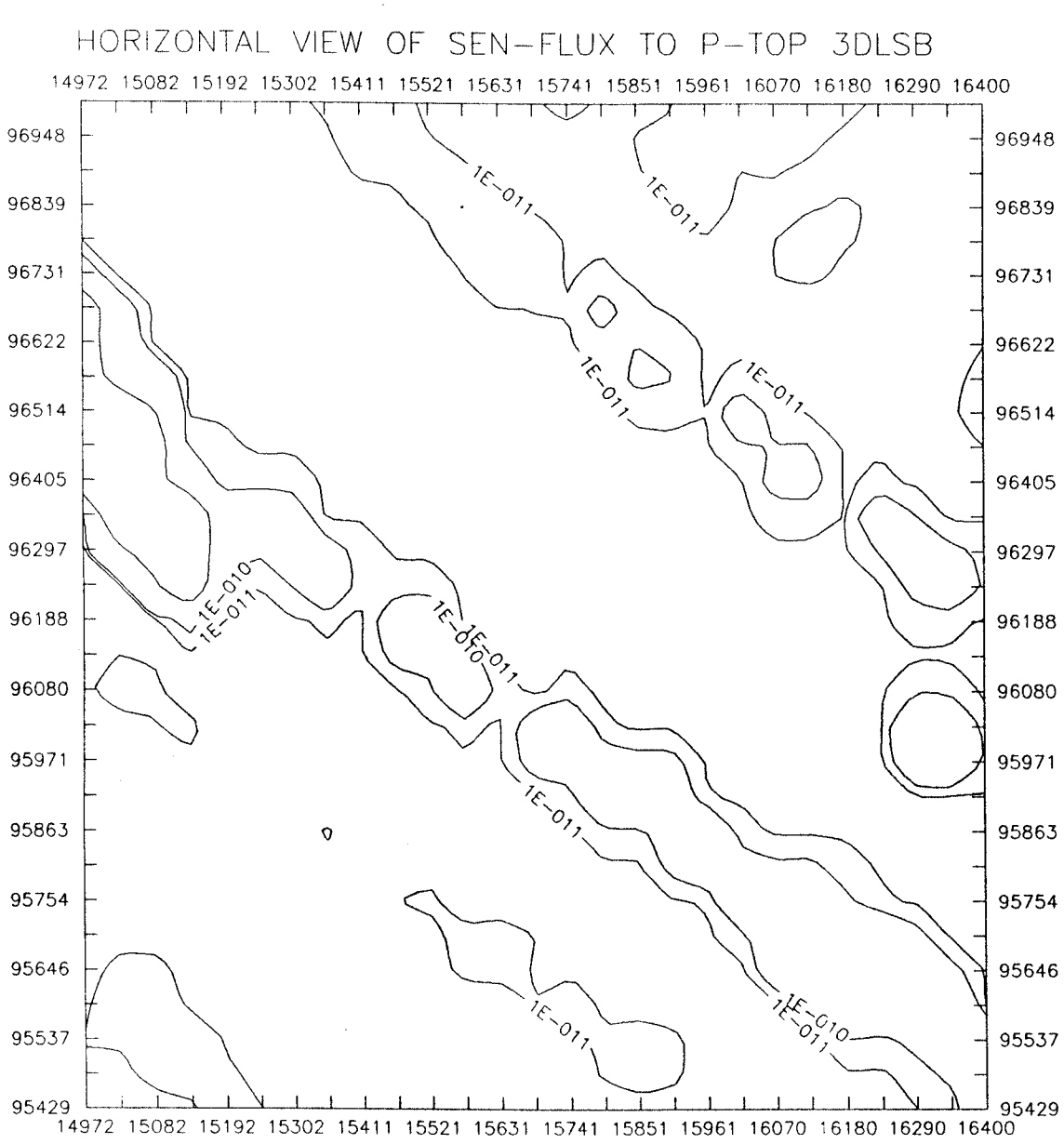


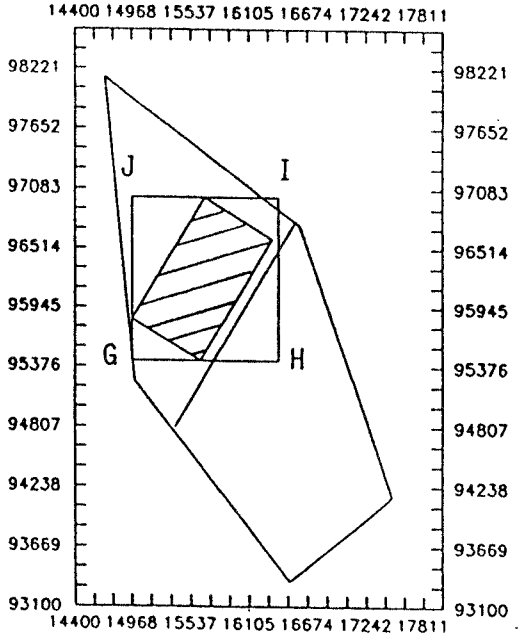


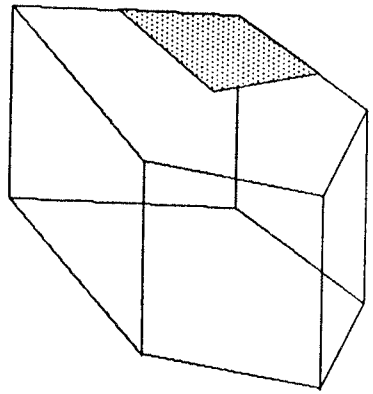

Figure C23. Contour lines in a horizontal section (z = -500 m) through the flow domain in case 3DLSB, showing the distribution of the flux sensitivity (1/s) to perturbation of the top boundary at the north-eastern corner.

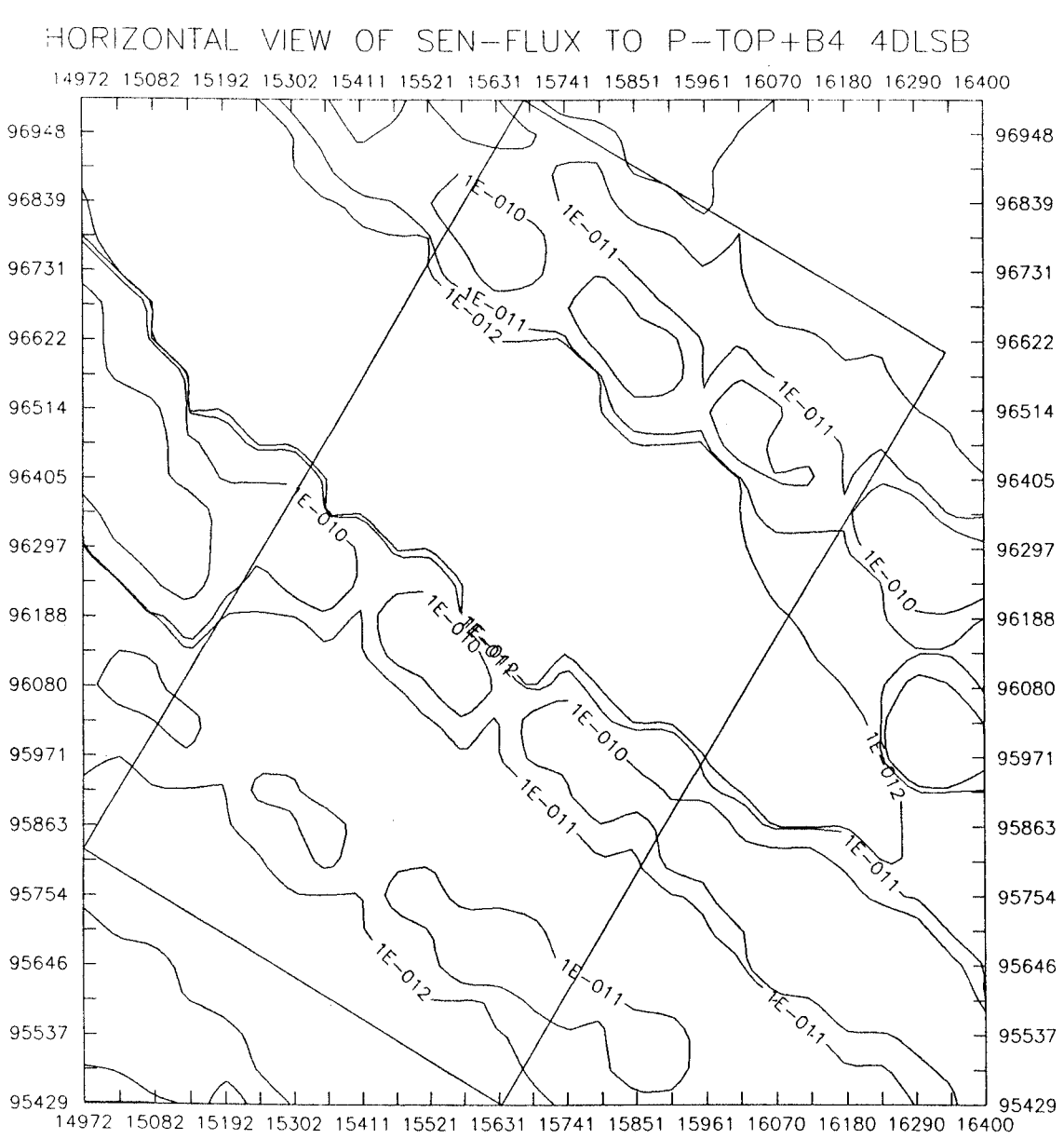


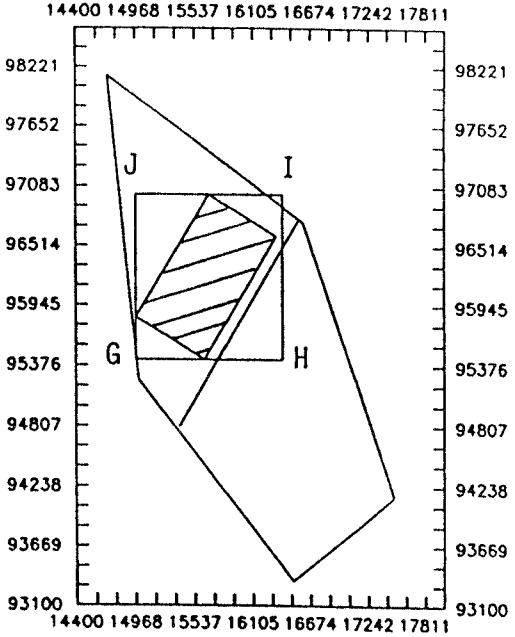


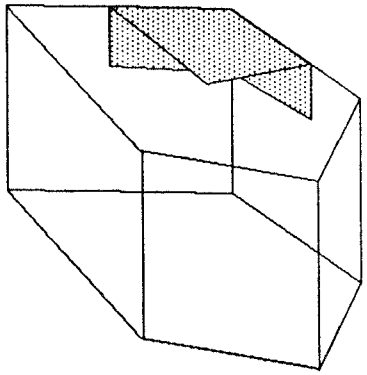

Figure C24. Contour lines in a horizontal section (z = -500 m) through the flow domain in case 3DLSB, showing the distribution of the flux sensitivity (1/s) to perturbation of the top boundary at the north-eastern corner including parts of the lateral boundaries.

# *List of SKB reports*

## Annual Reports

*1977-78*
TR 121
**KBS Technical Reports 1 – 120**
Summaries
Stockholm, May 1979

*1979*
TR 79-28
**The KBS Annual Report 1979**
KBS Technical Reports 79-01 – 79-27
Summaries
Stockholm, March 1980

*1980*
TR 80-26
**The KBS Annual Report 1980**
KBS Technical Reports 80-01 – 80-25
Summaries
Stockholm, March 1981

*1981*
TR 81-17
**The KBS Annual Report 1981**
KBS Technical Reports 81-01 – 81-16
Summaries
Stockholm, April 1982

*1982*
TR 82-28
**The KBS Annual Report 1982**
KBS Technical Reports 82-01 – 82-27
Summaries
Stockholm, July 1983

*1983*
TR 83-77
**The KBS Annual Report 1983**
KBS Technical Reports 83-01 – 83-76
Summaries
Stockholm, June 1984

*1984*
TR 85-01
**Annual Research and Development Report 1984**
Including Summaries of Technical Reports Issued during 1984. (Technical Reports 84-01 – 84-19)
Stockholm, June 1985

*1985*
TR 85-20
**Annual Research and Development Report 1985**
Including Summaries of Technical Reports Issued during 1985. (Technical Reports 85-01 – 85-19)
Stockholm, May 1986

*1986*
TR 86-31
**SKB Annual Report 1986**
Including Summaries of Technical Reports Issued during 1986
Stockholm, May 1987

*1987*
TR 87-33
**SKB Annual Report 1987**
Including Summaries of Technical Reports Issued during 1987
Stockholm, May 1988

*1988*
TR 88-32
**SKB Annual Report 1988**
Including Summaries of Technical Reports Issued during 1988
Stockholm, May 1989

*1989*
TR 89-40
**SKB Annual Report 1989**
Including Summaries of Technical Reports Issued during 1989
Stockholm, May 1990

*1990*
TR 90-46
**SKB Annual Report 1990**
Including Summaries of Technical Reports Issued during 1990
Stockholm, May 1991

## Technical Reports

### List of SKB Technical Reports 1991

TR 91-01
**Description of geological data in SKB's database GEOTAB**
**Version 2**
Stefan Sehlstedt, Tomas Stark
SGAB, Luleå
January 1991

TR 91-02
**Description of geophysical data in SKB database GEOTAB**
**Version 2**
Stefan Sehlstedt
SGAB, Luleå
January 1991

TR 91-03
**1. The application of PIE techniques to the study of the corrosion of spent oxide fuel in deep-rock ground waters**
**2. Spent fuel degradation**
R S Forsyth
Studsvik Nuclear
January 1991

TR 91-04
**Plutonium solubilities**
I Puigdomènech[1], J Bruno[2]
[1]Enviromental Services, Studsvik Nuclear, Nyköping, Sweden
[2]MBT Tecnologia Ambiental, CENT, Cerdanyola, Spain
February 1991

TR 91-05
**Description of tracer data in the SKB database GEOTAB**
SGAB, Luleå
April, 1991

TR 91-06
**Description of background data in the SKB database GEOTAB**
**Version 2**
Ebbe Eriksson, Stefan Sehlstedt
SGAB, Luleå
March 1991

TR 91-07
**Description of hydrogeological data in the SKB's database GEOTAB**
**Version 2**
Margareta Gerlach[1], Bengt Gentzschein[2]
[1]SGAB, Luleå
[2]SGAB, Uppsala
April 1991

TR 91-08
**Overview of geologic and geohydrologic conditions at the Finnsjön site and its surroundings**
Kaj Ahlbom[1], Sven Tirén[2]
[1]Conterra AB
[2]Sveriges Geologiska AB
January 1991

TR 91-09
**Long term sampling and measuring program. Joint report for 1987, 1988 and 1989. Within the project: Fallout studies in the Gideå and Finnsjö areas after the Chernobyl accident in 1986**
Thomas Ittner
SGAB, Uppsala
December 1990

TR 91-10
**Sealing of rock joints by induced calcite precipitation. A case study from Bergeforsen hydro power plant**
Eva Hakami[1], Anders Ekstav[2], Ulf Qvarfort[2]
[1]Vattenfall HydroPower AB
[2]Golder Geosystem AB
January 1991

TR 91-11
**Impact from the disturbed zone on nuclide migration – a radioactive waste repository study**
Akke Bengtsson[1], Bertil Grundfelt[1], Anders Markström[1], Anders Rasmuson[2]
[1]KEMAKTA Konsult AB
[2]Chalmers Institute of Technology
January 1991

TR 91-12
**Numerical groundwater flow calculations at the Finnsjön site**
Björn Lindbom, Anders Boghammar, Hans Lindberg, Jan Bjelkås
KEMAKTA Consultants Co, Stockholm
February 1991

TR 91-13
**Discrete fracture modelling of the Finnsjön rock mass**
**Phase 1 feasibility study**
J E Geier, C-L Axelsson
Golder Geosystem AB, Uppsala
March 1991

TR 91-14
**Channel widths**
Kai Palmqvist, Marianne Lindström
BERGAB-Berggeologiska Undersökningar AB
February 1991

TR 91-15
**Uraninite alteration in an oxidizing environment and its relevance to the disposal of spent nuclear fuel**
Robert Finch, Rodney Ewing
Department of Geology, University of New Mexico
December 1990

TR 91-16
**Porosity, sorption and diffusivity data compiled for the SKB 91 study**
Fredrik Brandberg, Kristina Skagius
Kemakta Consultants Co, Stockholm
April 1991

TR 91-17
**Seismically deformed sediments in the Lansjärv area, Northern Sweden**
Robert Lagerbäck
May 1991

TR 91-18
**Numerical inversion of Laplace transforms using integration and convergence acceleration**
Sven-Åke Gustafson
Rogaland University, Stavanger, Norway
May 1991

TR 91-19
**NEAR21 - A near field radionuclide migration code for use with the PROPER package**
Sven Norman[1], Nils Kjellbert[2]
[1]Starprog AB
[2]SKB AB
April 1991

TR 91-20
**Äspö Hard Rock Laboratory. Overview of the investigations 1986-1990**
R Stanfors, M Erlström, I Markström
June 1991

TR 91-21
**Äspö Hard Rock Laboratory. Field investigation methodology and instruments used in the pre-investigation phase, 1986-1990**
K-E Almén, O Zellman
June 1991

TR 91-22
**Äspö Hard Rock Laboratory. Evaluation and conceptual modelling based on the pre-investigations 1986-1990**
P Wikberg, G Gustafson, I Rhén, R Stanfors
June 1991

TR 91-23
**Äspö Hard Rock Laboratory. Predictions prior to excavation and the process of their validation**
Gunnar Gustafson, Magnus Liedholm, Ingvar Rhén, Roy Stanfors, Peter Wikberg
June 1991

TR 91-24
**Hydrogeological conditions in the Finnsjön area. Compilation of data and conceptual model**
Jan-Erik Andersson, Rune Nordqvist, Göran Nyberg, John Smellie, Sven Tirén
February 1991

TR 91-25
**The role of the disturbed rock zone in radioactive waste repository safety and performance assessment. A topical discussion and international overview.**
Anders Winberg
June 1991

TR 91-26
**Testing of parameter averaging techniques for far-field migration calculations using FARF31 with varying velocity.**
Akke Bengtsson[1], Anders Boghammar[1], Bertil Grundfelt[1], Anders Rasmuson[2]
[1]KEMAKTA Consultants Co
[2]Chalmers Institute of Technology

TR 91-27
**Verification of HYDRASTAR. A code for stochastic continuum simulation of groundwater flow**
Sven Norman
Starprog AB
July 1991

TR 91-28
**Radionuclide content in surface and groundwater transformed into breakthrough curves. A Chernobyl fallout study in an forested area in Northern Sweden**
Thomas Ittner, Erik Gustafsson, Rune Nordqvist
SGAB, Uppsala
June 1991

TR 91-29
**Soil map, area and volume calculations in Orrmyrberget catchment basin at Gideå, Northern Sweden**
Thomas Ittner, P-T Tammela, Erik Gustafsson
SGAB, Uppsala
June 1991

TR 91-30
**A resistance network model for radionuclide transport into the near field surrounding a repository for nuclear waste (SKB, Near Field Model 91)**
Lennart Nilsson, Luis Moreno, Ivars Neretnieks, Leonardo Romero
Department of Chemical Engineering,
Royal Institute of Technology, Stockholm
June 1991

TR 91-31
**Near field studies within the SKB 91 project**
Hans Widén, Akke Bengtsson, Bertil Grundfelt
Kemakta Consultants AB, Stockholm
June 1991

TR 91-32
**SKB/TVO Ice age scenario**
Kaj Ahlbom[1], Timo Äikäs[2], Lars O. Ericsson[3]
[1]Conterra AB
[2]Teollisuuden Voima Oy (TVO)
[3]Svensk Kärnbränslehantering AB (SKB)
June 1991

TR 91-33
**Transient nuclide release through the bentonite barrier - SKB 91**
Akke Bengtsson, Hans Widén
Kemakta Konsult AB
May 1991

TR 91-34
**SIMFUEL dissolution studies in granitic groundwater**
I Casas[1], A Sandino[2], M S Caceci[1], J Bruno[1], K Ollila[3]
[1]MBT Tecnologia Ambiental, CENT, Cerdanyola, Spain
[2]KTH, Dpt. of Inorganic Chemistry, Stockholm, Sweden
[3]VTT, Tech. Res. Center of Finland, Espoo, Finland
September 1991

TR 91-35
**Storage of nuclear waste in long boreholes**
Håkan Sandstedt[1], Curt Wichmann[1], Roland Pusch[2], Lennart Börgesson[2], Bengt Lönnerberg[3]
[1]Tyréns
[2]Clay Technology AB
[3]ABB Atom
August 1991

TR 91-36
**Tentative outline and siting of a repository for spent nuclear fuel at the Finnsjön site. SKB 91 reference concept**
Lars Ageskog, Kjell Sjödin
VBB VIAK
September 1991

TR 91-37
**Creep of OFHC and silver copper at simulated final repository canister-service conditions**
Pertti Auerkari, Heikki Leinonen, Stefan Sandlin
VTT, Metals Laboratory, Finland
September 1991

TR 91-38
**Production methods and costs of oxygen free copper canisters for nuclear waste disposal**
Hannu Rajainmäki, Mikko Nieminen, Lenni Laakso
Outokumpu Poricopper Oy, Finland
June 1991

TR 91-39
**The reducibility of sulphuric acid and sulphate in aqueous solution (translated from German)**
Rolf Grauer
Paul Scherrer Institute, Switzerland
July 1990

TR 91-40
**Interaction between geosphere and biosphere in lake sediments**
Björn Sundblad, Ignasi Puigdomenech, Lena Mathiasson
December 1990

TR 91-41
**Individual doses from radionuclides released to the Baltic coast**
Ulla Bergström, Sture Nordlinder
Studsvik AB
May 1991